Mid-channel proteolysis of the L-type voltage gated calcium channel and the potential role of amyloid-β precursor protein

Kathryn Abele Henckels

Submitted in partial fulfillment of the
requirements for the degree of
Doctor of Philosophy
in the Graduate School of Arts and Sciences

COLUMBIA UNIVERSITY

2014

Abstract

Mid-channel proteolysis of the L-type voltage gated calcium channel and the potential role of amyloid-β precursor protein

Kathryn Abele Henckels

L-type voltage-gated calcium channels are involved in many important physiological processes, including muscle contraction, hormone secretion and neuronal gene expression. These channels are regulated by many different mechanisms to tightly control calcium influx. Our lab has uncovered a new form of L-type channel regulation that involves the proteolysis of the channel in the main body of the α_1 subunit in response to increased intracellular calcium, channel activity and age. I investigated the immediate and long-term functional impact of mid-channel proteolysis on the $Ca_V1.2$ channel. Mid-channel proteolysis causes an acute change in gating and a decrease in channel activity over a longer time scale. Fragment channels result from proteolysis, and these fragments associate on the plasma membrane to form functional channels. These L-type fragment channels exhibit different biophysical properties than full-length $Ca_V1.2$. While fragment channels must combine so that all four domains are present to be functional, non-complimentary pairs containing more than four domains still produce discernible current. L-type fragment channels co-immunoprecipitate with the full-length $Ca_V1.2$, indicating that fragments bind to either the α_1 subunit or the channel complex. Some of these fragments cause a shift in inactivation and in the I-V curve of the channel, and one fragment comprising Domain IV and the C-terminus (fragment C2) inhibits full-length

$Ca_V1.2$ in a dominant negative manner. These results demonstrate the functional effects of mid-channel proteolysis.

L-type mid-channel proteolysis increases with animal age. Therefore, to identify the protease responsible for mid-channel proteolysis, I turned to proteases involved in aging diseases. Amyloid-β precursor protein (APP), a protein implicated in Alzheimer's disease (AD), modulates L-type channels and is itself extensively proteolyzed. One of those proteases is presenilin, the catalytic component to γ-secretase. I found that APP dramatically reduced human $Ca_V1.2$ current in *Xenopus* oocytes. The current-voltage relationship and inactivation profiles of $Ca_V1.2$ in the presence of APP mirrored those of the fragment channels. Moreover, a γ-secretase inhibitor, DAPT, completely reversed this effect. When an AD APP mutant was co-expressed with $Ca_V1.2$, currents were further diminished. Astonishingly, an APP mutant that protects against AD had the opposite effect, allowing larger $Ca_V1.2$ currents than wild-type APP.

Western blots stained with an antibody against $Ca_V1.2$ revealed a ~100 kD band when APP was coexpressed with the channel, which was absent in oocytes solely expressing $Ca_V1.2$. DAPT application reversed this effect, indicating the band was a product of presenilin proteolysis. A putative cut site was found on the α_1 subunit that would produce a band similar in size to the one observed in Western blots. When this site was mutated, the ~100 kD band no longer appeared when $Ca_V1.2$ was coexpressed with APP. Unfortunately, the $Ca_V1.2$ II-III loop antibody was later found to cross-react with APP. Therefore, additional experiments are necessary to determine whether the ~100 kD band is $Ca_V1.2$ Interestingly, APP induced mid-channel proteolysis was detected in primary neurons using imaging techniques. While the mechanism for APP-induced

inhibition of the channel is still unresolved, my data clearly shows this effect is mediated by presenilin. Whether or not presenilin is responsible for cutting $Ca_V1.2$ remains to be resolved.

Table of Contents

List of Figures ..... **iii**

Acknowledgements ..... **v**

Dedication ..... **vii**

Chapter 1: Introduction **1**

1.1 Overview of Voltage-Gated Calcium Channels **1**

1.1.1 The Subunits of Voltage-Gated Calcium Channels 1

1.1.2 Subtypes of VGCCs 6

1.1.3 Localization and Function of VGCCs 7

1.2 Regulation of VGCCs **10**

1.2.1 PKA and PKC 10

1.2.2 G-proteins 12

1.2.3 RGK proteins 13

1.2.4 Lipids 13

1.2.5 SNARE proteins 14

1.2.6 Calmodulin 15

1.3 Regulatory Proteolysis **15**

1.4 Splice Variants and Truncated HVA VGCCs **21**

1.4.1 Natural Truncations of L-type Channels 21

1.4.2 Ca_V1 Fragments as Transcription Factors 22

1.4.3 P/Q-type channel truncations 24

1.4.4 N-type channel Splice Variants 25

1.5 Thesis Introduction **26**

Chapter 2: Materials & Methods **28**

2.1 Molecular Biology 28

2.2 Protein Purification 29

2.3 RNA Synthesis 30

2.4 Oocyte Preparation & cRNA Injection 31

2.5 Electrophysiology 31

2.6 Rat Cortical Slices 32

2.7 HEK293 stable line creation and cell culture 34

2.8 Embryonic hippocampal neuron culture 34

2.9 Transfection 35

2.10 Co-Immunoprecipitation 36

2.11 Biotinylation of HEK293_$\beta_3\alpha_2\delta$ cells 36

2.12 SDS-PAGE and Western Blot 37

2.13 Immunofluorescent Staining and Confocal Microscopy 38

2.14 Data Analysis 39

Chapter 3: Functional Effect of Proteolysis of $Ca_V1.2$ **41**

3. 1 Introduction **42**

3.2 Results **43**

3.2.1 Mid-channel proteolysis of $Ca_V1.2$ 43

3.2.2 Activity-dependent proteolysis of $Ca_V1.2$ 46

3.2.3 Separation of the channel on the membrane ... 47
3.2.4 Age-dependent proteolysis of $Ca_V1.2$ ... 50
3.2.5 Identifying the protease site ... 52
3.2.6 Acute functional effect of mid-channel proteolysis ... 54
3.2.7 Long-term functional effect of mid-channel proteolysis ... 57
3.3 DISCUSSION ... 60
3.3.1 The importance of L-type mid-channel proteolysis ... 60
3.3.2 Identifying the protease and cut site ... 60
3.3.3 Functional effects of mid-channel proteolysis ... 61
3.3.4 Fragment channels are functional ... 62

Chapter 4: Functional Characterization of $Ca_V1.2$ Fragment Channels ... 64
4.1 INTRODUCTION ... 65
4.2 RESULTS ... 68
4.2.1 Fragment channels are functional as complementary pairs ... 68
4.2.2 Fragment channels have different biophysical properties ... 71
4.2.3 Surface expression of fragment channels ... 72
4.2.4 Dominant negative effects on the full-length channel ... 75
4.3 DISCUSSION ... 82
4.3.1 Fragment channels are functional ... 82
4.3.2 Effect of fragments on full-length $Ca_V1.2$ ... 83
4.3.3 Implications of fragment channels as products of mid-channel proteolysis ... 85

Chapter 5: $Ca_V1.2$ Function is Inhibited by APP and γ-secretase ... 86
5.1 INTRODUCTION ... 87
5.1.1 The calcium hypothesis of Alzheimer's Disease ... 87
5.1.2 APP Processing ... 90
5.1.3 L-type channel and Alzheimer's Disease ... 94
5.2 RESULTS ... 96
5.2.1 APP decreases L-type channel current and changes its biophysical properties ... 96
5.2.2 A ~100kD band appears in westerns when APP is coexpressed with $Ca_V1.2$ ... 98
5.2.3 DAPT reverses the effect on current and proteolysis ... 99
5.2.4 The ~100kD band occurs with rat $Ca_V1.2$ but not PQ channel ... 103
5.2.5 Potential cut sites on the channel – mutations change cleavage pattern ... 104
5.2.6 APP-induced proteolysis is not reproducible in neurons ... 107
5.2.7 APP-/- brain slices and neurons ... 110
5.2.8 There is no proteolysis in HEK 293 cells ... 112
5.2.9 APP and hL do not co-IP in HEK cells or oocytes ... 114
5.2.10 Effect of APP mutants on $Ca_V1.2$ current in oocytes ... 116
5.2.11 Imaging reveals APP-dependent proteolysis of $Ca_V1.2$ in neurons ... 119
5.3 DISCUSSION ... 121

Chapter 6: Concluding Remarks and Future Prospects ... 124
6.1 Mid-channel Proteolysis of $Ca_V1.2$ ... 124
6.2 The Fate and Function of Fragment Channels ... 125
6.3 The Effect of Amyloid-β Precursor Protein and Presenilin on $Ca_V1.2$ ... 127

References ... 130

Appendix ... 153

List of Figures

Figure 1.1	Molecular composition of VGCC complex	2
Figure 1.2	Schematic topology of α_1 subunit	4
Figure 1.3	The three subfamilies of VGCCs	7
Figure 1.4	Ca_V2 channel signaling complexes	11
Figure 1.5	Proteolytic cleavage of the C-terminus in β-adrenergic regulation	20
Figure 3.1	Mid-channel proteolysis of endogenous $Ca_v1.2$ in cortical neurons and its channel activity-dependent regulation.	43
Figure 3.2	Visualization of mid-channel proteolysis of $Ca_v1.2$ in the plasma membrane of cultured hippocampal neurons.	47
Figure 3.3	Mid-channel proteolysis is age-dependent and can be reversed *in vivo*	49
Figure 3.4	Thrombin and enterokinase are not the protease	51
Figure 3.5	Acute functional effect of mid-channel proteolysis	54
Figure 3.6	Long-term functional effect of mid-channel proteolysis	56
Figure 3.7	Fragment channels are functional when coexpressed	57
Figure 4.1	Fragment channels are functional when properly paired	67
Figure 4.2	Fragment channels have different biophysical properties than $Ca_V1.2$	69
Figure 4.3	Surface expression of fragment channels	71
Figure 4.4	Dominant negative effects of fragments on full-length $Ca_V1.2$	72
Figure 4.5	Fragments A1 and A2 affect the biophysical properties of $Ca_V1.2$ through an association with the channel complex	74
Figure 4.6	Fragments B1 and B2 associate with the channel complex but do not affect the biophysical properties of $Ca_V1.2$	76

Figure 4.7	Fragments C1 and C2 affect the biophysical properties of $Ca_V1.2$ and C2 strongly associates with the channel complex	78
Figure 5.1	Dysregulation of intracellular calcium (Ca^{2+}) in AD	85
Figure 5.2	Overview of APP processing	88
Figure 5.3	APP inhibits $Ca_V1.2$ peak current	92
Figure 5.4	Biophysical changes to $Ca_V1.2$ in the presence of APP	93
Figure 5.5	APP causes the appearance of a ~100 kD band in Western blots	95
Figure 5.6	DAPT reverses the effect APP has on $Ca_V1.2$	98
Figure 5.7	The ~100 kD band is L-type specific	100
Figure 5.8	Mapping the potential cut site in $Ca_V1.2$	102
Figure 5.9	$Ca_V1.2$ proteolysis patterns in rat neurons	105
Figure 5.10	Comparing proteolysis patterns of $Ca_V1.2$ in WT and APP-/- mice	107
Figure 5.11	$Ca_V1.2$ proteolysis is absent in the HEK293 β_3-$\alpha_2\delta$ stable line	109
Figure 5.12	There is no apparent association between hL and APP	111
Figure 5.13	APP mutants' effect on current and proteolysis of hL	114
Figure 5.14	APP FAD and protective mutant effects on the separation of surface LGH3	116

Acknowledgements

Many people have helped in enabling me to complete this PhD training over the past six years. First and foremost, I would like to thank my advisor Jian Yang. Jian urged me to join the PhD program when I was enrolled as a Master's student, and I could not be more grateful for his support. He has been a wonderful mentor over the years, providing me guidance yet allowing me the freedom to explore my own ideas.

I would also like to thank my advisory committee and defense committee members. Thank you Elizabeth Miller, Martin Chalfie and Ming Zhou for your invaluable advice throughout my time as a graduate student and for taking the time to serve on my committee. Thank you Steven Marx and Jamie Weiss for taking the time to read my thesis and attend my defense. Your expert opinions are very much appreciated.

There are many past and present members of the Yang Lab that I would like to thank. Yannis Michailidis started as a mentor and ended as an invaluable colleague. I am grateful for his patience, guidance and help over the years. Minghui Li, Zafir Buraei, Yong Yu and Kevin Zhang were always available to answer my questions and provide support. All of their personalities made the atmosphere of the lab warm and supportive. Lastly, I would like to thank the undergraduates that I had the pleasure of mentoring and whom both contributed to this work, Glynis Gordon and Morgan Goodman.

My friends and family have been a wonderful support system over the years. Nadia Propp, Jessica Brann and Aileen Fitzmaurice have always been there with professional and personal advice over the years. They have made my time in New York a wonderful experience. I also have to thank my Mother for her unwavering support

throughout my life. She has pushed me to take on more than I thought possible since I applied to undergrad. She was the only one that told me it was okay to leave a comfortable, well-paying job to move to the “big city”, not knowing a soul, to earn little to no money while paying double the rent just to pursue a higher degree. I appreciate her love and support more than she realizes.

Last, but certainly not least, I would like to thank my husband and best friend, Eric Henckels. I could not have done this without his love, motivation and support. And I suppose I should also thank my unborn son for not causing any medical drama during the writing of this thesis. I can’t wait to meet you.

To my Mother and Husband

Chapter 1

Introduction

1.1 Overview of Voltage-Gated Calcium Channels

Ion channels are transmembrane proteins that form pores in the plasma membrane to allow the passage of ions in and out of the cell. Voltage-gated ion channels open in response to changes in membrane potential, and include voltage-gated Na^+, K^+, Cl^- and Ca^{2+} channels. These are different than ligand-gated ion channels that open in response to a ligand binding, allowing for an influx of Na^+ or Ca^{2+} to locally depolarize the membrane. Voltage-gated channels are essential for all excitable cells. Voltage-gated calcium channels (VGCCs) not only aid in cell excitability, but they allow for the influx of calcium, a very important second messenger. Calcium triggers various signaling cascades that control many critical cellular processes. These include hormone secretion, neurotransmitter release, cell migration, gene transcription, and muscle contraction (Catterall, 2000). In response to changes in voltage across the membrane, and under the regulation of many other proteins, VGCCs allow the heart to beat, the kidney to function, and neurons to communicate with one another.

1.1.1 The Subunits of Voltage-Gated Calcium Channels

VGCCs consist of an assembly of subunits that together form a functional channel. The main transmembrane α_1 subunit associates with auxiliary subunits β, $\alpha_2\delta$

and sometimes γ (Figure 1.1) to form the VGCC complex. Although α_1 alone is able to conduct a current, the auxiliary subunits allow for proper gating (Perez-Reyes and Schneider, 1995). Coexpression of β is necessary for α_1 trafficking from the endoplasmic reticulum to the plasma membrane, therefore little α_1 will be expressed without β present in heterologous systems (Buraei and Yang, 2010). While many subtypes and splice variants exist for all subunits, the basic structure of the complex is similar for all VGCCs.

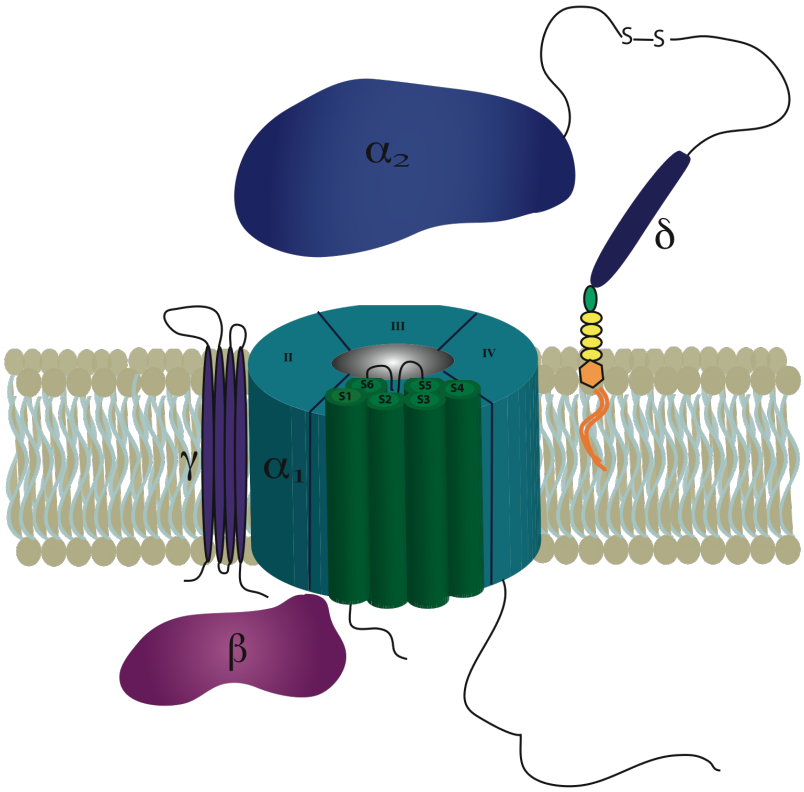

Figure 1.1 Molecular composition of VGCC complex. $Ca_V\alpha_1$ is the pore-forming subunit responsible for the biophysical and pharmacological properties of the channel. $Ca_V\beta$, $Ca_V\gamma$, and $Ca_V\alpha_2\delta$ are auxiliary subunits that modulate channel expression and gating.

The principal component of the calcium channel, the α_1 subunit, contains the voltage sensor and forms the pore through which Ca^{2+} ions flow (Figure 1.2). This subunit is responsible for most of the pharmacological properties of VGCCs (Catterall, 2000). The α_1 subunit consists of four homologous domains, each containing six hydrophobic transmembrane segments. Both the cytoplasmic N- and C-termini and the intracellular loops connecting the domains, often termed "linkers", contain binding sites for a multitude of proteins responsible for channel modulation and regulation. The pore-lining loops (P loops), which are made up of highly conserved glutamic acid residues between segments S5 and S6, reinsert into the membrane. Due to their negative charge they are responsible for the high Ca^{2+} selectivity of the pore (Yang et al., 1993). The S4 segment consists of positively charged lysines and arginines that create the voltage sensor, which swings outward opening the ion pore in response to depolarization (Bezanilla, 2002). The S6 segment is involved in inactivation of the channel, whereby the I-II linker region docks to the extracellular end of S6 in response to depolarization, essentially blocking the pore (Stotz et al., 2004). Ten different genes for α_1 have been identified in humans, all having different gene transcripts, but belonging to the same *CACNA1* family, although various splice variants exist (Jurkat-Rott and Lehmann-Horn, 2004). Expression of a particular α_1 subunit dictates the type of channel, high voltage activated (HVA) or low voltage activated (LVA), as well as the type of current conducted through that channel.

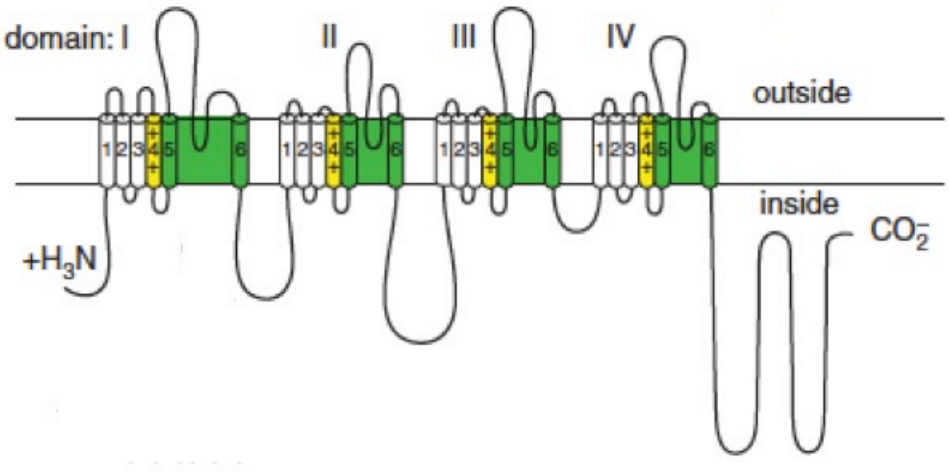

Figure 1.2 Schematic topology of α_1 subunit. Positively charged voltage-sensor S4 is in yellow and the pore forming segments S5, S6 and the P-loop are in green. Domains are denoted as I, II, III and IV. Both N- and C-termini are intracellular. (Modified from (Catterall, 2011)).

The cytosolic β subunit is a multifunctional protein in regards to the role it plays as part of the VGCC complex (Buraei and Yang, 2010). The β subunit acts as a chaperone to α_1, trafficking it out of the endoplasmic reticulum and to the plasma membrane (Raghib et al., 2001) Different β subtypes determine the subcellular location of the channel (Wittemann et al., 2000). The GK domain of β is absolutely necessary for channel expression on the membrane, regardless of whether the rest of the β subunit is present (He et al., 2007). The β subunit also greatly affects the activation and inactivation kinetics of the channel. There are four known human β subunit genes, each with splice variants, termed β_1, β_2 β_3 and β_4 (Birnbaumer et al., 1998) and each subtype of VGCC associates primarily with one specific β subtype (Reimer et al., 2000). β directly interacts with α_1 on the I-II linker (Chen et al., 2004), and this high-affinity binding site is termed the α_1-interaction domain (AID). A single β subunit molecule is

sufficient to provide full function and membrane expression of the channel (Dalton et al., 2005). β hyperpolarizes the voltage-dependence of activation of VGCCs (Dolphin, 2003) and increases the mean open time of the channel pore (Wakamori et al., 1999).

The α_2 and δ subunits are generally considered one subunit as they are encoded by the same gene (De Jongh et al., 1990). However, posttranslational modifications occur that cleave the translated protein into 143-kD α_2 and 27-kD δ subunits, which are then linked by a disulfide bond to form the α_2-δ complex (Jay et al., 1991). Several splice variants of α_2-δ are known, many with specific tissue expression (Klugbauer et al., 2003). Previous studies have reported that expression of the α_2-δ complex increases currents in α_1/β recombinant channels (Bangalore et al., 1996) and influences inactivation rates. Assembly of the α_2-δ complex with N-type channels increased the half-life of the channel (Bernstein and Jones, 2007), possibly tethering it to the membrane to impede internalization of the channel by mechanisms yet unexplored. The α_2δ subunit is also thought to assist with α_1 trafficking and stabilization of the VGCC complex on the plasma membrane (Dolphin, 2012).

The γ subunit is a hydrophobic glycoprotein with four transmembrane domains and cytoplasmic N- and C-termini (Black, 2003). The γ-subunit was found to be just over 25kD in size and co-purified with the other four subunits of the L-type Ca^{2+} channel (Sharp and Campbell, 1989). There are currently eight known γ genes in humans, all of the *CACNG* gene family (Black, 2003). Not all VGCC complexes require the γ subunit to function properly. Cardiac L-type channels have been found to associate with the γ

subunit (Yang et al., 2011) and γ was shown to cause activation to occur at more negative potentials, as well as speed up inactivation (Eberst et al., 1997) .

1.1.2 Subtypes of VGCCs

Two main types of VGCCs exist, high voltage activated (HVA) and low voltage activated (LVA), and they are further differentiated based on the type of α_1 subunit they express (Figure 1.3). The HVA channels consist of L-, P/Q-, N-, and R-type currents, while T-type currents are classified as LVA channels. They are subdivided into Ca_V1, Ca_V2, and Ca_V3 families, each of which have representative channels in *C. elegans* (Jeziorski et al., 2000), proving the phylogenic age of these proteins. The Ca_V1 and Ca_V2 channels are roughly 50% homologous to one another, whereas the Ca_V3 channels have only ~25% homology to the HVA channels (Figure 1.3), about the same as those channels share with Na^+ channels, indicating that T-type channels separated from HVA VGCCs around the same time as voltage-gated Na^+ channels did (Catterall, 2011). However, the differences between the channel subtypes are not only in their amino acid sequences, but in their tissue localization and function (described in detail below).

The L-type Ca^{2+} channels have four different gene transcripts, all specifying different α_1 subtypes. These are designated $Ca_v1.1$, $Ca_v1.2$, $Ca_v1.3$, and $Ca_v1.4$, which express α_{1S}, α_{1C}, α_{1D}, and α_{1F} respectively. P/Q-type channels are classified as $Ca_v2.1$ and express α_{1A}, N-type channels are classified as $Ca_V2.2$ and express α_{1B}, and R-type channels are classified as $Ca_V2.3$ and express α_{1E}. The T-type Ca^{2+} channels have three subtypes classified as $Ca_v3.1$, $Ca_v3.2$, and $Ca_v3.3$, which express α_{1G}, α_{1H}, and α_{1I} respectively.

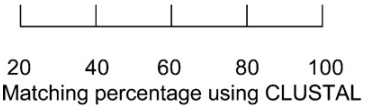

Protein	Gene	Chromosome	Primary tissues	Calcium current
$Ca_v1.1$ (a_{1S})	*CACNA1S*	1q32	skeletal muscle	L-type
$Ca_v1.2$ (a_{1C})	*CACNA1C*	12p13.3	heart smooth muscle brain, heart, pituitary, adrenal	L-type
$Ca_v1.3$ (a_{1D})	*CACNA1D*	3p14.3	brain, pancreas, kidney, ovary, cochlea	L-type
$Ca_v1.4$ (a_{1F})	*CACNA1F*	Xp11.23	retina	L-type
$Ca_v2.1$ (a_{1A})	*CACNA1A*	19p13	brain, cochlea, pituitary	P/Q-type
$Ca_v2.2$ (a_{1B})	*CACNA1B*	9q34	brain, nervous system	N-type
$Ca_v2.3$ (a_{1E})	*CACNA1E*	1q25-31	brain, cochlea, retina, heart, pituitary	R-type
$Ca_v3.1$ (a_{1G})	*CACNA1G*	17q22	brain, nervous system	T-type
$Ca_v3.2$ (a_{1H})	*CACNA1H*	16p13.3	brain, heart, kidney, liver	T-type
$Ca_v3.3$ (a_{1I})	*CACNA1I*	22q12.3-13-2	brain	T-type

Figure 1.3 The three subfamilies of VGCCs. A dendogram comparing the amino acid sequences between the subtypes of VGCC α_1 subunits. Gene name, chromosome location, tissue localization and type of current also listed. (Taken from (Jurkat-Rott and Lehmann-Horn, 2004)).

1.1.3 Localization and Function of VGCCs

L-type channels are involved in muscle contraction, hormone secretion and gene transcription (Catterall, 2011). $Ca_V1.1$ channels are predominately found in skeletal muscle and $Ca_V1.2$ channels are located in cardiac tissue and brain. $Ca_V1.3$ channels are generally found in the central nervous system (Catterall, 2000) and auditory hair cells (Platzer et al., 2000). $Ca_V1.4$ channels are expressed in the retina and are involved in phototransduction (Bech-Hansen et al., 1998). Neuronal L-type channels ($Ca_V1.2$ and $Ca_V1.3$) are found at postsynaptic synapses and in the soma, however they are also recruited to microdomains along distal dendrites and spines, which allows for easier synapse to nucleus communication (Leitch et al., 2009). L-type channels play a role in

gene transcription in neurons (Bean, 1989) and are involved in hormone secretion in endocrine cells (Milani et al., 1990). They are responsible for the contraction of cardiac and smooth muscle, and initiate rapid contraction in skeletal muscle by directly interacting with ryanodine-sensitive Ca^{2+} release channels (Catterall, 2011). L-type channels are known to be sensitive to phenylalkylamines, benzothiazapines, and dihydropyridines (Reuter, 1983) and are blocked by the spider toxin ω-agatoxin IIIA (Mintz et al., 1991). L-type channels are implicated in many disease states, including Duchenne muscular dystrophy (Friedrich et al., 2008), arrhythmias and hypertension (Triggle, 2006), Timothy syndrome (Barrett and Tsien, 2008), hypokalemic periodic paralysis and night blindness (Striessnig et al., 2004).

The P/Q-, R-, and N-type Ca^{2+} channels make up the Ca_V2 family and are widely expressed in neurons and chromaffin cells (Garcia et al., 2006). Ca_V2 channels are mainly involved in short-term synaptic plasticity (Catterall et al., 2013). P- and Q-type channels are derived from alternative splice variants of the same gene (Bourinet et al., 1999), and can be distinguished based on their sensitivities to various toxins. P-type channels are more sensitive to ω-AgaIVA, whereas Q-type channels are sensitive to ω-CMVIIC (Randall and Tsien, 1995). N-type channels are specifically blocked by the marine snail toxin, ω-conotoxin GVIA (Plummer et al., 1989). R-type channels are resistant to these toxins, thus termed "R" for resistant. P/Q- and N-type channels are abundant in presynaptic terminals and are involved in neurotransmitter release (Takahashi and Momiyama, 1993). N-type channels ($Ca_V2.2$) are found in neurons and neuroendocrine cells (Catterall and Few, 2008). In the spinal cord (Snutch, 2005) they are located in dorsal root ganglia and at the synaptic terminals in dorsal horn neurons that

connect to afferent sensory fibers (Perret and Luo, 2009). In the dorsal horn, they are found predominately in substance P containing cells (Altier et al., 2007; Snutch, 2005). $Ca_V2.2$ channels are responsible for the majority of synaptic processing of nociceptive information in dorsal horn neurons (Hatakeyama et al., 2001; Matthews and Dickenson, 2001). P/Q-type channels ($Ca_V2.1$) are found throughout the entire brain, but are expressed at particularly high levels in the cerebellum (Pietrobon, 2005b). $Ca_V2.1$ channels are also found in brain regions associated with the perception of pain, such as the trigeminal ganglia and brainstem nuclei (Pietrobon, 2005b). They play a major role at excitatory synapses (glutamate) and a lesser role at inhibitory synapses (GABA) (Timmermann et al., 2002). While $Ca_V2.2$ knockouts do not display an adverse phenotype besides higher threshold for pain (Pietrobon, 2005a), $Ca_V2.1$ knockout mice survive for only a few weeks, and display seizures and ataxia while alive (Jun et al., 1999). Also, a lack of N- and R-type channels can be compensated for, whereas deficiencies in P/Q-type channels cannot (Pietrobon, 2005a).

The T-type calcium channels make up the Ca_V3 family and are the LVA calcium channels, meaning they open at much more negative potentials than the other VGCCs (Carbone and Lux, 1984). T-type calcium channels are expressed throughout the body, and can be found in the brain, heart, kidney, sperm, smooth muscle and many endocrine organs (Perez-Reyes, 2003). They serve a major role in cardiac pacemaking and neuronal oscillations (Cueni et al., 2009) and are essential for sleep, motor coordination and learning. In contrast to the other VGCCs that require auxiliary subunits to function, Ca_V3 channels are believed to function as independent α_1 subunits (Catterall, 2011).

1.2 REGULATION OF VGCCS

With such a diverse range of functions, it is no surprise that VGCCs must be intricately regulated by a variety of mechanisms. Many proteins interact with VGCCs to regulate or modulate the channel (Figure 1.4). Kinases activate the channel through phosphorylation. G-proteins can bind to and inactivate the channel. Lipids in the membrane interact with the channel to stabilize it in the membrane and contribute to the channel's kinetics. Calcium binding proteins act as calcium sensors to control the channel in response to its environment. The VGCC subtypes are regulated by one, or many, of the following proteins in order to properly function.

1.2.1 PKA and PKC

VGCCs can be regulated by c-AMP dependent protein kinase A (PKA) and protein kinase C (PKC). L-type channels are phosphorylated by PKA, which enhances channel activity (to be discussed in detail below). Ca_V1 channels also directly bind to PKA anchoring proteins (AKAP) (Hulme et al., 2002). PKA has been found to enhance voltage-dependent facilitation of $Ca_V2.1$ channels (Tamse et al., 2003) and $Ca_V2.2$ channels to a lesser extent (Fukuda et al., 1996). Many different isoforms of PKC have been shown to co-immunopreciptitate with $Ca_V\alpha_1$ (Dai et al., 2009). PKC has an inhibitory effect on L-type channels, whereby phosphorylation of two sites on the N-terminus decreases current in both $Ca_V1.2$ (McHugh et al., 2000) and $Ca_V1.3$ (Baroudi et al., 2006) channels. In contrast, PKC phosphorylation of Ser^{1928} in the C-terminus, the same residue that is phosphorylated by PKA, upregulates $Ca_V1.2$ activity (Yang et al., 2005). PKC also phosphorylates Ca_V2 channels in the I-II loop, leading to an

upregulation of channel activity by antagonizing Gβγ (Zamponi et al., 1997). PKC phosphorylation of Ca_V2 channels in the synprint site interfere with syntaxin binding and cause a hyperpolarizing shift in voltage-dependent inactivation (Jarvis and Zamponi, 2001).

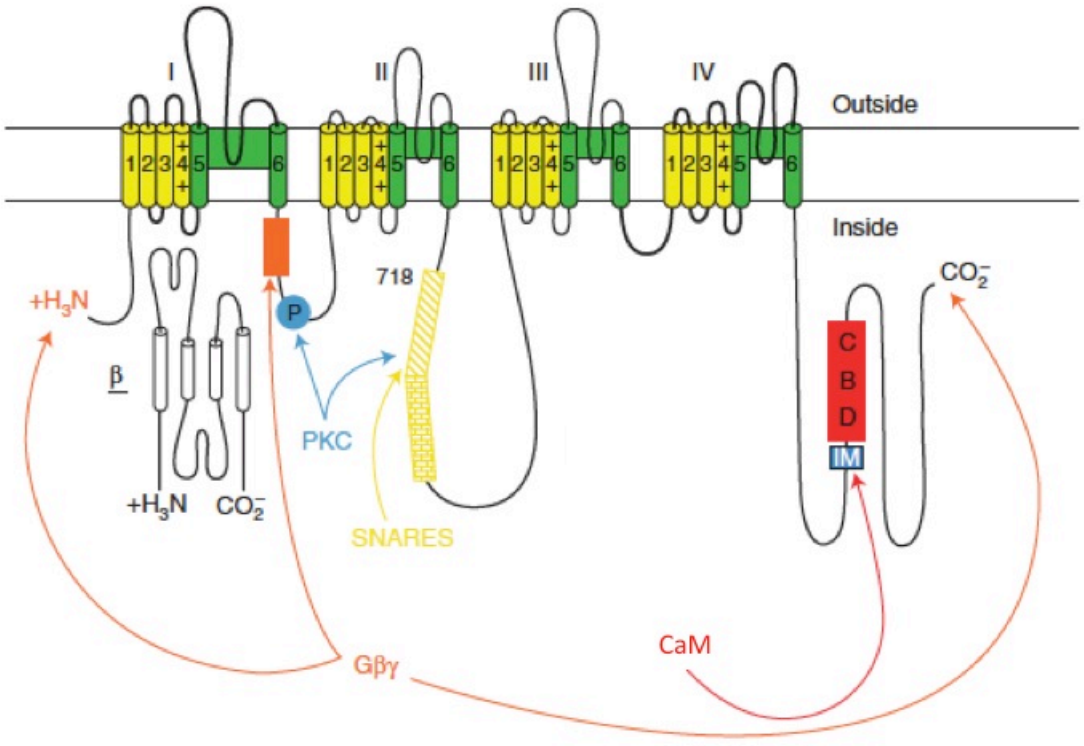

Figure 1.4 Ca_V2 channel signaling complexes. Sites of interaction of regulatory proteins are illustrated. Gβγ binds to the I-II loop, N- and C-termini. PKC phosphorylates residues on the I-II and II-III loop. SNARE proteins interact with the synprint site on the II-III loop. CaM binds to both the IQ- like motif (IM) and the CaM binding domain (CBD). β associates with the channel at in the AID of the I-II loop. (Modified from (Catterall, 2011)).

1.2.2 G-proteins

The G protein heterodimer Gβγ is known to inhibit P/Q- and N-type calcium channels (Herlitze et al., 1996; Ikeda, 1996) by causing a change in the voltage dependence of VGCCs so that more positive voltages are necessary for activation of the channel (Catterall, 2000). This inhibition is most prominent at hyperpolarized potentials and is transiently relieved by large depolarization steps that facilitate the channel (Zamponi and Currie, 2013). This inhibition is thus termed voltage-dependent inhibition. Gβγ appears to only inhibit members of the Ca_v2 family, suggesting its involvement in neurotransmitter release at the presynaptic terminal (Tedford and Zamponi, 2006). Gβγ binds to sites on the N-terminus, the I-II linker encompassing the AID and the C-terminus (Zamponi and Currie, 2013). When bound to α_1, Gβγ stabilizes the closed conformation of the channel and it is only after Gβγ dissociates that the channel can return to a state willing to open (Zamponi and Snutch, 1998). When β binds to the AID it induces a rigid alpha helical link with domain IS6. When the membrane is depolarized, this rigid alpha helix moves and disrupts the Gβγ binding pocket, which displaces Gβγ from the channel and relieves the inhibition (Zhang et al., 2008). The voltage-dependent inhibition is dependent on β; when β is not present Gβγ will not dissociate (Zhang et al., 2008). Protein kinase C can also reverse G-protein inhibition, most likely by interfering with the Gβγ binding domains through phosphorylation sites on the I-II linker (Zamponi et al., 1997).

1.2.3 RGK proteins

The RGK proteins, comprised of Rem, Rem2, Gem, and Rad, are all small GTP-binding proteins in the Ras protein family (Correll et al., 2008b) and act as inhibitors of VGCCs (Tedford and Zamponi, 2006). It was originally thought that RGK proteins act to sequester β in the ER to hinder α_1 trafficking to the membrane (Correll et al., 2008b). However, it is now known that Rem, Rad, and Gem are able to bind to the β-α_1 complex on the membrane without causing β to dissociate (Beguin et al., 2007; Fan et al., 2012). In fact, while Gem binds to α_1 directly, Gem inhibition requires β to also bind to α_1 to expose an inhibitory site on the channel (Fan et al.). Rem2 also forms a Rem2-β-α_1 complex at the plasma membrane, and localization of Rem2 to the plasma membrane is essential for its inhibitory effect on channel function (Correll et al., 2008a). RGK proteins impose their inhibitory effects by increasing channel endocytosis, decreasing the open probability of channels on the membrane, and inhibiting the movement of the voltage sensor in a GTP dependent manner (Yang and Colecraft, 2013).

1.2.4 Lipids

Lipids in the plasma membrane also regulate HVA VGCCs. Phosphatidylinositol-4,5-biphosphate (PIP2) stabilizes the channel in the plasma membrane and attenuates current rundown (Michailidis et al., 2007), and also produces voltage-dependent inhibition. HVA VGCC voltage-dependent inhibition occurs because of the slow hydrolysis of PIP2 and arachidonic acid in the plasma membrane. Interestingly, PIP2 induced voltage-dependent inhibition is reversed by PKA phosphorylation (Wu et al.,

2002). Gβγ inhibition also requires an ample amount of PIP2 on the plasma membrane (Rousset et al., 2004). Additionally, phosphatidylinositol-3,4,5-triphosphate (PIP3) promotes trafficking of the channels to the plasma membrane, increasing surface expression (Viard et al., 2004).

1.2.5 SNARE proteins

Neurotransmitters are released through a complex vesicular fusion process initiated by the influx of Ca^{2+} at the presynaptic terminal. The docking and fusion of vesicles is dependent on Ca^{2+} concentration within the presynaptic terminal where VGCCs interact with the SNARE protein complex of syntaxin, SNAP-25, and VAMP/synaptobrevin (Bajjalieh and Scheller, 1995). P/Q- and N-type channels physically couple to synaptic release complexes, ensuring Ca^{2+} influx occurs in close proximity to the release site (Sheng et al., 1998). This region of binding on the α_1 subunit has been termed the "synprint" site for synaptic protein interaction and is located in the II-III loop of Ca_V2 channels. In addition, SNARE proteins modulate channel gating, shifting the voltage-dependence of inactivation to more hyperpolarized potentials (Bezprozvanny et al., 1995; Zhong et al., 1999). Syntaxin may also act as a scaffolding protein, bringing Ca^{2+} channels and Gβγ into close proximity to allow inactivation of the channel (Evans and Zamponi, 2006), however this has only been demonstrated in N-type Ca^{2+} channels.

1.2.6 Calmodulin

Calmodulin (CaM) is a calcium binding protein that acts as a calcium sensor to regulate VGCCs in a biphasic manner. CaM contains four Ca^{2+} binding domains, two in the N-terminal lobe and two in the C-terminal lobe. While CaM is constitutively bound to the C-terminus of VGCCs, it binds specific regions on α_1, termed the calmodulin binding domain (CBD) and the IQ domain, depending on the amount of bound Ca^{2+} it holds (Catterall and Few, 2008). An N-terminal binding CaM site has also recently been uncovered (Simms et al., 2013). For Ca_V2 channels, when Ca^{2+} binds the C-terminal lobe of CaM, CaM binds the IQ domain prompting a fast calcium-dependent facilitation (CDF) of the channel (DeMaria et al., 2001). However, when Ca^{2+} also binds to the N-terminal lobe of CaM, CaM binds the CBD just downstream of the IQ site and causes a slower Ca^{2+} dependent inactivation (CDI) (Soldatov 2003). Therefore, Ca^{2+} influx causes an initial facilitated opening and a gradual Ca^{2+} induced closing of Ca_V2 channels. In contrast, Ca_V1 channels experience rapid CDI in response to Ca^{2+} binding the C-terminal lobe of CaM, a process that occurs within milliseconds of Ca^{2+} influx (Lee et al., 1985). This dual role of CaM in VGCC modulation provides positive and negative feedback in response to both local and global Ca^{2+} levels.

1.3 Regulatory Proteolysis

Proteases are yet another subset of proteins that can act on VGCCs to modulate their function. Two forms of $Ca_V1.1$ channel exist in the heart, full length (~220 kD) and truncated (~190 kD). Approximately 80% of $Ca_V1.1$ channels are truncated in the heart (De Jongh et al., 1991), and therefore the truncated channel is the predominant

physiological form. This truncated version is cleaved in the C-terminus between residues A1664 and N1665 of $Ca_V1.1$ in skeletal muscle (Hulme et al., 2005) and A1800 and N1801 of $Ca_V1.2$ in cardiac muscle (Fuller et al., 2010). The C-terminus is an important factor for VGCC function, affecting channel properties through the mechanisms mentioned above, like the interaction with calmodulin (Zuhlke and Reuter, 1998), the β subunit (Gao et al., 1997), cAMP-dependent protein kinase (PKA) (Sculptoreanu et al., 1993), and by targeting the channel to the plasma membrane (Gao et al., 2000). What purpose would this proteolysis serve if the C-terminus is so integral to channel function?

In skeletal muscle, excitation-contraction coupling is initiated by L-type channels (Catterall, 1991), which open and allow Ca^{2+} to enter acting as a second messenger. This is a tightly regulated process, requiring rapid phosphorylation of the Ca_V1 channel by PKA, which modulates channel activity (Johnson et al., 1994; Sculptoreanu et al., 1993), and is thought to underlie the "fight or flight" phenomenon. Basically, when faced with a threat, epinephrine and norepinephrine are released and activate the β-adrenergic system, which in turn activates L-type channels allowing muscle contraction to increase and the heart to beat faster (Bers, 2002). This mechanism has now been parsed out and the cleaved Ca_V1 C-terminal fragment plays a major role in the regulation of the "fight or flight" phenomenon.

Phosphorylation by PKA is crucial for channel modulation during β-adrenergic regulation, however it is anchored to the channel through sites on the the distal C-terminus, a region that is cleaved from the channel under physiological conditions. This modulation could only occur if the cleaved C-terminus reassociates with the channel. Indeed, this was found to be the case. The distal C-terminus and proximal C-terminus

co-immunoprecipitated when coexpressed in HEK-293 cells and also directly interacted in a yeast-two hybrid screen (Hulme et al., 2005). Functional studies revealed that when the C-terminus is removed from the channel by mutagenesis, an increase in peak current amplitude results (Wei et al., 1994). This has also been demonstrated using tsA201 cells with cardiac $Ca_V1.2$ channels truncated at 1821 (Hulme et al., 2006), at 1905, and those missing the PRD region (Gerhardstein et al., 2000). When truncated channels were coexpressed with the C-terminal fragment, a 20-fold inhibition occurred and even full-length channels were further inhibited by the C-terminal fragment (Hulme et al., 2006). In fact, it was found that channels missing only their last 147 residues displayed an increase in peak current amplitude compared to full-length channels, which was able to be reversed by addition of C-terminal fragments through direct association with α_1 (Gao et al., 2001). Arginines 1696 and 1697 on the proximal C-terminus interact with negatively charged residues (E2103, E2106, and D2110) on the distal C-terminal fragment via salt bridges to exert this inhibitory effect (Hulme et al., 2006). Therefore, it has been established that the C-terminal fragment that has been cleaved from α_1 can reassociate with the channel and act as an autoinhibitor. Besides an overall decrease in peak current amplitude, the C-terminal fragment shifts the voltage dependence of activation causing the channels open at higher voltages, however there is no effect on inactivation properties (Hulme et al., 2006).

Ca_V1 potentiation in both the heart and skeletal muscle is controlled by a rapid phosphorylation by PKA (Sculptoreanu et al., 1993). Two conserved phosphorylation sites in $Ca_V1.1$ (S1575 and T1579) and in $Ca_V1.2$ (S1700 and T1704) are regulated by the β-adrenergic system; S1575 phosphorylation is increased with isoproterenol, a β-

adrenergic receptor agonist, and decreased with propranolol, an antagonist (Emrick et al., 2010). These experiments were more relevant than past *in vitro* phosphorylation assays (Fuller et al., 2010; Johnson et al., 1997) because they were done using isolated rabbit skeletal muscle, whereby the animal was injected with these drugs while moving and breathing, and therefore are more physiologically relevant. While PKA has been primarily implicated in the β-adrenergic system, it was found that S1575 can be phosphorylated by both PKA and CAMKII (Emrick et al., 2010). On the other hand, T1579 is phosphorylated by casein kinase 2 (Emrick et al., 2010). PKA phosphorylation dramatically increases Ca_V1 current (Johnson et al., 1997), presumably by forcing the disassociation of the distal C-terminal fragment and relieving the autoinhibition.

PKA phosphorylation happens so rapidly, it was assumed that PKA must be stationed very close to the channel. An anchoring protein, AKAP-15 was identified that was integral to PKA phosphorylation. When a peptide that corresponded to 24 amino acids of a human AKAP protein was applied through a patch electrode on myotubes, it was able to inhibit channel current to the same extent that PKA inhibitors did (Johnson et al., 1994). AKAP-15 co-immunoprecipitates with $Ca_V1.1$ from skeletal muscle (Gray et al., 1997) and from tsa-201 cells (Gray et al., 1998), and confocal microscopy revealed it also colocalized with $Ca_V1.1$ in distinct areas (Gray et al., 1998). It wasn't confirmed that the two proteins directly interact until, using a yeast two-hybrid screen, AKAP-15 was found to bind to the distal C-terminal domain of $Ca_V1.1$ (residues 1774-1841) (Hulme et al., 2002). This interaction occurs through a leucine zipper (LZ) motif on AKAP-15 and a LZ-like motif on the $Ca_V1.1$ C-terminus. Furthermore, when either of the two regions were mutated to alanine, or a synthetic peptide comprising the LZ motif

of AKAP-15 was introduced to negatively compete with AKAP-15, PKA was unable to anchor to the channel, disrupting phosphorylation and voltage-dependent potentiation (Gray et al., 1998; Hulme et al., 2002). Therefore, AKAP-15 is responsible for targeting PKA to the channel.

While this mechanism has been established for $Ca_V1.1$, cardiac $Ca_V1.2$ is also truncated in the C-terminus at A1800 (Fuller et al., 2010). However, this residue does not appear to be required for proteolytic cleavage, since channels lacking this region were cleaved at the same rate as wild-type channels (Yang et al., 2013). $Ca_V1.2$ is also targeted by AKAP-15 and PKA in the same manner that $Ca_V1.1$ is. This mechanism has been reconstituted in non-muscle tsA-201 human embryonic kidney cells with $Ca_V1.2$ (Fuller et al., 2010) after transfection of the necessary molecular players, namely AKAP-15, PKA, $Ca_V1.2$ (1-1800) and the distal C-terminus. Furthermore, mice with $Ca_V1.2$ lacking the distal C-terminus developed cardiac hypertrophy and their β-andernergic pathway was disabled due to an inability of PKA to regulate $Ca_V1.2$ function (Fu et al., 2011). Cardiac myocytes from these mice also showed decreased surface expression of this truncated $Ca_V1.2$, which is most likely due to the role the C-terminus plays in trafficking the channel. AKAP-15 also had reduced expression. However, the required $Ca_V1.2$ PKA phosphorylation sites may be different than $Ca_V1.1$. It was recently found that cardiac myocytes taken from transgenic mice with mutated $Ca_V1.2$ phosphorylation sites (S1700A and T1704A) still exhibited isoproterenol- and forskolin-induced β-adrenergic stimulation (Yang et al., 2013). $Ca_V1.2$ channels in the hippocampus also undergo extensive C-terminal cleavage in response to NMDA receptor activation, which was blocked by calpain inhibitors (Hell et al., 1996). Calpains are activated by depolarization

(Roehm et al., 2008) and also require calcium, therefore it seems plausible that calpains could be responsible for Ca_V1 proteolysis. The 190 kD form of $Ca_V1.2$ also appears in uterine smooth muscle and its expression levels are regulated by hormones during pregnancy (Helguera et al., 2002).

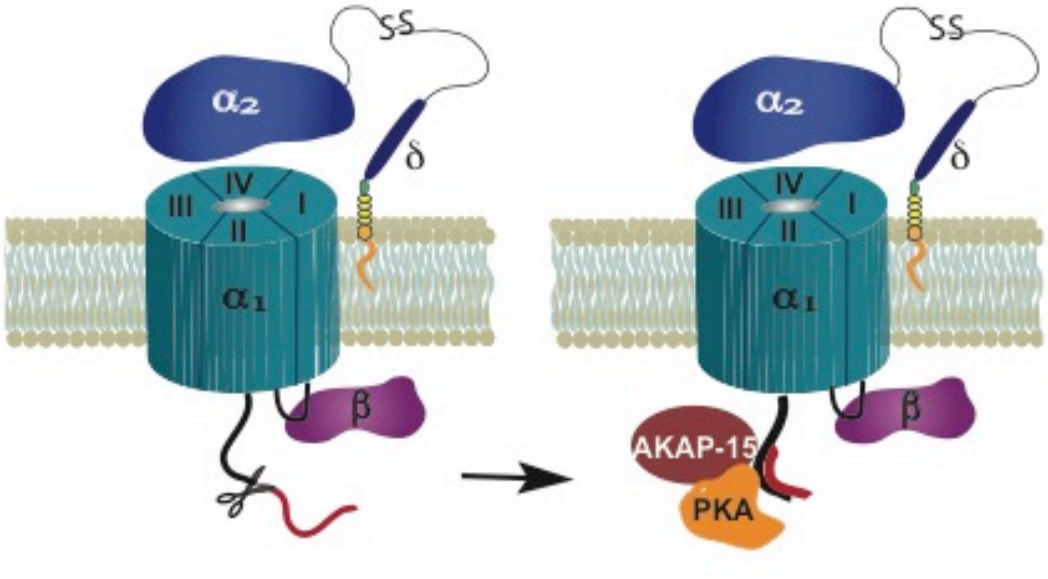

Figure 1.5 Proteolytic cleavage of the C-terminus in β-adrenergic regulation. The distal C-terminus (red) is cleaved from the channel and reassociates with the proximal C-terminus causing inhibition of the channel. AKAP-15 and PKA are docked close to this site. When activated by the β-adrenergic pathway, PKA phosphorylation dislodges the distal C-terminus, relieving the inhibition. (Modified from (Abele and Yang, 2012)).

In summary, under normal physiological conditions, Ca_V1 is proteolyzed by calpains and the cleaved distal C-terminus reassociates with the channel to inhibit its

function. AKAP-15 binds to the C-terminal fragment and recruits PKA to the scene (Figure 1.5). In a "fight or flight" scenario the β-adrenergic system is activated, in turn activating PKA. It is thought that PKA then phosphorylates the channel, which forces the distal C-terminus apart from the channel, releasing inhibition and greatly enhancing the activity of the channel. It is this mechanism that is believed to be responsible for excitation-contraction coupling.

1.4 Splice Variants and Truncated HVA VGCCs

The α_1 subunit is normally 190-260 kD depending on the subtype of channel, however many different forms of α_1 exist in both the natural and disease state. Some alternate forms of α_1 are developmentally regulated, others are tissue specific. Alternative splicing produces much smaller transcripts from sections of the channel to perform other functions, such as initiating transcription. Disease mutations cause early truncations resulting in nonfunctional channels that interfere with full-length channels. All of these channel fragments affect the excitability and health of the cell.

1.4.1 Natural Truncations of L-type Channels

Two different truncated $Ca_V1.2$ channels are produced by alternative splicing in the II-III loop (Wielowieyski et al., 2001). Both of these two-domain fragments contain domains I and II and a unique C-terminal tail. Another naturally occurring $Ca_V1.2$ channel truncated in domain II was found to act in a dominant-negative fashion, inhibiting full-length $Ca_V1.2$ current (Cox and Fromme, 2013). While proteolysis of

$Ca_V1.3$ has not been reported, a truncated form of the channel exists naturally that occurs through alternative splicing (Singh et al., 2008). The truncated version of $Ca_V1.3$ incorporates an alternative exon 42 that encodes a stop codon after the IQ domain in the C-terminus. This splice variant changes the gating and biophysical properties of the channel. Truncated $Ca_V1.3$ channels inactivate much faster, due mainly to enhanced CDI, and they activate at more negative potentials than full length $Ca_V1.3$. A developmentally regulated ascidian homologue of the L-type channel thought to originate from an alternative start site results in a three-domain channel beginning in the middle of domain II (Okagaki et al., 2001). While this channel did not prove to be functional, it strongly inhibited the full-length channel when coexpressed in *Xenopus* oocytes (Okagaki et al., 2001).

1.4.2 Ca_V1 Fragments as Transcription Factors

It has been well established that one of the many functions of L-type channels is to control gene expression, however it was always thought to occur through calcium-mediated activation of transcription factors or signaling proteins (Bean, 1989). Another mechanism for transcriptional activation that is mediated by L-type channels has been discovered; that the C-terminus of $Ca_V1.2$ is itself a transcription factor (Gomez-Ospina et al., 2006). The C-terminal fragment, termed CCAT (*c*alcium *c*hannel *a*ssociated *t*ranscriptional regulator), was found to translocate to the nucleus predominately in inhibitory neurons. CCAT is larger than the distal C-terminus fragment reported by the Catterall group; it appears as 75kD in western blots and comprises the last 503 amino acids of the C-terminus. Interestingly, the appearance of this fragment is

developmentally regulated, gradually becoming more prominent in the nucleus starting at age P1 through adulthood. Furthermore, CCAT translocates to the nucleus in an activity-dependent manner. When L-type channels were stimulated with either KCl or glutamate, less CCAT was detected in nuclei. The converse was also true whereby the presence of EDTA caused a significant increase in the amount of CCAT in the nucleus of neurons. While it was initially assumed the full-length channel is proteolyzed to cleave CCAT from the channel, further experiments identified an exonic promoter and alternative start site that produced the CCAT fragment (Gomez-Ospina et al., 2013). At the gene expression level, 16 mRNAs were found to be upregulated and 31 genes were downregulated in cells transfected with CCAT, and CCAT itself bound to the enhancer of the Connexin 3.1 gene. In addition, CCAT appeared to increase neurite growth in cerebellar granule neurons.

Another group reported the $Ca_V1.2$ C-terminus as exhibiting transcriptional properties, although they focused on cardio myocytes (Schroder et al., 2009). A 37kD C-terminal fragment was found to localize to the nucleus, interact with the $Ca_V1.2$ promoter, and ultimately act as a repressor, downregulating $Ca_V1.2$ levels. Schoder, et al. reported that the N-terminal truncated C-terminal fragment (1906-2171) showed the greatest nuclear presence, where that reported in Gomez-Ospina, et al. did not find this region necessary for nuclear translocation. This discrepancy could be due to the cell systems the experiments were performed in, or possibly the species and variant of $Ca_V1.2$ they were using.

1.4.3 P/Q-type channel truncations

Another of the HVA VGCCs also undergoes proteolysis on its C-terminus. Two sizes of the P/Q-type channel have been isolated, 220kD and 170kD (Kordasiewicz et al., 2006). The cleaved C-terminus translocates to the nucleus, however it is unclear whether it participates in transcription. It does appear to be linked to spinocerebellar ataxia type 6, where the expanded polyglutamine track in the C-terminus causes this fragment to become toxic to cells (Kordasiewicz et al., 2006; Kubodera et al., 2003). In addition, another short form of the channel, 95kD, has been isolated that comprises the N-terminus to the middle of the II-III linker (Scott et al., 1998). This short form of the P/Q channel interacts with β and is glycosylated. It has yet to be determined whether this 95 kD form of $Ca_V2.1$ is a splice variant or the result of posttranslational proteolysis, although a splice variant causing a truncation in the II-III linker has been reported (Soong et al., 2002).

Genetic channelopathies of the P/Q-type channel that result in a truncated channel cause a form of absence epilepsy and episodic ataxia in humans (Pietrobon, 2010). A case was reported whereby a child with absence seizures and ataxia had a frameshift mutation in the CACNA1A gene that gave rise to a truncated C-terminus and complete loss of function of the channel (Jouvenceau et al., 2001). The *leaner* (tg^{la}) mouse has a frameshift mutation that causes a truncated C-terminus and results in ataxia and absence seizures (Fletcher et al., 1996). Episodic ataxia type two (EA2) is a disorder caused by a truncated $Ca_V2.1$ channel that inhibits wild-type $Ca_V2.1$ channels (Jeng et al., 2008). This dominant-negative effect is caused by increased proteasomal degradation, whereby the mutant form interacts with the wild-type channel to promote ER retention and premature

degradation (Mezghrani et al., 2008). Truncated N-type channels were constructed to mimic these EA2 mutations (Raghib et al., 2001) and were found to induce the same dominant-negative effect through increased degradation of full-length channels (Page et al., 2010).

1.4.4 N-type channel Splice Variants

Two main N-type α_1 subunits have been identified, one 240kD and the other 210kD, and these are predominately located in dendrites (Westenbroek et al., 1992). At least six different splice variants of $Ca_V2.2$ are expressed in sympathetic ganglia cells, with two of the variants responsible for 60-85% of the channels. These variants differ in three areas of the coding region and one in the 3'UTR, with the majority of the variants expressed only differing in one residue (A415) (Lin et al., 1997). In individual DRG neurons, multiple isoforms of the N-type channel can be expressed. It was found that in a single neuron, $Ca_V2.2$ was expressed with and without exon e18a (Bell et al., 2004). N-type channels, as all other HVA channels, are alternatively spliced, allowing for differences in biophysical properties depending on the tissue, cell type, or time of development. For example, exon e18a located within the II-III loop of $Ca_V2.2$ is developmentally regulated, where it's expression steadily increases from birth through adulthood in rat superior cervical ganglia (Gray et al., 2007).

1.5 Thesis Introduction

Truncated channels formed by proteolysis, splicing, an alternative start site, or a frame-shift mutation are responsible for very specific physiological functions. C-terminal proteolysis of the cardiac $Ca_V1.2$ channel during β-adrenergic regulation exemplifies the importance of VGCC proteolysis in channel regulation in the fight or flight response. The C-terminal fragment of neuronal $Ca_V1.2$ illustrates the direct involvement of VGCCs in gene expression. Although proteolysis of Ca_v2 channels has not been extensively observed, many short forms of $Ca_V2.1$ and $Ca_V2.2$ are known to exist as a result of alternative splicing or disease-causing mutations. These truncated forms of Ca_V2 channels markedly change the function and expression of their full-length counterparts. Considering all the regions of α_1 that are necessary for proper regulation, it is no surprise that channels lacking those sites behave differently than full-length channels. These truncated VGCCs are relevant in overall cell excitability and cellular function.

Our lab has discovered a new form of $Ca_V1.2$ produced by proteolysis within the body of the α_1 subunit. This mid-channel proteolysis is regulated by the activity of the channel and results in fragment channels that remain on the plasma membrane. What is the physiological purpose of this type of regulation? For example, does it simply aid in degradation of the channel or do the products of mid-channel proteolysis have alternate functions? Furthermore, what effect does this have on the full-length channel's function? And lastly, what protease is involved in this regulation? Would the disruption of mid-channel proteolysis lead to disease or a dysfunction in calcium signaling? This thesis will attempt to answer these questions in the subsequent chapters.

In chapter 3 of this thesis, I focus on the functional effects mid-channel proteolysis exerts on $Ca_V1.2$. The channel behaves differently immediately after the channel is cut, as well as many hours after proteolysis occurs. Mid-channel proteolysis results in fragment channels that can remain on the plasma membrane. Chapter 4 serves to characterize the functions of these L-type fragments, as well as the effect they have on full-length channels. Chapter 5 identifies a potential protease involved in mid-channel proteolysis. Presenilin appears to cleave $Ca_V1.2$ through the coexpression of amyloid-β precursor protein (APP), reducing peak current and shifting biophysical properties. The involvement on these two proteins ties mid-channel proteolysis to Alzheimer's disease (AD), and APP mutants that lead to AD have a more extreme effect on $Ca_V1.2$ function.

Chapter 2

Materials & Methods

2.1 Molecular Biology

For two-electrode voltage clamp (TEVC) and inside-out macropatch recordings in *Xenopus* oocytes, cDNAs encoding various constructs were sub-cloned into a modified oocyte expression vector pGEMHE. Rat brain $Ca_v1.2$ (UniProt P22002-5) and rabbit $Ca_V2.1$ (GenBank accession number X57477) were used as controls. Rat skeletal muscle $\alpha_2\delta$ (GenBank accession number M21948) and rat brain β_3 (GenBank accession number M88751) were co-injected into all oocytes to allow for optimal α_1 expression. The P/Q channel carrying the TEVp cutting motif (ENLYFQG) at three different locations was engineered by using splice-by-overlap PCR. The ENLYFQG motif was inserted between G419-A420 in loop I-II, L1096-S1097 in loop II-III, and G1218-P1219 in loop II-III of $Ca_V2.1$. Tobacco etch virus protease (TEVp) (Addgene Plasmid 8827) was also cloned into pGEMHE for TEVC experiments. For the fragment channels, A1 (residues M1-D449), A2 (E450-L2143), B1 (M1-S866), B2 (M867-L2143), C1 (M1-W1216) and C2 (Y1217-L2143) were truncated using PCR into the backbone of $Ca_V1.2$. Human $Ca_V1.2$ (UniProt Q13936**)** was used in the Alzheimer's disease (AD) experiments (Chapter 5). Potential cut site mutants (hL_4xAla, hL_4xIle, and hL_4xVal) were made using splice-by-overlap PCR techniques on human $Ca_V1.2$. Neuronal isoform APP-695 (Entrez Gene 351) was used as the backbone to make APP mutants (A598T, A598V and V642F) using PCR.

For imaging in primary neurons, a modified rat $Ca_V1.2$ (UniProt P22002-5) was made by attaching GFP to the N-terminus and adding a HA tag to domain III (termed LGH3). LGH3 was inserted into a modified mammalian expression vector peGFP-C3. The thrombin and enterokinase triple mutant was made by splice-by-overlap PCR using LGH3 as the backbone. APPwt, APP_A598T and APP_A598V were subcloned into pcDNA3.1(-) for neuronal expression.

For co-immunoprecipitations (co-IP) and Westerns in HEK293_$\beta_3\alpha_2\delta$ cells relating to the fragment channels (Chapter 4), the full-length rat $Ca_V1.2$ channel and fragments were tagged with either HA or Flag on the N-terminus and cloned into pcDNA3.1(-). For co-IP and Westerns in HEK293_$\beta_3\alpha_2\delta$ cells relating to the AD experiments (Chapter 5), the human $Ca_V1.2$ channel and APP were tagged with either HA or Flag on the N-terminus and cloned into pcDNA3.1(-).

2.2 Protein Purification

For protein synthesis in *E.coli*, DE3 bacteria was used for cDNA transformation and protein expression. Tobacco etch virus protease (TEVp) (Addgene Plasmid 8827: pRK793) contains a MBP molecule for enhanced expression, a TEV recognition site (ENLYFQG) and a polyhistidine-tag at the N-terminus of TEV. Transformed DE3 bacteria were cultured at 37 ^oC until OD_{600} reached 0.6 and then induced at room temperature by 0.8 mM IPTG for 16 hours. Cells were collected at 1000 g for 10 minutes and resuspended in a lysis solution containing 50 mM Tris-HCl, 250 mM NaCl, 2.5% glycerol and 7 mM β- mercaptoethanol (pH 7.8). Resuspended bacteria were sonicated

with a Branson digital sonifier, followed by centrifugation at 10,000 g for 30 minutes. The supernatant was collected and incubated with Ni-NTA His•Bind beads (Novagen) in the presence of 30 mM imidazole at 4 °C for 1 hour. Proteins were eluted from the beads with 300 mM imidazole in the lysis solution. Proteins were concentrated and further purified using overnight dialysis to remove imidazole from the solution.

2.3 RNA Synthesis

cRNAs were transcribed from 6-8 μg template DNA that was linearized overnight and then purified with phenol (pH 8.0)/chloroform extraction and ethanol precipitation. An *in vitro* transcription reaction was set up for each RNA using the purified DNA template, 2 μL T7 RNA polymerase (100 units, New England Biolabs), 15 μL G(ppp)G RNA Cap structure analog (10 mM, New England Biolabs), 4 μL rNTP (100 mM, Roche), 5 μL DTT (100 mM, Pierce), 7.2 μL MgCl2 (50 mM), 4 μL T7 RNA polymerase transcription buffer (New England Biolabs), 1.5 μL RNAse Inhibitor (15 units, Invitrogen), and 10.8 μL DEPC treated water (Ambion). The transcription reaction proceeded at 37°C for 2.5-3 hours. The RNA product was then purified with phenol (pH 5.2)/chloroform extraction and ethanol precipitation and diluted to 1 μg/μL in DEPC-treated water. The concentration was determined using formaldehyde agarose gel electrophoresis and comparing to a RNA ladder (Invitrogen).

2.4 Oocyte Preparation & cRNA Injection

Ovarian lobes were obtained from adult *Xenopus* laevis (Xenopus I and Xenopus Express) under 0.5% tricaine anesthesia. Stages V–VI oocytes were prepared by treatment with 0.5 mg/mL collagenase A (Roche) for 1.5–2.5 h under 250 rpm shaking in OR2 solution (82.4 mM NaCl, 2.5 mM KCl, 1 mM $MgCl_2$, and 5 mM hepes (pH 7.6)), and then rinsed two times (15 min each) with ND96 solution (96 mM NaCl, 2.5 mM KCl, 1 mM $MgCl_2$, 5 mM hepes, 1.8 mM $CaCl_2$, 100 units/mL penicillin, and 100 μg/mL streptomycin (pH7.6)). Single defoliculated oocytes were individually selected. cRNAs were synthesized *in vitro*, and varying amounts (0.2–5 ng) were injected into selected oocytes in various combinations. Recordings were performed 3–5 d after injection.

2.5 Electrophysiology

For whole-oocyte recordings by TEVC, electrodes were filled with 3 mM KCl and had a resistance of 0.5–1 MΩ. The bath solution contained 10 mM BaCl2, 5 mM KCl, 60 mM tetra-ethyl ammonium hydroxide, 20 mM NaOH, and 5 mM HEPES (pH 7.4 with methane-sulfonic acid). To obtain I-V curves, the current was evoked every 2 sec by a +10 mV pulse for 60 ms from a holding potential of -80 mV. For inactivation curves, a prepulse of 10 mV was delivered before a 5 sec +10 pulse, followed by a 10 mV test pulse before a 55 sec recovery at -80 mV. All data were analyzed with Clampfit and were represented as mean ± SD.

For inside-out macropatch, electrodes had a diameter of 15-30 μm and a resistance of 0.2-0.4 MΩ when filled with a solution containing 45 mM $BaCl_2$, 80 mM KCl, 10 mM HEPES (pH 7.3 with KOH). The bath solution contained 125 mM CsCl, 4

mM NaCl, 10 mM HEPES, 10 mM EGTA (pH 7.3 with KOH). Cs^+ was included to reduce the influence of endogenous potassium channels. No PIP_2 or MgATP were added to avoid any interference on TEV protease activity. The purified TEV protease or its catalytically inactive mutant C151A was perfused in the bath solution for 2 min, followed by 1 min of wash. Recordings were obtained before protease application (0 min), and after wash (3 min). To construct activation curves, macroscopic currents were evoked from a holding potential of -80 mV by 5-ms depolarizations ranging from -40 mV to +100 mV in 20-mV increments at 2 s intervals. Tail currents were recorded by repolarization to -40 mV, regardless of the preceding test pulse, normalized by that after depolarization to +100 mV, and plotted against the test potentials. All data were analyzed with Clampfit and were represented as mean ± SD.

For the DAPT experiments, oocytes were treated with DAPT dissolved in ND96 media (50 μM final concentration) for 24-48 hours before recordings. Oocytes were stored at 18°C.

All experiments were performed at 22°C.

2.6 Rat Cortical Slices

Male Sprague-Dawley rats were purchased from Taconic Farms and housed in a controlled environment animal facility (stable temperature and regular light-dark cycle. Animals were anesthetized by injection of a mixture of ketamine (80 mg/kg in saline) and xylazine (8 mg/kg). Dissections were performed by removing the brain and immediately submerging it in a sucrose saline solution (27 mM $NaHCO_3$, 1.5 mM NaH_2PO_4, 2.55 mM

KCl, 222 mM sucrose) bubbling with 95% O_2 at 4°C. The cortices were then placed on a Vibratome stage (V-1500 sectioning system), and horizontal slices of 400 μm were obtained from each hemisphere while bubbling in ice-cold sucrose solution. Slices were transferred to a bubbled incubation chamber of 35-37°C, filled with artificial cerebrospinal fluid (ACF: 119 mM NaCl, 26 mM $NaHCO_3$, 1.25 mM NaH_2PO_4, 2.5 mM KCl, 15 mM glucose, 1 mM myo-inositol, 2 mM pyruvate, 0.4 mM ascorbic acid) and left there to recover for 15 minutes. After recovery, slices were split into treatment groups in the ACS solution, bubbling with 95% O_2 at room temperature. Treatments lasted for 20-30 minutes before slices were moved to an ACS solution on ice containing biotin (Pierce) to label surface proteins. For the rest of the procedure, all steps were performed on ice. After a 40 minute biotin treatment, a quenching solution was added and slices were collected. Slices were washed twice with ice cold 1x PBS containing protease inhibitor cocktail and stored at -80°C until further use. Tissues were homogenized and lysed using Pierce lysis buffer plus 1:50 protease inhibitor cocktail (Halt cocktail, Pierce) rotating at 4°C for 45-60 minutes. Samples were centrifuged to remove cell debris, and supernatant was incubated with neutravidin agarose bead slurry column (Pierce) for 90-120 minutes rotating at 4°C. Samples were then centrifuged and collected as "flow-through" samples presumed to contain all cytoplasmic proteins. The neutravidin agarose beads were then washed four times using Pierce wash buffer with 1:1000 protease inhibitor cocktail. Surface proteins were eluted using SDS with 53 mM DTT by rotating for 45-60 minutes at 37°C and collected by centrifugation. Samples were stored at -80°C until being further used.

2.7 HEK293 stable line creation and cell culture

The pIRES-eGFP vector (neomycin resistant) was modified so that it contained β_3 before the IRES sequence and $\alpha_2\delta$ in place of the GFP after the IRES sequence. This plasmid was then transiently transfected into HEK293 cells (detailed in 2.8). 16 hours post-transfection, the media was removed and new media (DMEM, 10% FBS, 1% Pen/Strep) containing 2mg/mL geneticin (Gibco) was added to the cells for selection. After one week, surviving cells were spilt and moved to a new plate and maintained with 1mg/mL geneticin. Expression of β_3 and $\alpha_2\delta$ was confirmed with Western blot (detailed in 2.11.)

Cells were maintained at 37°C in DMEM media supplemented with 10% FBS, 100 U/mL penicillin, 100 μg/mL streptomycin and 1mg/mL geneticin. When cells reached 85% confluency, they were rinsed using 1x PBS (Gibco) and then split using 0.5% trypsin-EDTA solution (Gibco).

2.8 Embryonic hippocampal neuron culture

Pregnant Sprague-Dawley rats were anesetized using the carbon dioxide chamber and embryos were quickly removed at age E17-E19. Embryos were rinsed with 70% ethanol and immediately placed in ice cold 1x Hank's buffer (Invitrogen) containing 5.54 mM glucose and supplemented with 1:200 penicillin and streptomycin (Sigma). The hippocampal dissection was performed in a laminar flow hood with embryo brains submerged in the ice cold 1x Hank's buffer. Once the hippocampi were isolated, they were incubated at 37°C for 15 minutes in 0.125% trypsin in Hank's buffer. They were

then washed three times with plating media (DMEM media (Gibco) supplemented with 10% fetal bovine serum (Hyclone) and 10% F-12 (Invitrogen)) to remove traces of trypsin. Hippocampi were triturated with polished glass pipettes, counted and plated on poly-D-lysine/laminin-coated (Sigma) glass coverslips or tissue treated petri dishes in plating media. 16h later and then every 3-4 days, the culture medium was replaced in a 1:1 ratio with neurobasal medium (Invitrogen) supplemented with B-27 (1:50) and 0.5 mM I-glutamax (Invitrogen). Neurons were kept in an incubator at 37°C in a 5% CO_2 humid atmosphere for up to 2 weeks.

2.9 Transfection

Hippocampal neurons were transfected between DIV10-13. Neurobasal media was removed and saved and 1-1.5 μg of DNA / 1μL Lipofectamine 2000 (Invitrogen) in 100 μl Opti-MEM (Invitrogen) was added for each 12 mm (diameter) coverslip. Neurons were then incubated at 37°C. After 40 minutes the DNA:lipofectamine solution was removed and the neurobasal media was returned to the plates. Neurons were allowed to recover for 36-48 hours post-transfection before prepping for western blot or imaging.

HEK 293 cells were transfected using Lipofectamine 2000 (Invitrogen) according to the manufacture's directions. 16 hours post-transfection, the DNA:lipofectamine solution was removed and fresh DMEM media was added. HEK 293 cells were processed 40-48 hours post-transfection.

2.10 Co-Immunoprecipitation

HEK 293 cells were collected 40-48 hours post-transfection. Cells were washed twice with PBS + 1:1000 protease inhibitor cocktail (Pierce) and then scraped in the same solution. Cells were centrifuged at 1000 g for 5 minutes and the pellet was lysed in lysis buffer (Pierce) with 1:50 protease inhibitors for 1 hour at 4°C while rotating. After vortexing the lysate was centrifuged at 10,000 g for 10 minutes to pellet cell debris. A portion of the supernatant was removed and set aside as "input" sample and the remainder was incubated with monoclonal anti-Flag (Clone M2) antibody coated affinity gel (Sigma) or monoclonal anti-HA (Clone HA-7) antibody coated affinity gel for 2 hours rotating at 4°C. Affinity gel was washed four times with TBS containing 250 mM NaCl and 1:1000 protease inhibitor cocktail (Pierce). Tagged proteins of interest were then eluted using the Flag (Sigma) or HA (Genscript) peptide dissolved in RIPA buffer (Sigma) according to manufactures' instructions. SDS was added to all samples and the samples were incubated at 37°C for 1 hour before being analyzed using SDS-PAGE or frozen at -80°C until further use.

2.11 Biotinylation of HEK293_$\beta_3\alpha_2\delta$ cells

Neurons and HEK 293 cells were biotinylated using the Surface Protein Isolation Kit (Pierce). Biotin was dissolved in cold PBS and cells were gently washed with cold PBS before adding the biotin mixture to the plates. Plates were then incubated at 4°C for 25-30 minutes with gentle shaking. Afterwards, a quenching solution (Pierce) was added for 5 minutes to stop the biotin reaction. Cells were washed twice with PBS + 1:1000 protease inhibitor cocktail (Pierce) and then scraped in the same solution. Cells were

centrifuged at 1000 g for 5 minutes and the pellet was lysed in lysis buffer (Pierce) with 1:50 protease inhibitors for 1 hour at 4°C while rotating. After vortexing, the lysate was centrifuged at 10,000 g for 10 minutes to pellet cell debris. The supernatants were removed and incubated with a neutravidin agarose bead slurry column (Pierce) by rotating for 2 h at 4°C to bind surface-biotinylated proteins, followed by 3-4 PBS washes in the presence of protease inhibitors (1:250) after whatever did not bind to the beads was collected (cytoplasmic proteins). The beads were finally incubated with SDS sample buffer supplemented with 53 mM DTT for 30-45 minutes at 37°C to elute biotinylated proteins, which were collected by centrifugation and analyzed by SDS-PAGE.

2.12 SDS-PAGE and Western Blot

For SDS-PAGE, samples were run in 6% acrylamide (BioRad) gels cast in the laboratory or 4-12% precast gradient gels (Invitrogen). Electrical transfer to PVDF membranes (BioRad) was performed in a standard 25 mM Tris, 192 mM glycine, pH~8.3 buffer supplemented with 0.002% SDS for 90 min at 90 V at 4°C. Methanol was not added to the transfer buffer to facilitate the transfer of large proteins. Membranes were blocked by gently shaking for 1 hour at room temperature with blocking buffer (Odyssey) and 1xPBS at a 1:1 ratio. Membranes were incubated with primary antibody overnight at 4°C. Membranes were washed in 1x PBS containing 0.2% Tween-20 (PBST). After four 5 minute PBST-washing steps, secondary antibody in blocking buffer/PBST was applied and membranes were shaken at room temperature for 1 hour. After four 5 minute washes with PBST, protein bands were visualized using enhanced chemiluminescence reagents (Pierce) on X-ray film (Kodak).

Primary antibodies were used at 1:500-1:1000 dilutions. Antibodies were as follows: rabbit polyclonal anti-$Ca_V1.2$ II-III loop (Sigma), rabbit polyclonal anti-HA (Sigma), mouse monoclonal anti-Flag M2 (Sigma), rabbit monoclonal anti-Na^+/K^+-ATPase (Abcam), rabbit polyclonal anti-APP Y188 (Abcam), rabbit monoclonal anti-presenilin 1 (Cell Signaling), and rabbit polyclonal anti-β-actin (Sigma). Secondary antibodies, goat anti-rabbit and goat anti-mouse (SantaCruz Biotechnologies) were used at 1:2000 dilution.

2.13 Immunofluorescent Staining and Confocal Microscopy

Immunofluorescence staining of hippocampal neurons was performed 24-36 hours post-transfection. The culture medium was removed and the transfected neurons grown on glass coverslips were briefly rinsed with PBS before being fixed in PBS supplemented with 2% paraformaldehyde-4% sucrose for 15 minutes at room temperature. Cells were washed briefly in PBS, then blocked in a non-permeabilizing (detergent-free) blocking buffer consisting of 0.5% fish gelatin and 10% goat serum in PBS for 1 hour at room temperature. To visualize surface HA tags, the coverslips were incubated with a primary antibody against HA (mouse monoclonal anti-HA, Covance) for 1 hour at room temperature in PBS containing 0.5% fish gelatin and 10% goat serum, then washed with PBS four times. The goat anti-mouse secondary antibody conjugated with the Alexa594 fluorophore (Invitrogen) was added to the coverslips for 1 hour at room temperature in the same buffer composition. The stained coverslips were finally washed four times with PBS and once with distilled water, then mounted on imaging slides using an anti-fade reagent (Biomeda).

Confocal imaging was performed using a spinning disc confocal microscope upgraded from an inverted Nikon Eclipse TE2000-S microscope. Confocal optics consisted of a spinning disc confocal scanner unit (CSU10, Yokogawa) rotating between 1200 and 2500 rpm and a CCD high resolution digital B/W ORCA-ER camera (Hamamatsu). Images were acquired using either a 100x or a 60x color-corrected objective lens (Nikon). The GFP (green) laser line used 491 nm and 520 nm as excitation and emission wavelengths, respectively. The Alexa594 (red) laser optical path consisted of a 561 nm excitation source and a 591 nm emission filter. Laser sources and equipment were from Spectral. Optical filters were sputter-coated to minimize chromatic aberration (Chromas). Confocal optical slice thickness (z-axis) was 300 nm in all cases. Confocal images for each fluorophore in double-labeling experiments were always acquired separately (sequential scans, every 300 nm) rather than simultaneously, to further minimize optical bleedthrough.

2.14 Data Analysis

For imaging, resulting images were processed using the Volocity (PerkinElmer) image analysis software package and MatLab. In ensemble %Frequency-above-threshold vs. NCI curves using data pooled from multiple neurons, the X-axis consisted of step thresholds used to bin the entire population of NCI values. Typically, a group of ~15 neurons produced ~150,000-200,000 voxels. In these cases, X-axis thresholds were a sequence of logarithmically spaced numbers generated by MatLab to represent values between 0.1 and 10. Y-axis data points from all the neurons in any given group were averaged and plotted as mean± SE.

For electrophysiology, all data were analyzed using Clampfit. Peak current was represented as mean ± SE. I-V and activation curves were generated after normalizing currents to peak current and represented as a percentage ± SE at various voltages. Inactivation curves were generated from dividing peak current at +10 mV test pulse by the peak current at +10 mV pre-pulse for each voltage and represented as a percentage ± SD.

Chapter 3

Functional Effect of Proteolysis of $Ca_V1.2$

THE BIOCHEMISTRY EXPERIMENTS LINKING MID-CHANNEL PROTEOLYSIS TO CHANNEL ACTIVITY WERE DONE BY IOANNIS MICHAILIDIS WITH ASSISTANCE PROVIDED BY KATHRYN ABELE HENCKELS. THE IMAGING AND AGING EXPERIMENTS WERE PERFORMED BY IOANNIS MICHAILIDIS . THE THROMBIN/ENTEROKINASE AND ALL FUNCTIONAL EXPERIMENTS WERE DONE BY KATHRYN ABELE HENCKELS. KEVIN ZHANG PARTIALLY CONTRIBUTED TO THE INSIDE-OUT MACROPATCH RECORDINGS AND GLYNIS GORDON ASSISTED WITH THE PRODUCTION OF THE TEV PROTEASE.

3. 1 INTRODUCTION

Voltage gated calcium channels (VGCCs) control many critical physiological processes, including hormone secretion, neurotransmitter release, cell migration, gene transcription, and muscle contraction (Catterall, 2000). In response to changes in voltage across the membrane, and under the regulation of many other proteins, these channels allow the heart to beat, the kidney to function, and neurons to communicate with one another. Many genetic diseases can be attributed to mutations in these channels, such as familial hemiplegic migraine (Pietrobon and Striessnig, 2003), long QT syndrome (Gargus, 2006), Timothy syndrome (Barrett and Tsien, 2008), and epilepsy (Zamponi et al., 2009). Also, VGCC dysfunction has been associated with Alzheimer's disease, Parkinson's disease (Mattson, 2007), and chronic pain (Snutch, 2005). Due to having such a diverse range of functions, VGCCs are regulated by many pathways and mechanisms.

Proteolysis as a regulatory mechanism has been reported for a variety of ion channels. Epithelial sodium channels are targeted by the protease furin, which cleaves a small section of the α_1 subunit, releasing an inhibitory segment and activating the channel (Kleyman et al., 2009). The AMPA receptor undergoes a C-terminal cleavage mediated by calpain which alters the channel's properties (Bi et al., 1996). The voltage gated Na^+ channel α_1 subunit is also proteolyzed by calpain (von Reyn et al., 2009) and its associated β_2 subunit is proteolyzed by β- and γ-secretase (Kim et al., 2005). Proteolysis of the L-type calcium channel as a form of regulation has also been reported. $Ca_V1.2$ is cleaved in the C-terminus and this distal C-terminal fragment then binds to the proximal C-terminus, still attached to α_1, to act as an autoinhibitor to the channel (Hulme

et al., 2006). Our lab has uncovered a new form of proteolysis of the L-type voltage gated calcium channel, $Ca_V1.2$, which is termed mid-channel proteolysis because it occurs within the body of the α_1 subunit.

3.2 RESULTS

3.2.1 Mid-channel proteolysis of $Ca_V1.2$

The $Ca_V1.2$ α_1 subunit has a predicted molecular weight of 190-240 kD. The α_1 subunit consists of four homologous domains, each containing six hydrophobic transmembrane segments, connected by intracellular loops and flanked by an intracellular N- and C-terminus. The three intracellular loops are referred to as the I-II loop, the II-III loop and the III-IV loop.

Mid-channel proteolysis was first discovered in biotinylated cortical slices from six-week-old rats. Western blots of surface proteins probed with an antibody against the II-III loop revealed two bands, one at the predicted 240 kD and one at 150 kD. This pattern was seen repeatedly with subsequent experiments. This 150 kD band has been previously observed (Gomez-Ospina et al., 2006; Sakurai et al., 1995; Scott et al., 1998; Westenbroek et al., 1995), but has yet to be explained. Our lab observed the 150 kD fragment so consistently that we decided to investigate it further.

Using antibodies from three regions of the channel; the N-terminus, the II-III loop and the C-terminus (Figure 1a) it could be determined which section of the channel the 150 kD band comprised. The 150 kD band was present with the II-III loop antibody (Figure 1b and 1c) and the C-terminus antibody (Figure 1d), and a ~90 kD band was

present with the N-terminus antibody (Figure 1e). This pattern of bands would only be produced if the channel was being cut within the II-III loop (Figure 1a). The other bands detected by the N- and C-terminal antibodies suggest that the channel is extensively proteolyzed. Moreover, these channel segments are found on the plasma membrane.

Unfortunately, there is no $Ca_V1.2$ knockout mouse available because deletion of $Ca_V1.2$ is embryonic lethal (Seisenberger et al., 2000), and therefore samples taken from a knockout cannot be used to confirm this band is calcium channel. However, since multiple $Ca_V1.2$ antibodies stained the 150 kD band, it is undoubtedly not an artifact. The 150 kD band was also sent for mass spectrometry analysis and was found to be L-type calcium channel. After confirming the 150 kD fragment is a smaller L-type calcium channel, the big question is why would this channel form exist?

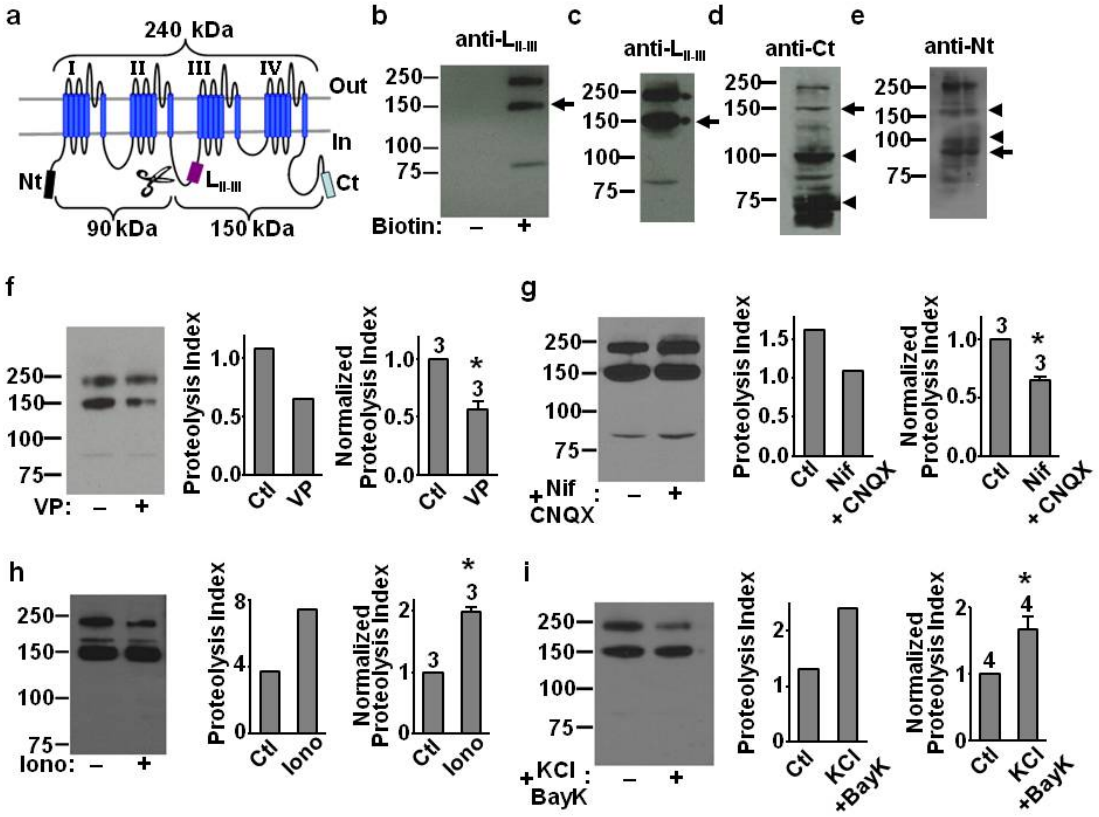

Figure 3.1 Mid-channel proteolysis of endogenous $Ca_v1.2$ in cortical neurons and its channel activity-dependent regulation. (a) Topology of $Ca_v1.2$ with epitope locations for three antibodies (anti-L_{II-III}, anti-Ct and anti-Nt) indicated and predicted molecular masses for full-length $Ca_v1.2$ and two fragment-channels generated by a presumed proteolytic cut (scissors). b, Western blot with anti-L_{II-III} of native $Ca_v1.2$ in surface-biotinylated and non-biotinylated cortical slices (from 6-week old rats), showing a 150-kDa band (arrow). (c-e) Western blot with anti-L_{II-III} (c), anti-Ct (d) or anti-Nt (e) of native $Ca_v1.2$ from the same sample of surface-biotinylated cortical slices. (f-i) Activity-dependent regulation of mid-channel proteolysis. Left: representative Western blot with anti-L_{II-III} of $Ca_v1.2$ in cortical slices treated with either vehicle (control) or the indicated reagent(s) before surface biotinylation: (f) verapamil (65 µM, 2 hr); (g) nifedipine (10 µM, 2 hr) and CNQX (21.5 µM, 2 hr); (h) ionomycin (3 µM, 45 min); (i) BayK8644 (14 µM, 40 min) and 65 mM KCl (40 min). Middle: bar graph depicting the proteolysis index (intensity ratio of 150-kDa/240-kDa band) for the representative gel. Right: summary graph showing data pooled from the indicated number of independent experiments. Data in bar graphs are represented as mean±s.e.m. and asterisks denote statistical differences, with $P<0.01$. Modified from (Michailidis IE, Abele-Henckels K, et al. Neuron. 2014. In Press).

3.2.2 Activity-dependent proteolysis of $Ca_V1.2$

Mid-channel proteolysis could occur as a way to regulate calcium influx. One method to test this hypothesis is to measure the ratio between the 150 kD and 240 kD bands in response to channel activity. Using densitometry, the proteolysis index was calculated for each sample. Rat cortical slices were treated with various L-type channel activators and inhibitors, biotinylated and then ran on Western blots. All experiments were done quickly at 4°C and in the presence of protease inhibitor cocktail to minimize sample preparation degradation.

When the channel was inhibited with application of the phenylalkylamine Verapamil, a L-type calcium channel blocker, mid-channel proteolysis decreased about 50% (Figure 3.1 f). The same effect was observed when the dihydropyridine Nifedipine, another L-type calcium channel blocker, was applied to cortical slices in the presence of CNQX, an AMPA receptor antagonist (Figure 3.1 g). These results demonstrate that when the channels are prevented from opening, either through direct inhibition or combined with lower cell excitability, mid-channel proteolysis is reduced. When a calcium channel ionophore, ionomycin, was added to neurons, forcing an influx of calcium into the cells, mid-channel proteolysis increased (Figure 3.1 h). The same effect was seen when neurons were treated with a combination of high KCl and BayK8644, a L-type channel agonist (Figure 3.1 i). Therefore, enhanced cell excitability, increased intracellular calcium and activation of L-type channels increase mid-channel proteolysis.

These results were also replicated in biotinylated, cultured hippocampal neurons. Mid-channel proteolysis appears to be a regulated event, since the channel is proteolyzed in response to channel activity. The increase in proteolysis in response to increased

channel activity hints that the purpose may be to down-regulate functional channels on the membrane. These results also rule out the 150 kD band being a product of sample preparation degradation, since that is not regulated and would happen in the processing of the samples and not during the drug treatment of the neurons.

3.2.3 Separation of the channel on the membrane

$Ca_V1.2$ channel fragments reside on the plasma membrane, but do they remain associated after proteolysis? One way to answer this question is to visualize the fragments using confocal microscopy. $Ca_V1.2$ was modified to include GFP on the N-terminus and a HA tag on an extracellular loop of Domain III, a construct called LGH3 (Figure 3.2 a). Using an anti-HA primary antibody and an Alexa-594 secondary antibody under non-permeabilized conditions, surface LGH3 could be visualized. Surface channels would appear red (HA staining) and green (GFP). Channels that had not yet reached the membrane would only appear green.

In most cases, red signal clustered with green signal, which is expected of intact surface channels where the red and green signals are on the same protein. Interestingly, there were many instances of red signal without green signal along dendrites (Figure 3.2 b and c). This indicated that domain III of the channel was dissociating from the N-terminal half of the channel on the membrane. In order to quantify this, an algorithm was developed that scanned each dendrite and detected any red "voxels", which are essentially objects made of pixels of similar intensity. For each voxel the intensity of green signal and red signal was measured and the red/green ratio was determined. This ratio was termed the non-colocalization index (NCI). A value of 1 represents

colocalization; for every red signal there is a green signal. A value greater than 1 represents a higher red signal than there is green signal, indicating separation of fragments and thus proteolysis. This measurement method was tested comparing two dendrites, and the dendrite with obvious red-only clusters (Segment y) had a right-shift in the NCI curve (Figure 3.2 d). NCI values were calculated for all dendrites of a neuron and then many neurons were averaged per treatment group. In an additional control test, the same batch of neurons transfected with LGH3 was split in two and the NCI was measured and averaged for each group. The NCI values for the two groups overlapped completely (Figure 3.2 e), validating the analysis method.

In western blots, several bands were observed with both the N- and C-terminal antibodies. One explanation for this pattern is that the channel is cleaved in several locations. If this is true, the NCI should increase as the HA tag is moved further away on the channel from GFP. Constructs were made with a HA tag on Domain I (LGH1) and on Domain II (LGH2) to compare to LGH3. As expected, the NCI decreased as the HA tag moved closer to GFP (Figure 3.2 f). This not only substantiates the analysis method, since separation of red and green should not happen when they are very close together, but also indicates the channel can be cleaved in multiple locations along the α_1 subunit.

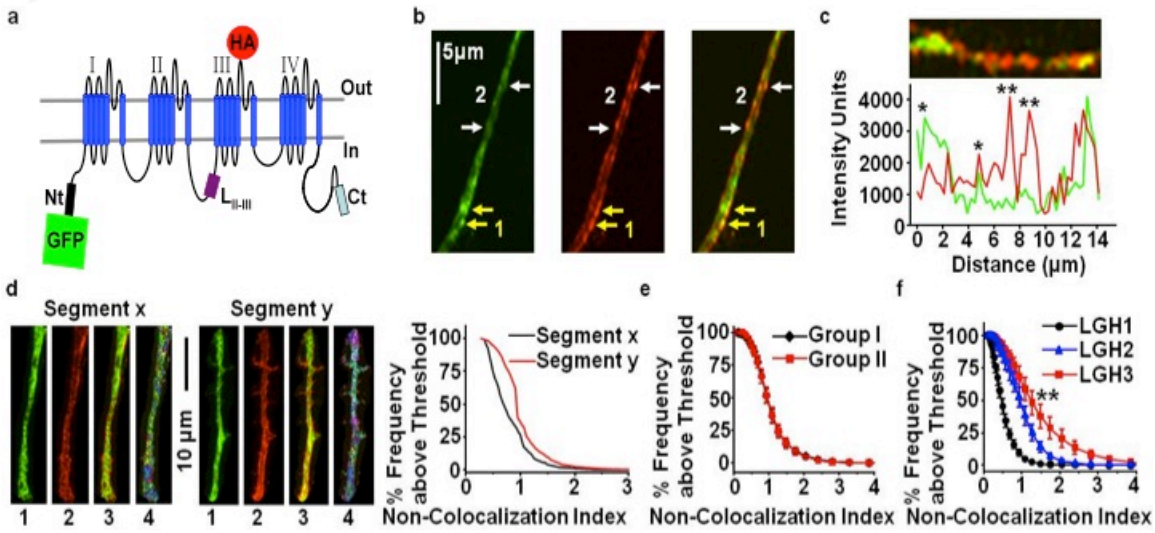

Figure 3.2 Visualization of mid-channel proteolysis of $Ca_v1.2$ in the plasma membrane of cultured hippocampal neurons. (a) LGH3 construct with a N-terminal GFP and a HA tag on an extracellular loop of Domain III. Antibody epitope locations are also indicated. (b) Confocal images of a representative dendritic segment of a neuron expressing LGH3. Left: surface and intracellular LGH3 indicated by GFP. Middle: surface LGH3 indicated by anti-HA+Alexa594 secondary antibodies. Right: overlay. Clusters of red/green colocalization and non-colocalization are marked by yellow and white arrows, respectively. (c) Fluorescence intensity profile (bottom) of a dendritic segment (top). Exemplar clusters of red/green colocalization and non-colocalization are marked by * and **, respectively. (d) Quantification of red/green colocalization in two dendritic segments displaying visually different extents of mid-channel proteolysis. Left and middle: images of GFP (lane 1), HA-Alexa594 (lane 2), overlay (lane 3) and the "voxels" selected according to our analysis protocol (lane 4). Right: cumulative distribution of the non-colocalization index (NCI) for the two selected dendritic segments. (e) Ensemble cumulative distribution of NCI from the dendrites of two randomly selected groups of neurons (n=15 each, same culture) expressing LGH3. (f) Cumulative distribution of NCI from the dendrites of neurons expressing LGH1 (n=23), LGH2 (n=15) and LGH3 (n=13). Taken from (Michailidis IE, Abele-Henckels K, et al. Neuron. 2014. In Press).

3.2.4 Age-dependent proteolysis of $Ca_V1.2$

L-type channel activity has been implicated in aging and aging diseases (Moyer et al., 1992; Thibault and Landfield, 1996; Thibault et al., 1998). Therefore, the extent of mid-channel proteolysis could vary depending on the age of the animal. To test this hypothesis, cortical slices were isolated from rats of various age groups (10 days, 6 weeks, 6 months and 16 months) and processed in parallel. Mid-channel proteolysis increased with the animals' age (Figure 3.2 a). While the 6-month-old and 16-month-old rats had less full-length $Ca_V1.2$ on the membrane than younger rats, there was a large increase in the ratio of the 150 kD band / 240 kD band, indicating increased mid-channel proteolysis. When 16-month-old rats were treated for 3-5 weeks with an oral dose of Verapamil, a L-type channel blocker, mid-channel proteolysis was slightly reduced (Figure 3.3 b), indicating that age-induced mid-channel proteolysis is partially reversible and dependent on channel activity.

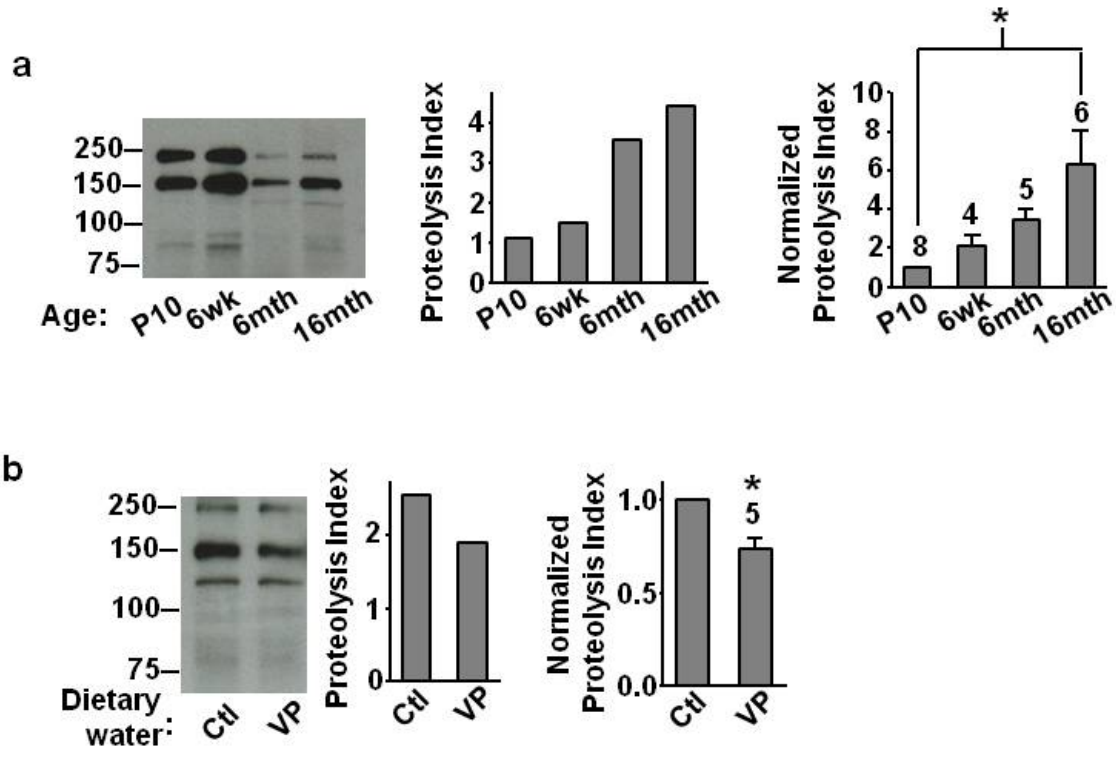

Figure 3.3 Mid-channel proteolysis is age-dependent and can be reversed *in vivo*. (a) Left: representative Western blot with anti-L_{II-III} of native $Ca_v1.2$ in surface-biotinylated rat cortical slices from the indicated age groups. Middle: proteolysis index for the representative gel. Right: summary graph showing data pooled from the indicated number of independent experiments. (b) Left: representative Western blot with anti-L_{II-III} of native $Ca_v1.2$ in surface-biotinylated cortical slices from 16-month old rats fed with water with or without verapamil for 3-5 weeks. Middle: proteolysis index for the representative gel. Right: summary graph showing data pooled from five independent experiments. Data in bar graphs are represented as mean±s.e.m. and asterisks denote statistical differences, with $P<0.01$. Taken from (Michailidis IE, Abele-Henckels K, et al. Neuron. 2014. In Press).

3.2.5 Identifying the protease site

Based on the molecular weights of the bands present in western blots, it was likely that the channel was being cut near or within the II-III loop. The first step to try and identify a protease was to run the channel sequence through PeptideCutter (ExPASy) to determine if any potential protease candidates cut in that region. The results included two proteases that potentially cut the channel in the II-III loop: enterokinase and thrombin. Enterokinase had potential cut sites in both the I-II loop (K490) and the II-III loop (K803), while thrombin only cut the channel once in the II-III loop (R888). All other proteases included in the results either cut the channel too many times or cut in the C-terminus, so those were excluded from mid-channel proteolysis candidates.

Using our confocal imaging method, we wanted to see whether mutating these "cut sites" would shift the NCI curve to the left, indicating less proteolysis than the wild-type channel. Each enterokinase and thrombin cleavage site was mutated by changing the consensus residues to glycines in LGH3. A triple mutant, where all three sites were mutated, was also made. This construct (TripMut) and wild-type LGH3 were transfected into rat hippocampal neurons. In case mid-channel proteolysis only occurs with increased channel activity, each group was also subjected to a 30 minute 65 mM KCl treatment 48 hours post-transfection. The neurons were then fixed, stained and imaged to see whether the triple mutation changed red-green separation.

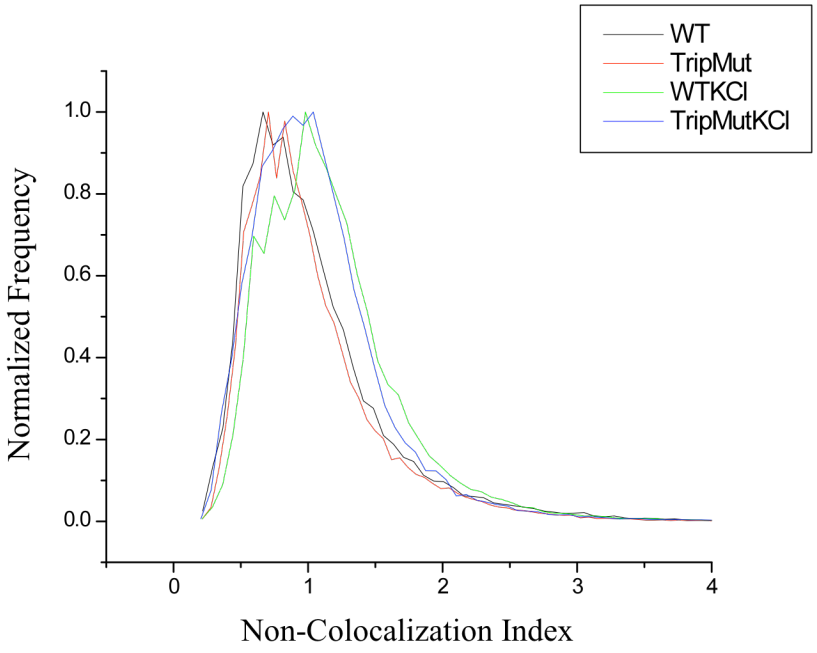

Figure 3.4 Thrombin and enterokinase are not the protease. Normalized distribution graph depicting red-green co-localization along dendrites of neurons expressing LGH3 (WT) or LGH3 with thrombin and enterokinase sites mutated (TripMut). Also shown are neurons treated with 65 mM KCl for 30 minutes before fixation. There is no change in the NCI between WT and TripMut.

There was no change between the wild-type channel and the triple mutant under normal conditions or when the channel was activated with KCl (Figure 3.4). The KCl treatment did shift the NCI curve to the right, as expected, but the triple mutation showed no difference compared to wild-type. Therefore, it appears that the mutated residues are not the cut sites involved in mid-channel proteolysis. Neither thrombin nor enterokinase is likely to be the protease.

3.2.6 Acute functional effect of mid-channel proteolysis

If the observed proteolysis occurs in response to channel activity, functional studies are necessary to demonstrate what effect that cleavage has on channel function. One way to investigate the acute functional effects of channel cleavage is to insert a protease site into the channel and, using inside-out macropatch, perfuse the protease while measuring current in real-time. In order to use this method effectively, the P/Q-type calcium channel must be used because it experiences less current run-down than L-type calcium channels.

An appropriate protease would be one that is highly specific, stable at room temperature, does not require calcium for activity, and does not naturally cut the channel. The tobacco etch virus protease (TEVp) meets these criteria, and because it is from a plant virus, it has very few mammalian targets. TEVp is a cysteine protease used often in protein purification experiments because it can be grown to a large scale in bacteria and purified and is catalytically active at a range of temperatures. Since inside-out macropatch recording measures all the effects the perfused protease has on the channel, other variables besides channel cleavage need to be controlled for, such as the protease binding to the channel. Therefore, a catalytically inactive TEVp was engineered to serve as a control since it presumably retains all wild-type properties except its ability to cut the channel.

TEVp is a small protein (27 kD) and therefore is more difficult to express in bacteria. To circumvent this problem, maltose binding protein (MBP) was tethered N-terminally to a TEVp containing a six histidine repeat with a TEVp cut site in between the two proteins. Once the protein is translated in DE3 cells, TEVp cuts itself from MBP

and the 27 kD protease can be purified using nickel beads. The catalytically inactive TEVp (TEVp_mut) was made by mutating cysteine 151 to an alanine (C151A). This mutant TEVp is unable to cut itself from MBP (42 kD), and therefore is a ~70 kD protein when purified with nickel beads (Figure 3.5 a). In order to remove the MBP, active TEVp without a His tag was incubated with the TEVp_mut overnight at 4°C and TEVp_mut was subsequently purified using nickel beads and concentrated.

TEVp recognizes the sequence ENLYFQG and cuts between the Q and G. I inserted the TEVp recognition sequence site once in the I-II loop and twice in the II-III loop of $Ca_V2.1$ (Figure 3.5 b) using PCR mutagenesis. Three sites were added to increase the likelihood that a cut site is accessible to the protease. Four days following microinjection of cRNA into *Xenopus* oocytes, inside out macropatch recording was performed. The current was recorded from a patch until a baseline was reached and then the protease was perfused over the cytoplasmic side of the patch while the current was being recorded. After 2 minutes, the patch was perfused with the control bath solution to measure if the protease effect was reversible. This method was tested with trypsin as a positive control, since trypsin cuts the channel hundreds of times, and the current was quickly and irreversibly abolished after trypsin perfusion. Before the experiment, I also confirmed that TEVp was functional by incubating TEVp with its substrate for five minutes and using SDS-PAGE to confirm that the substrate was cut.

When TEVp_wt was perfused over the wild-type PQ channel containing no TEVp cut sites, there was no observable effect on channel current. When the catalytically inactive TEVp (TEVp_mut) was perfused over the PQ channel containing three TEVp cut sites (PQ_tev), no effect was seen on the current. However, when the TEVp_wt was

perfused over the mutant channel (PQ_mut), an irreversible left shift was seen in the activation curve (Figure 3.5 c). The channel was still functional, however there was an immediate change in gating properties. The channel may have remained functional after being cut because the two halves were held in close proximity on the membrane.

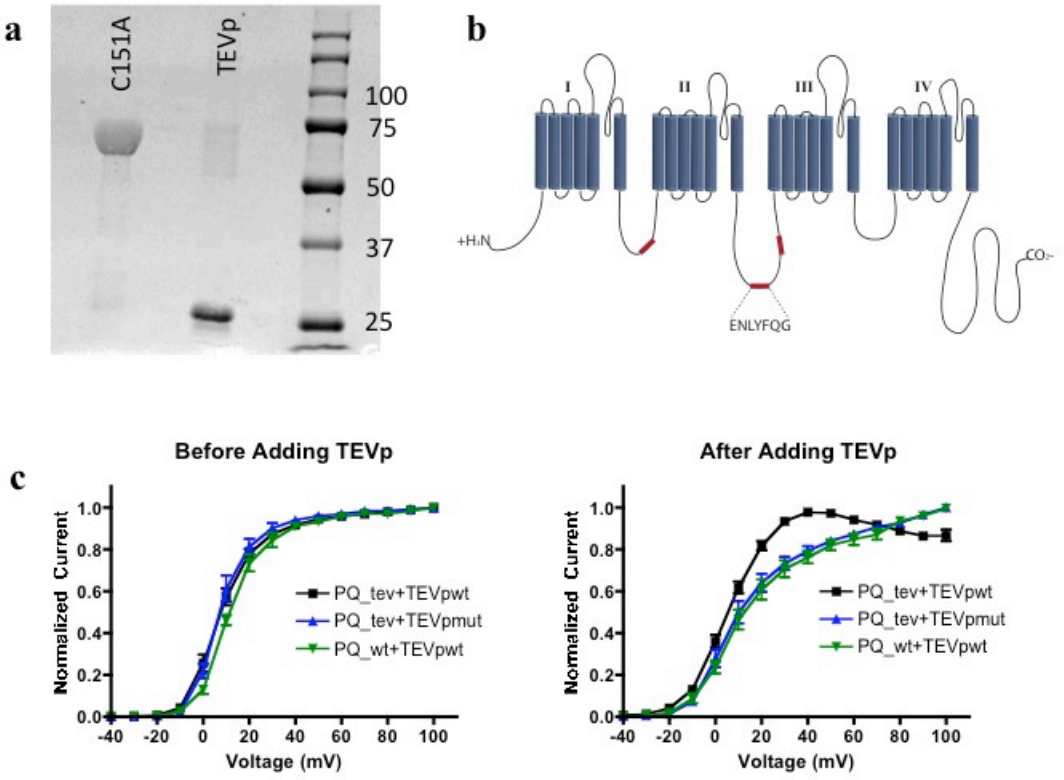

Figure 3.5 Acute functional effect of mid-channel proteolysis. (a) Western blot stained with anti-TEVp primary antibody to show catalytically inactive (TEVp C151A) and WT TEVp after purification with nickel beads. (b) P/Q channel with three TEV recognition sites construct (PQ_tev). (c) Current was recorded at +10 mV before and after addition of protease. A shift in the activation curve was seen only when active, TEVpwt was added to patches expressing PQ_tev. Catalytically inactive TEV (TEVpmut) and PQ_wt channels exhibited no change in current. N>7. Error bars represent ±SE.

3.2.7 Long-term functional effect of mid-channel proteolysis

After deciphering the immediate effect of proteolysis, I wanted to test the effect on a longer time scale. What happens to channel function hours after the channel is cut? I made wild-type TEVp RNA and injected into *Xenopus* oocytes along with wild-type PQ channel or the TEVp mutant PQ channel. All oocytes were also injected with $\alpha_2\delta$ and β_3. Recordings were done 4 or 5 days after injection to allow for sufficient time for protein expression. This should allow the cleaved channel time to separate on the membrane, which would be more relevant to what we observed *in vivo*. Wild-type PQ channel showed no change in current when TEVp was co-expressed (Figure 3.6). Without TEVp present, PQ_mut had current that was similar to PQ_wt, although the peak amplitude was slightly smaller (Figure 3.6). However, when PQ_mut was expressed with TEVp, the current was dramatically reduced (Figure 3.6). These data suggest that the long-term effect of mid-channel proteolysis is decreased channel function and down-regulated calcium current.

The long-term effect of proteolysis appears to be a reduction rather than a total abolishment of current. Is the residual current produced because not all of the channels are proteolyzed or because proteolyzed channels remain functional? To answer this question, I examined whether two complementary "fragment channels" can still form a functional channel. *Xenopus* oocytes expressing a truncated $Ca_V1.2$ containing either domains I-II or domains III-IV (Figure 3.7 a) were evaluated by TEVC. When the fragment channels were coexpressed, currents were approximately 60% of full-length $Ca_V1.2$ (FL) currents (Figure 3.7 b). When expressed alone they were completely nonfunctional (Figure 3.7 b). $Ca_V\beta$ binds to the AID in the I-II loop and traffics the

channel to the surface, therefore both fragment channels most likely assemble together prior to reaching the membrane. No dominant-negative effect on peak current amplitude was seen when one fragment channel was expressed along with the full-length channel (Figure 3.7 b), contrary to what as has been reported with N-type channels (Raghib et al., 2001).

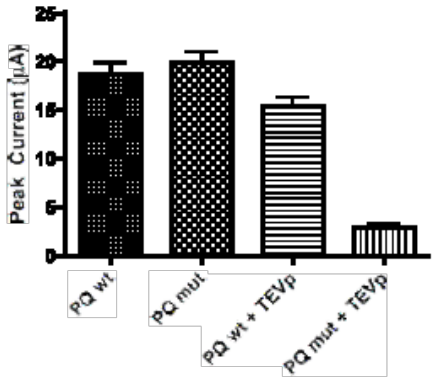

Figure 3.6 Long-term functional effect of mid-channel proteolysis. Comparison of peak current recorded at +10 mV by TEVC in oocytes expressing the indicated constructs with or without co-expression of TEV protease. Currents were normalized by the WT response. N > 10 for each group. Error bars represent ±SE. Expression of TEV protease had no effect on WT channels but did decrease the current of the mutated channel.

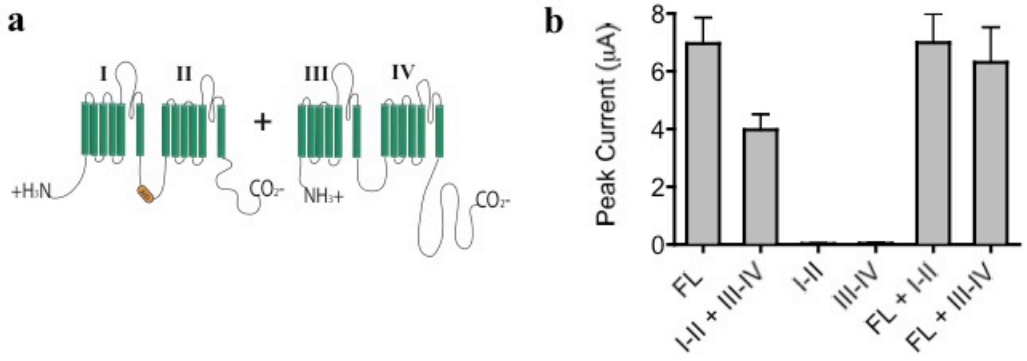

Figure 3.7 Fragment channels are functional when coexpressed. Two-electrode voltage clamp experiments recorded at +10mV on fragment channel constructs expressed in *Xenopus* laevis oocytes. (a) Fragment channel construct. (B) Peak current amplitude of full-length $Ca_V1.2$ (FL), when fragment pairs are co-expressed (I-II + III-IV), when fragments are expressed alone, and when each fragment is co-expressed with the full-length $Ca_V1.2$. N>10 for all groups.

3.3 DISCUSSION

3.3.1 The importance of L-type mid-channel proteolysis

The L-type voltage-gated calcium channel, $Ca_V1.2$, plays an important role in many cellular functions. Calcium influx through the channel not only changes cell excitability (Mahapatra et al., 2012), but activates various signaling cascades eventually causing a change in gene expression (Ma et al., 2012). Therefore, these channels have to be tightly regulated by a multitude of mechanisms, some redundant, to ensure that there is an optimal intracellular calcium concentration. Our lab has uncovered a new form of regulation of $Ca_V1.2$, termed mid-channel proteolysis, which serves to down-regulate calcium influx through the proteolysis of the α_1 subunit. This is different than the C-terminal proteolysis that occurs with 80% of $Ca_V1.2$ channels in the heart (Hulme et al., 2006). Our lab has shown that mid-channel proteolysis is dependent on the activity of the channel and the age of the animal. I have shown that the acute effect of the channel being cut is an immediate change in gating properties. The resultant "fragment channels" can remain on the membrane and associate to form functional channels. Perhaps many different forms of $Ca_V1.2$ naturally reside on the membrane and together are responsible for the total $Ca_V1.2$ current.

3.3.2 Identifying the protease and cut site

While thrombin and enterokinase were ruled out as potential proteases, many other proteases were considered. Due to mid-channel proteolysis being correlated to age, proteases involved in Alzheimer's disease were prime candidates. Many experiments

were done, as described in Chapter 5, to investigate the role γ-secretase plays in $Ca_V1.2$ proteolysis. While γ-secretase activity does have an effect on $Ca_V1.2$ current (Chapter 5, Figure 5.6), it is still unclear whether this is due to directly cutting the channel or through an indirect mechanism. Another viable candidate is calpain, a calcium activated protease assumed to be involved in the C-terminal proteolysis of $Ca_V1.2$ (Hell et al., 1996; Hulme et al., 2006). Applying a cocktail of calpain inhibitors to neurons expressing LGH3 resulted in a significant decrease in mid-channel proteolysis (Appendix, Figure 3a and b), however it did not abolish proteolysis completely and therefore other proteases are most likely involved. The ubiquitin-proteasome system, which is involved in degradation of proteins (Hershko and Ciechanover, 1998), might also be involved. A cocktail of ubiquitin inhibitors was added to neurons expressing LGH3 and resulted in a decrease in mid-channel proteolysis (Appendix, Figure 3c), as did mutating a putative ubiquitin site on the channel itself (Appendix, Figure 3d). PEST sequences are also involved in the ubiquitin-proteasome system, signaling the protein for degradation (Rechsteiner and Rogers, 1996). Two PEST sequences on the channel (Catalucci et al., 2009) were mutated, and one mutation (PEST1) practically abolished mid-channel proteolysis (Appendix, Figure 3). The exact cut site on the channel has yet to be identified and other potential proteases are likely to be involved.

3.3.3 Functional effects of mid-channel proteolysis

The inside-out macropatch experiments allowed me to observe in real-time the immediate effect on the channel being cut. It is not surprising that the channel was still functional after proteolysis, given the time scale of the measurements. The channel is a

properly formed tetramer held in place by non-covalent interactions with itself and the lipids in the plasma membrane. A simple nick of a cytoplasmic loop would not cause the channel to immediately dissociate, however it would have an effect on gating, which was observed (Figure 3.5 c). It seems reasonable that over a longer time scale the cut channel could separate, possibly by internalization or movement of one fragment within the membrane. These new fragment channels could therefore remain on the membrane without being associated with its partner. On this longer time scale you would expect a decrease in overall current, since upon separation, fragments cannot form a functional pore. This was seen in the TEVC experiment when TEVp was co-expressed with PQ_tev (Figure 3.6). One caveat of this experiment is that it does not reflect what occurs physiologically. TEVp is being constitutively over-expressed and is not cutting the channel in the regulated manner that mid-channel proteolysis occurs. Another caveat is that I was unable to control for where the channels were cut. The channel could be cut in the ER before surfacing or at the plasma membrane. A Western done by a colleague in the lab showed that these fragments are present on the plasma membrane after being cut by TEVp (Appendix, Figure 5). The final experiment described in this chapter proved that fragment channels are able to associate with one another and traffic together to the plasma membrane (Figure 3.7).

3.3.4 Fragment channels are functional

My finding that the two fragment channels can together form a functional channel on the membrane opens up many more questions. Do they traffic together to the plasma membrane? Is their reduced current a product of decreased surface expression, or is their

functionality impaired because they are separate proteins? Do they exhibit distinct biophysical properties? It does not appear that full-length channel current amplitude is affected by the presence of a fragment channel, however there could still be an impact on the full-length channel's gating properties. Only one set of fragment channels was tested here, however the channel can also be cut in other loops. It would therefore be interesting to evaluate the behavior of other fragment pairs. All of these questions will be addressed in the following chapter.

Chapter 4

Functional Characterization of $Ca_V1.2$ Fragment Channels

ALL OF THE EXPERIMENTS IN THE FOLLOWING CHAPTER WERE COMPLETELD BY KATHRYN ABELE HENCKELS.

4.1 INTRODUCTION

The α_1 subunit of voltage gated calcium channels (VGCCs) has four homologous domains, each containing six hydrophobic transmembrane segments, connected by intracellular loops and flanked by an intracellular N- and C-terminus (Catterall, 2000). The four domains come together in the membrane to form the pore that allows for Ca^{2+} influx. The β subunit binds to the I-II loop of α_1 and is necessary for surface expression (Buraei and Yang, 2010). It has been shown that $Ca_V\beta$ masks an ER retention signal in the I-II loop to allow α_1 to traffic to the membrane (Bichet et al., 2000), however there is also evidence that it protects α_1 from proteasomal degradation once it has left the ER (Waithe et al., 2011). The N- and C-termini are also very important in channel function, as both contribute to channel gating. Both the N- and C-terminus bind calmodulin, a calcium sensor that is responsible for calcium-dependent inactivation (CDI) and calcium-dependent facilitation (CDF) of the channel (Ben Johny et al., 2013). The C-terminus has also been recently associated with anchoring the channel to the plasma membrane through interactions with α-actinin (Hall et al., 2013).

The α_1 subunit can be extensively spliced (Lipscombe et al., 2013), and splice variants have been discovered that only contain partial α_1 subunits (Okagaki et al., 2001; Wielowieyski et al., 2001), which raises the possibility that VGCCs can form functional channels out of smaller α_1 fragments. This is not such a farfetched concept, since voltage-gated potassium channels are proteins containing six transmembrane domains that form a tetramer in the plasma membrane to conduct potassium (MacKinnon, 2003). There are also many naturally occurring disease-causing mutations that result in truncated

α_1 subunits (Pietrobon, 2010). For example, episodic ataxia Type-2 mutants cause truncated $Ca_V2.1$ channels and act in a dominant-negative manner with wild-type $Ca_V2.1$ channels by causing their retention in the ER (Jeng et al., 2008). A naturally occurring $Ca_V1.2$ α_1 subunit truncated in domain II was found to act in a dominant-negative fashion inhibiting full-length $Ca_V1.2$ current (Cox and Fromme, 2013).

N-type fragment channels reflecting a channel cut in the II-III loop were found to form functional channels with no differences in gating properties compared to full-length $Ca_V2.2$ (Raghib et al., 2001). Both fragments caused a decrease in current amplitude when coexpressed with full-length $Ca_V2.2$ and the fragment containing domain I was found to inhibit surface expression of $Ca_V2.2$ by interfering with channel synthesis (Raghib et al., 2001). This occurs when the fragment channel containing the N-terminus (Page et al., 2010) binds to $Ca_V2.2$ and initiates the unfolded protein response in the ER causing immediate protein degradation (Page et al., 2004). These are not naturally occurring fragment channels however, but they do provide insights into how truncated disease mutants can exert their dominant-negative effects on wild-type channels.

Mid-channel proteolysis of $Ca_V1.2$ produces fragment channels that remain on the plasma membrane for an unknown time and function. They may themselves form functional channels, although for reasons stated above, they would have to combine to include all four domains and both termini. They may also exert an effect on other full-length $Ca_V1.2$ channels on the membrane that have not yet been cleaved. Since it is still unclear where mid-channel proteolysis occurs in the cell, fragment channels could be created before reaching the plasma membrane and bind to full-length channels to influence trafficking and degradation. In this chapter, I investigate whether fragment

channels formed from cleavage of $Ca_V1.2$ in the I-II loop, II-III loop and III-IV loop are functional. I also evaluate whether they have distinct biophysical properties and if they can form functional channels with non-complimentary pairs. Their ability to associate with and influence the function of full-length $Ca_V1.2$ is also assessed.

4.2 RESULTS

4.2.1 Fragment channels are functional as complementary pairs

When $Ca_V1.2$ is split into two fragments, these fragment channels can still function if they are properly paired, albeit at less capacity than full-length $Ca_V1.2$ ($Ca_V1.2$_FL). This was shown with fragments resulting from a cut in the II-III loop (Chapter 3, Figure 3.7), however the channel can be cut in multiple places along the α_1 subunit (Chapter 3, Figure 3.2 f). Therefore, I decided to make sets of fragment channels reflecting proteolysis in the I-II loop (A1 + A2), the II-III loop (B1 + B2), and the III-IV loop (C1 + C2) (Figure 4.1 a). All three pairs of fragment channels were injected into *Xenopus* oocytes along with β_3 and $\alpha_2\delta$ and peak current was measured using TEVC to evaluate fragment channel function. Peak current was measured at + 10 mV and compared to the $Ca_V1.2$_FL current levels. When expressed along with their complimentary fragment, fragment channel pairs produced current that averaged ~40% of $Ca_V1.2$_FL current (Figure 4.1 b). This indicates that all three pairs of fragment channels can properly pair together on the plasma membrane and function in response to membrane depolarization. When these fragments were expressed alone, with β_3 and $\alpha_2\delta$ but without their complimentary fragments, they were non-functional (Figure 4.1 c). This result clearly shows that in order for the channel to produce current, four domains have to be present to form the pore and the N- and C-termini are critical for channel function. However, do the pairs have to be properly matched? What if there were *five* domains, a N-terminus and a C-terminus present? In most cases, when fragments were paired with a non-complimentary fragment they were non-functional (Figure 4.1 d).

However, fragments C1 and B2 did produce a small amount of current when paired, demonstrating that an extra domain, while impeding proper function, can in some cases be pushed out of the way so that a pore can form (Figure 4.1 d). The A1 + A2 pair exhibited lower currents than previously, and after repeated attempts I could still not find a batch of oocytes that produced 40% full-length current with A1 + A2. Also, B1 + B2 exhibited higher currents than usual in these oocyte batches. This could have been due to the quality of the injected RNA or differences in translation machinery for these particular batches of oocytes.

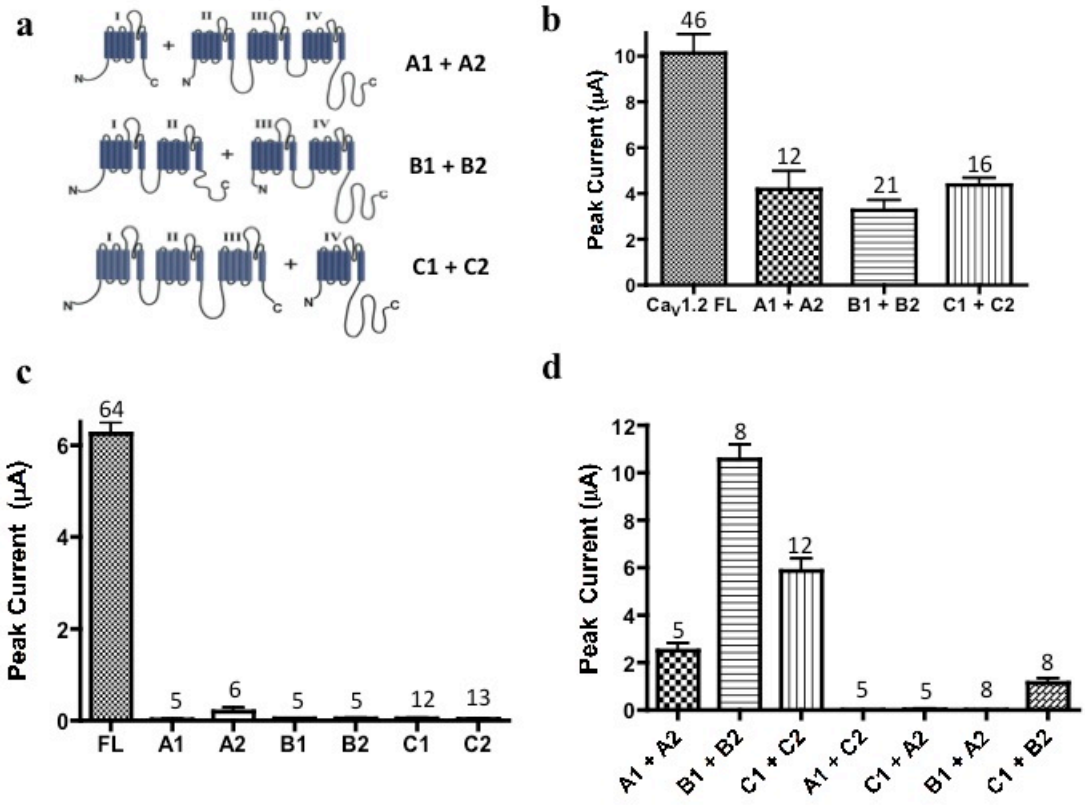

Figure 4.1 Fragment channels are functional when properly paired. (a) Schematic of the three sets of fragment channels cut in the I-II loop (A1 + A2), the II-III loop (B1 + B2) or the III-IV loop (C1 + C2). (b) Peak whole-cell currents recorded from oocytes at -10 mV to 0 mV expressing the full-length channel (Ca$_V$1.2 FL) or indicated fragment pairs. (c) Peak whole-cell currents recorded from oocytes at -10 mV to 0 mV expressing the full-length channel (FL) or indicated fragments without their complementary pair. (d) Peak whole-cell currents recorded from oocytes at - 0 mV expressing the indicated fragment pairs. Fragments paired with their complementary partner produced current, while fragments paired with a non-complimentary fragment produced little to no current. Error bars for all graphs reflect ±SE and the numbers above each bar represent the N.

4.2.2 Fragment channels have different biophysical properties

All three fragment pairs have been found to be functional, but do they display differences in gating? Fragment channels were injected into *Xenopus* oocytes along with β_3 and $\alpha_2\delta$ and the current-voltage relationship was determined by recording the peak Ba^{2+} current at a set applied voltage ranging from -50 mV to +60 mV. The current from each voltage was normalized to the peak current that occurred; -10 mV for $Ca_V1.2$_FL and 0 mV for each of the fragment channel pairs. All three fragment channel pairs displayed the same +10 mV shift in their current-voltage relationship (Figure 4.2 a). This suggests that the two halves of the channel being disconnected makes the channel slightly harder to open since a higher depolarization is needed for the channel to exhibit peak current influx.

The same fragment pairs were tested for their inactivation properties to see if the fragments had difficulty recovering from voltage-dependent inactivation. A pre-pulse of +10 mV was applied before a voltage between -50 mV and +30 mV was applied for 5 sec, which was followed by a test pulse of +10 mV. Again all three fragment channel pairs displayed the same inactivation profile, one that was shifted +10 mV from the $Ca_V1.2$_FL channel (Figure 4.2 b). This implies that the fragments have decreased inactivation compared to the full-length channel.

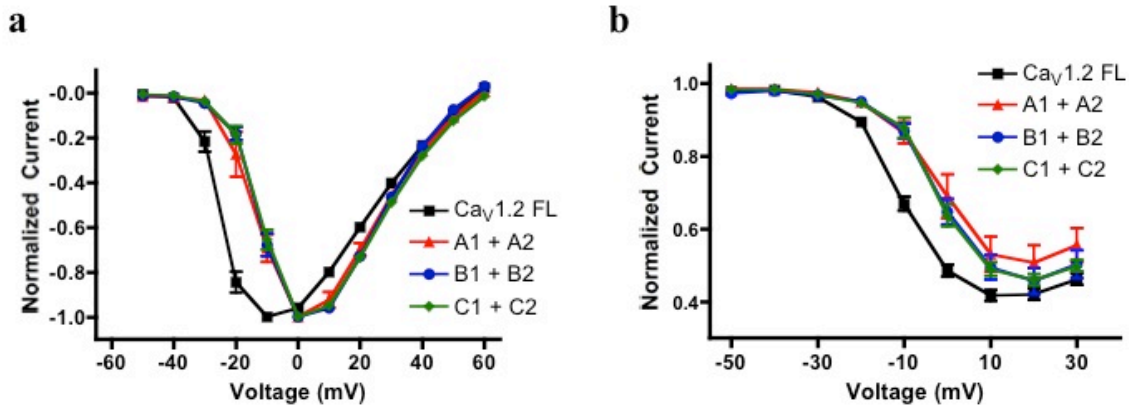

Figure 4.2 Fragment channels have different biophysical properties than $Ca_V1.2$. (a) The current-voltage relationship of full-length $Ca_V1.2$ (black, ■, N = 45) compared to fragments A1 + A2 (red, Δ, N = 12), B1 + B2 (blue, O, N = 15) and C1 + C2 (green, ◆, N = 15). (b) Inactivation curve of full-length $Ca_V1.2$ (black, ■, N = 29) compared to fragments A1 + A2 (red, Δ, N = 6), B1 + B2 (blue, O, N = 18) and C1 + C2 (green, ◆, N = 14). Error bars for both graphs reflect ±SE.

4.2.3 Surface expression of fragment channels

The fragment channels, while functional, have smaller currents compared to $Ca_V1.2$_FL. Is this due to the inherent nature of the two channel segments not being connected, or is surface expression an issue due to inadequate trafficking? One way to determine this is to look at the overall surface expression of the fragments compared to the surface expression of the full-length channel. This can be done using biotinylation and separating surface proteins from cytoplasmic proteins using streptavidin beads. Unfortunately, the oocytes membranes became too unhealthy after shaking during a 45-minute incubation with biotin. For this reason, another model system would have to be used.

HEK 293 cells do not endogenously express $Ca_V1.2$, and therefore make for a good model system to examine surface expression of $Ca_V1.2$ and the fragment channels. However, in order for $Ca_V1.2$ to traffic to the membrane efficiently and function properly, $Ca_V\beta$ and $Ca_V\alpha_2\delta$ also have to be expressed. Three to four different proteins (especially when two of them are as large as α_1 and $\alpha_2\delta$) are too difficult to simultaneously transfect. Therefore, making a stable line constitutively expressing β_3 and $\alpha_2\delta$ was the best option. I modified a pIRES vector so that upstream of the IRIS sequence was the β_3 gene and downstream was the $\alpha_2\delta$ gene. Whatever is upstream of IRES is translated at a higher rate than what comes after IRES and $\alpha_2\delta$, while important for $Ca_V\alpha_1$ function, is not as critical as β_3. HEK 293 cells were transfected with this construct and selected using geneticin (G418). This stable line (HEK293_$\beta3\alpha2\delta$) was now ready for transfection followed by biotinylation.

To be able to distinguish one fragment channel from the other, I decided to use two different tags. The fragment containing the N-terminus had a Flag-tag and the fragment comprising the C-terminus had a HA-tag. Both complimentary fragment channels were transfected together to replicate the condition that fragments were recorded from. As controls, I used LGH3, because it contained a HA tag, and a Flag-tagged $Ca_V1.2$. Comparing the amount of surface protein to the cytoplasmic protein, and then comparing that to the control allows for an estimate on the trafficking ability of the fragment channels. B1 + B2 and C1 + C2 seemed to have equal surface expression compared to the controls (Figure 4.3). Interestingly, A1 + A2 appeared to have slightly greater surface expression than the controls (Figure 4.3), which is contrary to the electrophysiology experiments where A1 + A2 had much less current that the full-length

channel and usually less current than the other fragment pairs. For the HA-tagged channels there seemed to be much less surface expression overall, including with the control LGH3, but this is most likely due to the antibody staining. This experiment does not allow for quantification due to the quality of the Western blots, but it does demonstrate that the surface expression of fragment channels is comparable to full-length $Ca_V1.2$.

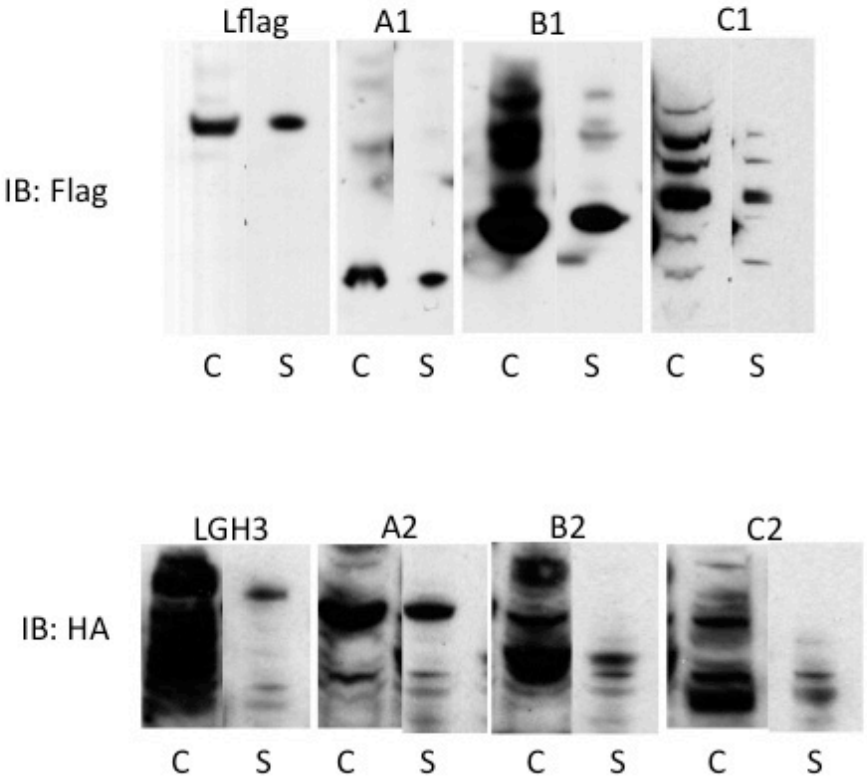

Figure 4.3 Surface expression of fragment channels. HEK293_β3α2δ cells were biotinylated 48-hours post-transfection and surface proteins were separated from cytoplasmic proteins using streptavidin beads (Thermo). (Top) Western of full-length $Ca_V1.2$ (Lflag) or indicated fragments containing a N-terminal Flag-tag and stained with an anti-Flag primary antibody. Cytoplasmic (C) and surface (S) proteins for each condition are shown. (Bottom) Western of full-length $Ca_V1.2$ (LGH3) or indicated fragments containing a N-terminal HA-tag and stained with an anti-HA primary antibody. Cytoplasmic (C) and surface (S) proteins for each condition are shown.

4.2.4 Dominant negative effects on the full-length channel

Next, I wanted to examine whether these fragment channels have an effect on full-length channel function. I had already observed that fragments B1 + B2 did not decrease $Ca_V1.2$_FL current (Chapter 3, Figure 3.7 b), however I did not investigate whether they had any effect on the biophysical properties of $Ca_V1.2$_FL. The other fragments could have differing effects on $Ca_V1.2$_FL as well. I first tested each of the individual fragments with $Ca_V1.2$_FL to see whether they had a dominant negative effect on peak current amplitude. C2 was the only fragment that produced a significant decrease in peak current (Figure 4.4). This initial C2 result was very interesting, but I wanted to examine further the effect these fragments were having on $Ca_V1.2$_FL. Even if they don't decrease peak $Ca_V1.2$_FL current, do they change the current-voltage relationship or inactivation profile of $Ca_V1.2$_FL? Also, do they physically interact with $Ca_V1.2$_FL?

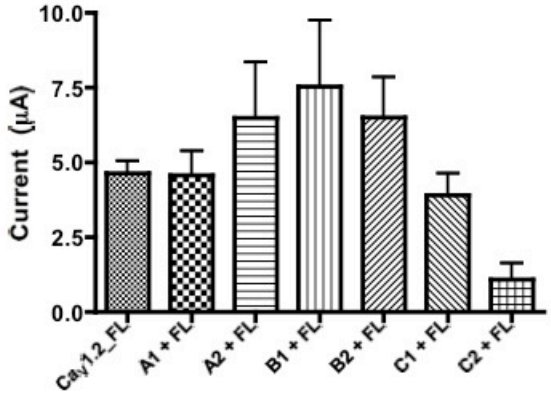

Figure 4.4 Dominant negative effects of individual fragments on full-length $Ca_V1.2$. Peak whole-cell currents recorded from oocytes at -10 mV to 0 mV expressing the full-length channel ($Ca_V1.2$ FL, N = 24) alone or with the indicated fragment A1 (N = 9), A2 (N = 8), B1 (N = 8), B2 (N = 14), C1 (N = 6), and C2 (N = 7). C2 produced a dramatic decrease in current amplitude. Error bars represent ±SE.

4.2.4.1 Fragment A1 & A2

Fragments A1 and A2 were individually coexpressed with $Ca_V1.2\_FL$, β_3, and $\alpha_2\delta$ in *Xenopus* oocytes. The current-voltage relationship and inactivation profile were determined according to methods described above. Both A1 and A2 had an effect on the biophysical properties of $Ca_V1.2\_FL$. The I-V curve of $Ca_V1.2\_FL$ was shifted to the right (Figure 4.5 a) and inactivation was increased (Figure 4.5 b). To determine whether this was due to a direct interaction between A1/A2 and $Ca_V1.2\_FL$, co-immunoprecipitations were done. Flag-tagged $Ca_V1.2\_FL$ (L-flag) and HA-tagged fragments (A1-HA and A2-HA) were transfected into HEK293_β3α2δ cells and lysates were incubated with anti-Flag or anti-HA beads. Untransfected cells and cells transfected solely with L-flag or A1/A2-HA served as controls. Fragments A1 (Figure 4.5 c) and A2 (Figure 4.5 d) were clearly able to be pulled down with L-flag, indicating that they associate with the full-length channel either by directly binding to α_1 or through interaction with auxiliary subunits such as β_3 and $\alpha_2\delta$.

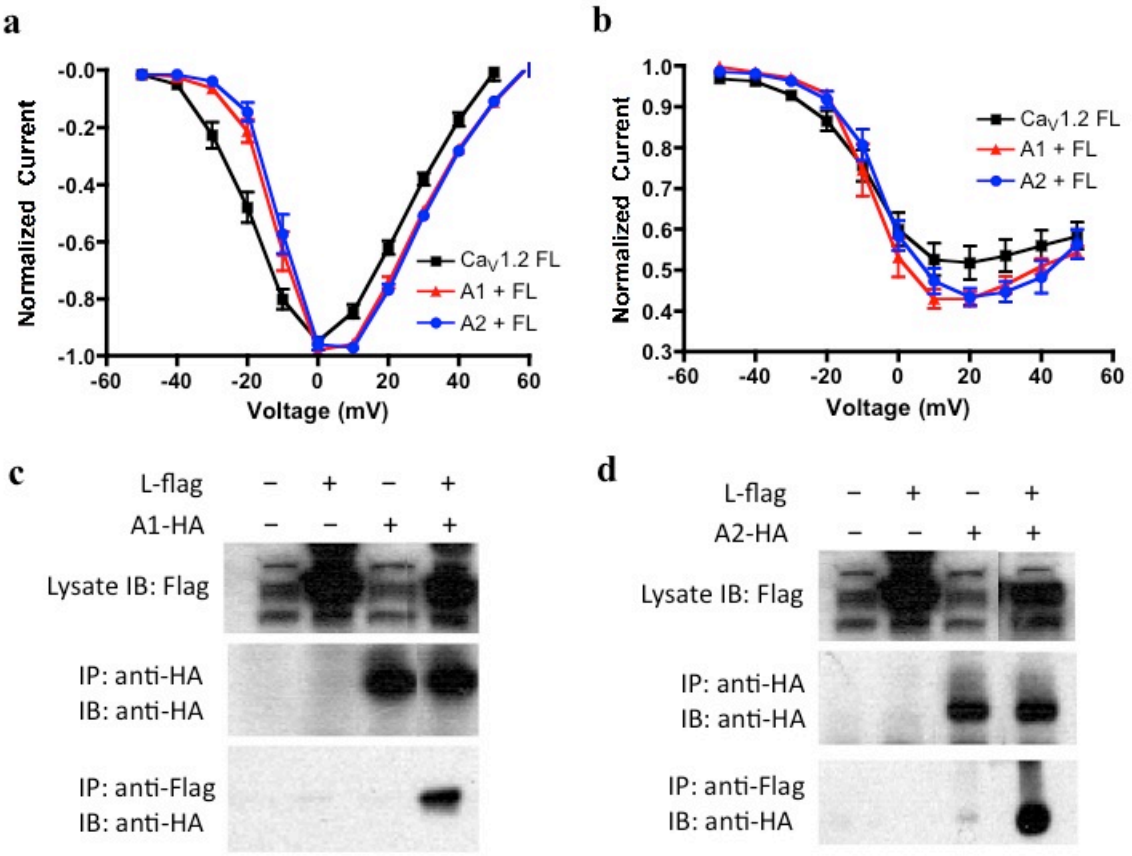

Figure 4.5 Fragments A1 and A2 affect the biophysical properties of $Ca_V1.2$ through an association with the channel complex. (a) I-V curve of $Ca_V1.2$_FL (black, ■, N = 31) is shifted to the right when coexpressed with either A1 (red, Δ, N = 9) or A2 (blue, O, N = 7). (b) Inactivation of $Ca_V1.2$_FL (black, ■, N = 14) is increased when coexpressed with either A1 (red, Δ, N = 5) or A2 (blue, O, N = 4). Error bars for both graphs reflect ±SE. (c) Western blot showing that A1 interacts with the channel complex. A1-HA co-immunoprecipitates with L-flag. (d) Western blot showing that A2 interacts with the channel complex. A2-HA co-immunoprecipitates with L-flag.

4.2.4.2 Fragment B1 & B2

Fragments B1 and B2 were individually coexpressed with $Ca_V1.2$_FL, β_3, and $\alpha_2\delta$ in *Xenopus* oocytes. The current-voltage relationship and inactivation profile were determined according to methods described above. Neither B1 nor B2 had a significant effect on the biophysical properties of $Ca_V1.2$_FL. The I-V curve of $Ca_V1.2$_FL remained the same when coexpressed with B1 or B2 (Figure 4.6 a) and $Ca_V1.2$_FL inactivation did not change when coexpressed with B1 or B2 (Figure 4.b b). To determine whether there was still an interaction between B1/B2 and $Ca_V1.2$_FL, co-immunoprecipitations were done. Flag-tagged $Ca_V1.2$_FL (L-flag) and HA-tagged fragments (B1-HA and B2-HA) were transfected into HEK293_$\beta3\alpha2\delta$ cells and lysates were incubated with anti-Flag or anti-HA beads. Untransfected cells and cells transfected solely with L-flag or B1/B2-HA served as controls. Fragments B1 (Figure 4.6 c) and B2 (Figure 4.6 d) were both able to be pulled down with L-flag, indicating that they associate with the full-length channel complex.

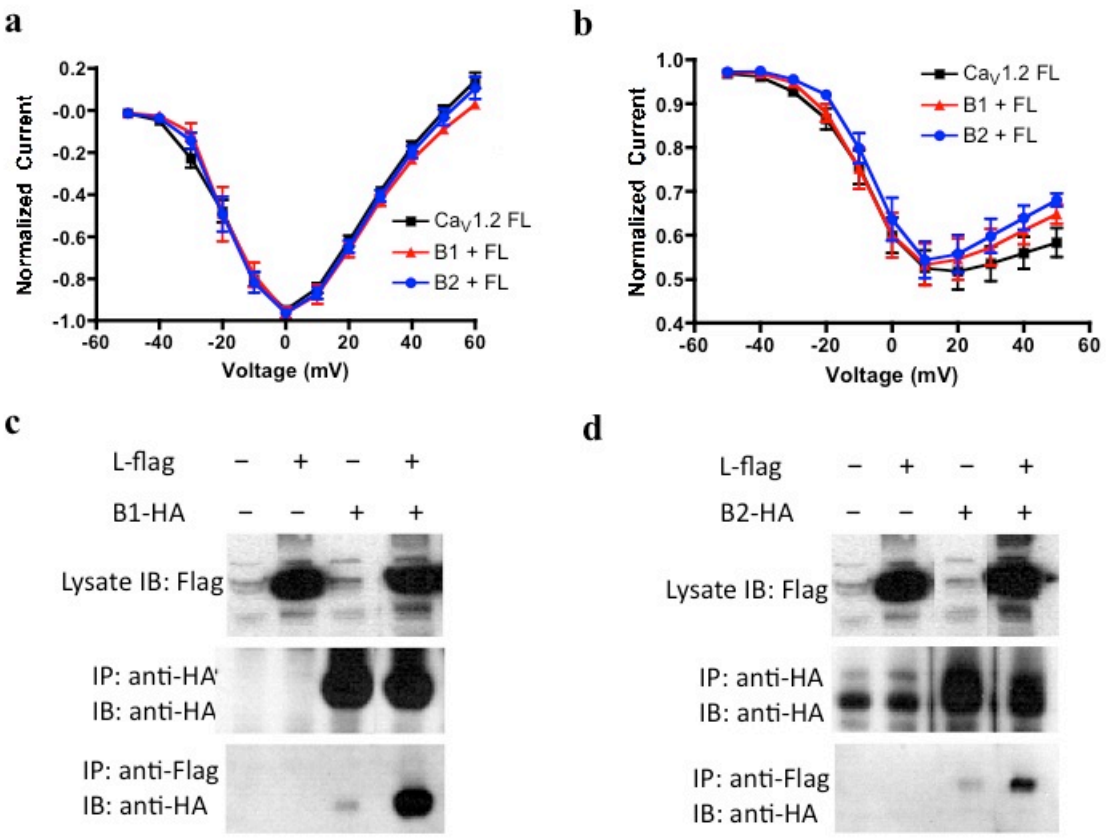

Figure 4.6 Fragments B1 and B2 associate with the channel complex but do not affect the biophysical properties of $Ca_V1.2$. (a) There is no change in the I-V curve of $Ca_V1.2$_FL (black, ■, N = 31) when coexpressed with either B1 (red, Δ, N = 8) or B2 (blue, O, N = 14). (b) There is no significant change in the inactivation of $Ca_V1.2$_FL (black, ■, N = 14) when coexpressed with either B1 (red, Δ, N = 9) or B2 (blue, O, N = 9). Error bars for both graphs reflect ±SE. (c) Western blot showing that B1 interacts with the channel complex. B1-HA co-immunoprecipitates with L-flag. (d) Western blot showing that B2 interacts with the channel complex. B2-HA co-immunoprecipitates with L-flag to a lesser degree than B1-HA.

4.2.4.3 Fragment C1 & C2

Fragments C1 and C2 were individually coexpressed with $Ca_V1.2\_FL$, β_3, and $\alpha_2\delta$ in *Xenopus* oocytes. The current-voltage relationship and inactivation profile were determined according to the methods described above. C2 had a slight effect on the I-V curve, as it seemed to shift the reversal potential to less positive voltages (Figure 4.7 a). The small shift C2 imposed on $Ca_V1.2\_FL$ inactivation is inconclusive due to the low sample size (Figure 4.7 b). C1, however, had a striking effect on the biophysical properties of $Ca_V1.2\_FL$. The I-V curve of $Ca_V1.2\_FL$ was shifted to the left (Figure 4.7 a) and the inactivation was dramatically increased (Figure 4.7 b). To determine whether this was due to a direct interaction between C1/C2 and $Ca_V1.2\_FL$, co-immunoprecipitations were done. Flag-tagged $Ca_V1.2\_FL$ (L-flag) and HA-tagged fragments (C1-HA and C2-HA) were transfected into HEK293_β3α2δ cells and lysates were incubated with anti-Flag or anti-HA beads. Untransfected cells and cells transfected solely with L-flag or C1/C2-HA served as controls. Fragment C1 did co-immunoprecipitate with the channel, however a small amount of C1-HA was pulled down by the Flag beads themselves (Figure 4.7 c). Therefore, no definitive conclusion can be made from this experiment. Fragment C2 (Figure 4.7 d) was able to be cleanly pulled down with L-flag, indicating that it does associate with the full-length channel complex.

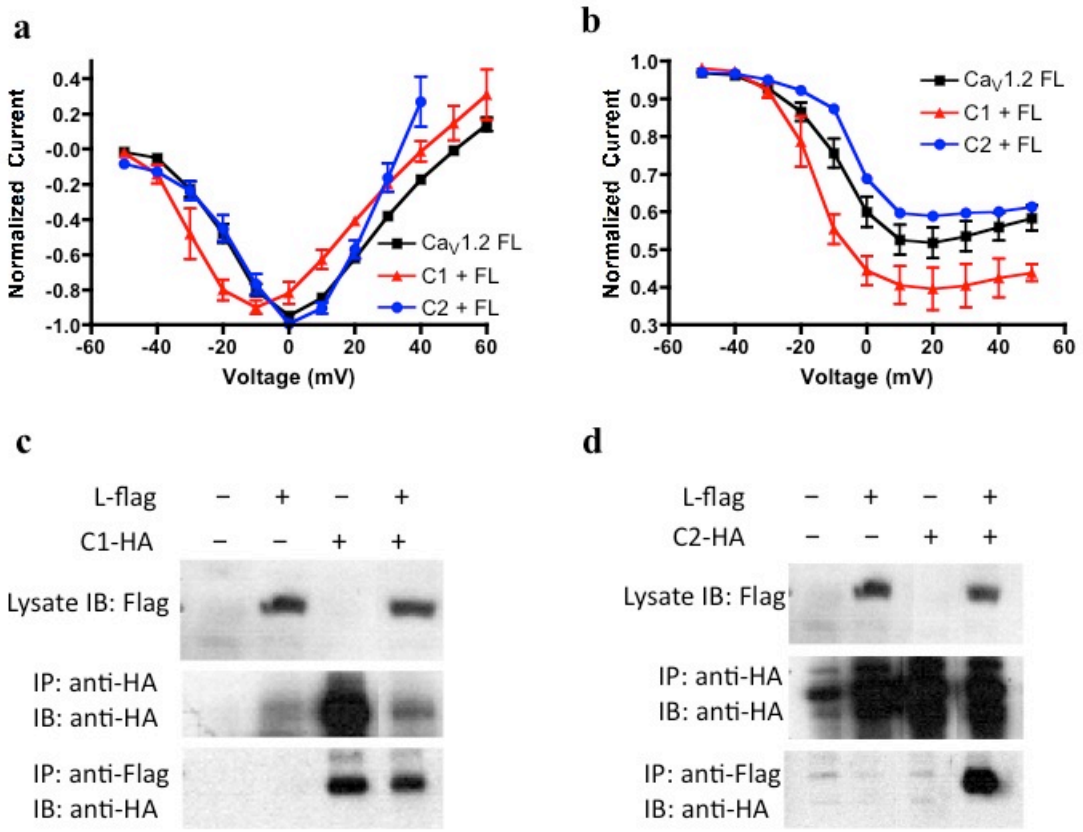

Figure 4.7 Fragments C1 and C2 affect the biophysical properties of $Ca_V1.2$ and C2 strongly associates with the channel complex. (a) I-V curve of $Ca_V1.2$_FL (black, ■, N = 31) when coexpressed with either C1 (red, Δ, N = 7) or C2 (blue, O, N = 7) C1 causes a left shift in the I-V curve while C2 seemed to change the reversal potential of $Ca_V1.2$_FL to +35 mV. (b) Inactivation curve of $Ca_V1.2$_FL (black, ■, N = 14) when coexpressed with either C1 (red, Δ, N = 3) or C2 (blue, O, N = 1). C1 dramatically increased inactivation, while C2 is inconclusive because of the low N. Error bars for both graphs reflect ±SE. (c) Western blot showing that C1 does not interact with the channel complex. C1-HA co-immunoprecipitates with L-flag, however a small amount of it is also pulled down by Flag beads without L-flag present. Therefore, this result is inconclusive. (d) Western blot showing that C2 interacts with the channel complex. C2-HA co-immunoprecipitates with L-flag.

4.3 DISCUSSION

4.3.1 Fragment channels are functional

Two-domain fragments of the N-type VGCC ($Ca_V2.2$) have been found to be functional when paired with their complementary partner (Raghib et al., 2001), however they did not exhibit differences in gating. In contrast, when $Ca_V1.2$ is split into two-domain fragments these channels are not only functional (Figure 4.1 b), but have unique biophysical properties (Figure 4.2). In addition, other varieties of $Ca_V1.2$ fragment channels reflecting cleavage in any one of the three intracellular loops (Figure 4.1 a), all produce current when paired with their complementary fragment (Figure 4.1 b). Moreover, they all share the same shift in their current-voltage relationship and inactivation profile (Figure 4.2). All fragments shifted the I-V curve to the right, reflecting a channel that is more difficult to open. Voltage-dependent inactivation also decreased with all the fragment pairs, indicating that once the channel is opened it is harder to close than when the channel is one continuous subunit. These results fit with a recombinant channel that is less fluid in it's gating due to not being properly joined together. It could also signify that interruptions in the intracellular loops disrupt the binding of regulatory proteins important in channel kinetics.

The observation that the fragment pairs have less current than the full-length channel can be a result of a few different factors. For instance, it is possible that this is a trafficking issue resulting in less surface expression than the full-length channel. This is a likely scenario, as it must be difficult to traffic together to the plasma membrane since only the fragment containing the I-II loop binds $Ca_V\beta$ to aid in exit from the ER.

However, this does not appear to be the case. Biotinylation experiments reveal that fragment channels have comparable, if not greater, surface expression than full-length channels (Figure 4.3). Therefore, the dampened peak current must be an inherent property of fragment channels paired together, perhaps a difference in gating, or of the two fragments being dissociated from one another in the membrane. The later seems likely in light of imaging experiments of LGH3 that show dissociated domains III and IV present on the plasma membrane (Chapter 3).

It does appear that for fragment channels to be functional their combination does need to contain all four domains, since fragments expressed alone produced no current (Figure 4.1 c). Interestingly, it does not appear to be the rule that the channel must contain only four domains. When a fragment containing domains I, II and III (C1) was coexpressed with a fragment containing domains III and IV (B2), functional channels resulted on the membrane (Figure 4.1 d), although with much smaller current than when fragments were properly paired. This unexpected result hints to the possibility that the channel can form a pore on the membrane by "kicking out" one of the extra domains. It also means that the same interactions between fragment channels may happen between a full-length channel and a smaller fragment, possibly affecting the overall functionality of the channel.

4.3.2 Effect of fragments on full-length $Ca_V1.2$

None of the fragments except C2 imposed a dominant-negative effect on the channel. C2 is interesting because it did not appear to change the biophysical properties of the full-length channel, however it reduced peak current. This is the same effect

Domain I had on the $Ca_V2.2$ channel (Raghib et al., 2001), which was later found to be due to the N-terminus interacting with the channel (Page et al., 2010). Possibly, the C-terminus of $Ca_V1.2$ interacts with full length $Ca_V1.2$, inhibiting its current (Hulme et al., 2006). Clearly, C2 binds to the full-length channel complex (Figure 4.7 d) and could be interfering with other proteins necessary for channel function. For example, it could disrupt $Ca_V1.2$ binding to α-actinin, which would impede surface expression (Hall et al., 2013). It could also affect $Ca_V1.2$ synthesis, whereby the fragment binds to the channel in the ER triggering the unfolded protein response, as was found with the N-type channel (Page et al., 2004) or just induce rapid protein degradation (Mezghrani et al., 2008). More experiments are needed to determine if the interaction between C2 and $Ca_V1.2\_FL$ results in less surface expression or direct inhibition of the channel.

Fragments A1 and A2 both had a small, but significant effect on the IV-curve and inactivation of $Ca_V1.2\_FL$ (Figure 4.5 a and b). Co-immunoprecipitations revealed that both fragments physically interact with the channel or channel complex (Figure 4.5 c and d). Regardless, this interaction did not decrease current (Figure 4.4) and therefore this interaction must only be affecting gating of $Ca_V1.2\_FL$. Surprisingly, fragments B1 and B2 had no effect on the current or gating of $Ca_V1.2\_FL$ (Figure 4.4 and 4.6). In the literature it is mainly fragments containing two domains that do the most damage to full-length channel function (Cox and Fromme, 2013; Okagaki et al., 2001; Raghib et al., 2001). B1 and B2 did bind to the channel complex however, and it is unclear how this interaction would not have some effect on channel function. C1 had a major effect on the inactivation of $Ca_V1.2\_FL$ and shifted the I-V curve to the left. Unfortunately, because of

the background binding in the co-immunoprecipitation experiment, it is inconclusive whether this is due to a direct interaction with the channel complex.

4.3.3 Implications of fragment channels as products of mid-channel proteolysis

The data gathered on the fragment channels has many implications for the aftermath of mid-channel proteolysis. The products of the channel being cut in any of the intracellular loops can associate to form functional channels. They can traffic together to the plasma membrane if the cleavage takes place in the ER, or remain on the plasma membrane if the cleavage occurs there. They can also interact with full-length channels that are already on the plasma membrane, changing gating properties. They can bind to the channel complex, including α_1, potentially affecting surface expression and protein degradation. If mid-channel proteolysis occurs as a way to regulate calcium, fragment channels are one way it exerts its effect. Not only can the proteolysis of the channel cause the two fragments to separate, abolishing current, but the fragments can then interact with other channels and proteins to further impact calcium influx. It is possible that the currents from VGCCs are actually a compilation of various forms of α_1, all working together to control calcium levels.

Chapter 5

$Ca_V1.2$ function is inhibited by APP and γ-secretase

ALL OF THE EXPERIMENTS PERFORMED IN THE FOLLOWING CHAPTER WERE COMPLETED BY KATHRYN ABELE HENCKELS. UNDERGRADUATE MORGAN GOODMAN ASSISTED IN THE CLONING OF THE APP MUTANTS.

5.1 INTRODUCTION

5.1.1 The calcium hypothesis of Alzheimer's Disease

Alzheimer's disease (AD) is strongly correlated with age and is characterized by progressive cognitive decline, memory loss, and impaired speech and spatial abilities (Albert, 2011). Two main types of AD exist, sporadic late-onset AD and genetic, early onset familial AD (FAD). In brain tissue, AD causes amyloid plaque deposition, which is generated from the amyloid-β precursor protein (APP), neurofibrillary tangles and selective neuronal loss (LaFerla, 2002). AD has been linked to erratic calcium signaling at the cellular level (Berridge, 2010; Green and LaFerla, 2008; LaFerla, 2002; Supnet and Bezprozvanny, 2010). In normal aging, neurons gradually lose their ability to tightly control calcium fluxes and recover from calcium load (Mattson, 2007); this deficit is exacerbated in AD.

APP is metabolized by two independent pathways (to be expanded on in 5.1.2). One pathway produces amyloid-β (Aβ), which is thought to contribute to a remodeling of calcium signaling pathways. When APP is processed in the amyloidogenic pathway, Aβ peptides are released to the extracellular space. These Aβ peptides can activate NMDA receptors causing an influx in calcium (Ye et al., 2004), and even form calcium leak channels themselves on the plasma membrane (Arispe et al., 1993). In addition, APP metabolism itself is enhanced by an increase in intracellular calcium (Pierrot et al., 2004), resulting in a positive feedback loop to further disrupt calcium homeostasis (Figure 5.1). Downstream effects of increased calcium include activation of calcineurin (Kuchibhotla et al., 2008) and calpains (Nixon et al., 1994), both exerting an effect on synaptic

plasticity. In postmortem brains of AD patients, an increase in levels of calpain and other calcium-dependent proteases has been observed (Green and LaFerla, 2008). Calbindin, a calcium buffer, has been observed to be downregulated in AD (Palop et al., 2003). Mitochondrial disruptions also result, leading to a depletion of ATP that causes enhanced membrane depolarization (Manczak et al., 2006; Toman and Fiskum, 2011) and increased facilitation of VGCCs on the plasma membrane.

Another consequence of this modified calcium signaling is an increase in the amount of calcium released from the endoplasmic reticulum (ER). Presenilin, a protease (discussed in detail below) intimately related to APP processing and AD, causes an increase in calcium release by $InsP_3$ (Cheung et al., 2008). This in turn increases the expression of the ryanodine receptor, the major Ca^{2+} release channel in the ER (Chan et al., 2000; Stutzmann et al., 2006) and of the sarco/endoplasmic reticulum ATPase (SERCA) pump, which refills ER Ca^{2+} stores (Green et al., 2008), all of which contribute to marked changes in calcium dynamics. Presenilins can even form passive calcium leak channels themselves in the ER and familial AD (FAD) mutations in presenilin prevent this, causing dysfunctional calcium signaling (Tu et al., 2006).

Increased calcium levels lead to disruptions in synaptic plasticity, long-term depression (LTD) and long-term potentiation (LTP), all factors contributing to learning and memory (Berridge, 2010). Aberrant calcium signaling also leads to apoptosis (Mattson, 2007), which could be the contributing factor to neuronal death in AD. Intriguingly, mutations in APP or presenilin that are linked to AD tend to intensify calcium dyshomeostasis, further validating the hypothesis that calcium plays a role in the onset and progression of AD.

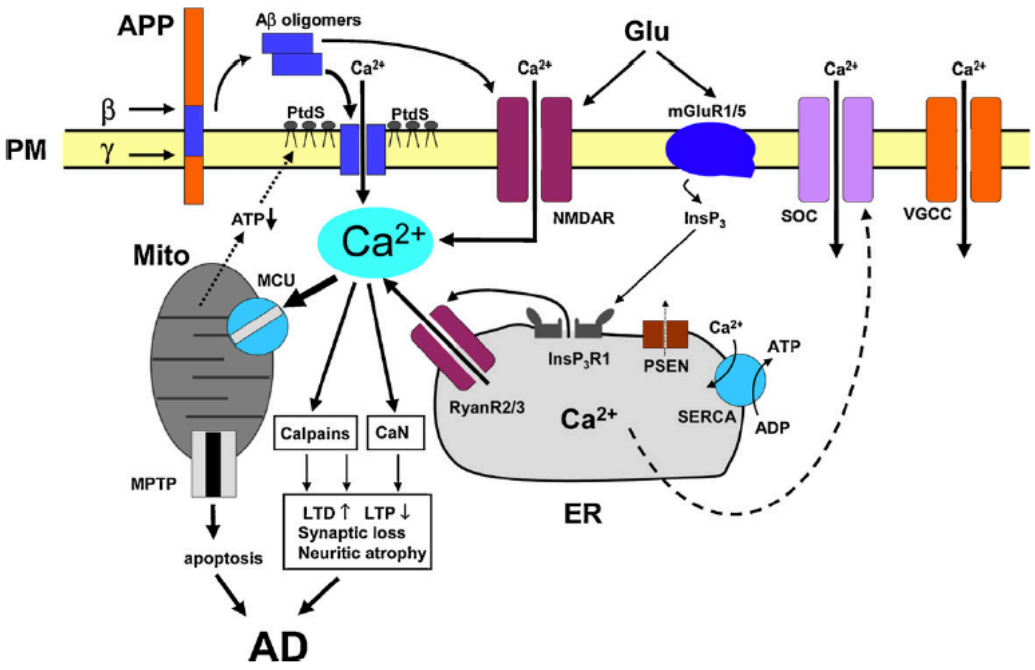

Figure 5.1 Dysregulation of intracellular calcium (Ca^{2+}) in AD. APP is cut by β- and γ-secretases to yield Aβ peptides that form oligomers in the extracellular space. These Aβ oligomers can activate NMDARs or insert into the membrane to form Ca^{2+} permeable pores, leading to an influx of Ca^{2+}. An overload of intracellular Ca^{2+} activates calpains and calcineurin and depletes ATP from the mitochondria. This leads to changes in synaptic plasticity and membrane integrity, which depolarizes the membrane, facilitating the activation of VGCCs. In the ER, presenilins form Ca^{2+} leak channels and increase the expression of SERCA. More Ca^{2+} is released from InsP3Rs and RyanRs. All of these cause altered Ca^{2+} signaling pathways that lead to synaptic loss, apoptosis and AD. Taken from (Supnet and Bezprozvanny, 2010).

5.1.2 APP Processing

To date the main focus of APP research has been on its relation to AD, specifically the Aβ product of metabolism. APP is, however, evolutionarily a highly conserved protein (Coulson et al., 2000) and must serve a function other than contributing to a devastating disease. Most of what is known of APP's function has come from studying knockout mice. APP has been reported to be involved in neuronal migration (Young-Pearse et al., 2007), neurogenesis, (Ma et al., 2008), neurite growth (Sabo et al., 2003), cell movement (Sabo et al., 2001), spatial learning and long-term potentiation (Tremml et al., 1998). How APP mechanistically exerts these effects and how it behaves in a non-disease state remains elusive.

APP is a type-1 membrane protein comprising a large extracellular N-terminus, a one-pass transmembrane segment and a short, intracellular C-terminus region (Kang et al., 1987). APP is metabolized by two independent pathways (De Strooper, 2010; Jacobsen and Iverfeldt, 2009), both involving a multitude of proteases (Figure 5.2). The non-amyloidogenic pathway, initiated by cleavage of APP by α-secretase (Postina, 2012), does not cause the production of Aβ and thus is not considered to contribute to AD. Instead, the products of α-secretase cleavage yield the soluble N-terminus, sAPPα and the membrane-bound C83. C83 is then cut by γ-secretase generating p3 and the APP intracellular domain (AICD), which can travel to the nucleus and aid in gene transcription (Cao and Sudhof, 2001). The amyloidogenic pathway begins when APP is cleaved by β-secretase (Vassar et al., 1999). This releases the soluble N-terminus, sAPPβ, and leaves the membrane-bound C99 as a target for γ-secretase. C99 is cleaved by γ-secretase to release the AICD and one of two forms of Aβ (Esler and Wolfe, 2001). The more

common, non-disease causing product of Aβ is Aβ-40. If however, Aβ is cut to yield a 42-residue peptide (Aβ-42), this disease form aggregates in the extracellular space leading to amyloid plaques (Iwatsubo et al., 1994), a hallmark symptom of AD.

All FAD APP mutations either flank or are located within the Aβ region, and are thought to disrupt normal processing by the secretases, creating more Aβ-42 (Wolfe, 2012). Most of the other FAD mutations occur in presenilin, a component of γ-secretase, which will be expanded on below. Recently, a protective APP mutant was found in an Icelandic population that had a single residue substitution from an alanine to a threonine in the β-secretase cut site of APP. This decreased the incidence of AD in people and dramatically decreased secreted Aβ in HEK cells (Jonsson et al., 2012). The same mutation was found in a Finnish woman that lived to the age of 104 (Kero et al., 2013). This protective effect is proposed to work through inhibiting β-secretase cleavage of APP.

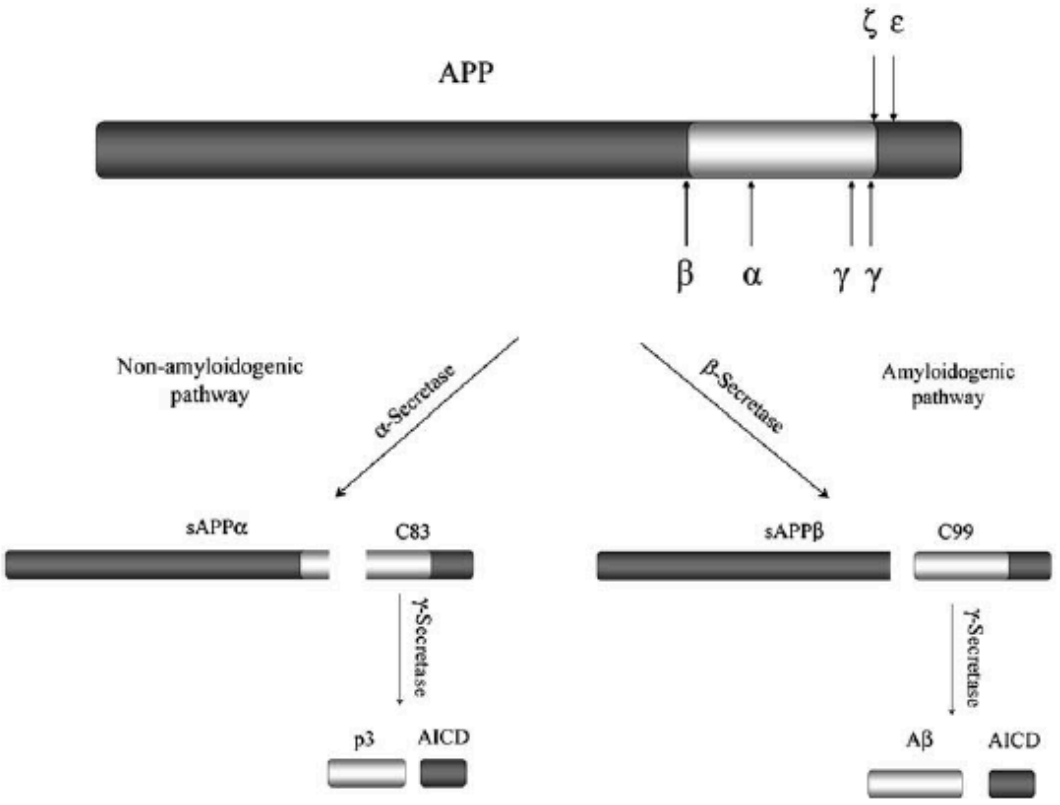

Figure 5.2 Overview of APP processing. APP is first cleaved by α- or β-secretase, which leads to the secretion of N-terminal sAPPα or sAPPβ. The remaining C-terminal membrane-bound C83 or C99 are cleaved by γ-secretase, generating AICD and either p3 or Aβ. Taken from (Jacobsen and Iverfeldt, 2009).

γ-secretase is a multimeric complex consisting of presenilin, PEN-2, nicastrin, and APH-1 (Selkoe and Wolfe, 2007). Presenilin is the catalytic component of γ-secretase and many presenilin mutations lead to AD. Presenilin contains nine transmembrane segments and has two catalytic aspartate residues in S6 and S7 that come together to cleave membrane bound proteins (Li et al., 2013). While presenilin does not have a

defined cut site and has even been referred to as the "proteasome of the membrane" (Kopan and Ilagan, 2004), it is thought to predominately cleave type-1 membrane proteins after most of the ectodomain has been removed (Selkoe and Wolfe, 2007; Struhl and Adachi, 2000). The most studied substrates of γ-secretase are APP and Notch (Lathia et al., 2008).

Recently, new targets of γ-secretase have been identified, including ion channel subunits. The β subunit of the voltage-gated sodium channel $Na_V1.1$ is cleaved by presenilin, driving transcription of the α_1 subunit resulting in increased surface expression of $Na_V1.1$ (Kovacs et al., 2010) and facilitating cell adhesion and migration (Kim et al., 2005). The KCNE1 and 2 subunits of voltage-gated potassium channels are also cleaved by presenilin (Sachse et al., 2013). While most of the known γ-secretase substrates are type-1 membrane proteins, the glutamate receptor subunit 3 is cleaved by γ-secretase in the membrane re-entry loop that forms the pore (Meyer et al., 2003). γ-secretase cleavage of these proteins regulates many neuronal functions including synaptic transmission and cell excitability. It was found using PS-1 knockout hippocampal neurons that γ-secretase regulates spontaneous neurotransmitter release in a calcium dependent fashion (Pratt et al., 2011). γ-secretase is found at synapses and has been shown to modulate synaptic activity by cleaving and downregulating synaptic proteins (Restituito et al., 2011). Intriguingly, PS-1 knockout mice have increased L-type current (Cook et al., 2005).

5.1.3 L-type channel and Alzheimer's Disease

In the hippocampus of AD brains there is increased expression of L-type channels and a lower cell density compared to healthy brains (Coon et al., 1999). L-type channel blockers have been shown to reduce symptoms of AD in *in vitro* cell systems, mice and humans. Verapamil, diltiazem, isradipine, and nimodipine all decreased Aβ42 toxicity in MC65 cells (Anekonda et al., 2011). A selective L-type channel blocker, S-312-d, rescued primary rat cortical neurons from Aβ-induced death (Yagami et al., 2004). Verapamil reversed Aβ-induced depression of long term potentiation in the hippocampus (Freir et al., 2003). Nimodipine slowed progression of AD in a clinical trial (Lopez-Arrieta and Birks, 2002; Tollefson, 1990). In an AD mouse model expressing two common FAD mutations, $Ca_V1.2$ expression in astrocytes increased along with increased Aβ plaques in an age-dependent manner (Willis et al., 2010). $Ca_V1.2$ current density was markedly reduced in hippocampal slice preps of a double AD mouse model, with knock-in APP and presenilin mutants, compared to wild-type mice (Thibault et al., 2012). In APP-/- mouse striatum, $Ca_V1.2$ expression and Ca^{2+} currents were increased compared to wild-type and APP-/- mice in which APP was reintroduced using lentiviral infection (Yang et al., 2009). All of these findings point to a close association between $Ca_V1.2$ and AD, or at least $Ca_V1.2$ and proteins involved in AD such as APP and presenilin.

Our lab has shown that mid-channel proteolysis of $Ca_V1.2$ occurs in response to increased Ca^{2+} levels and channel activity. It is believed to be a regulatory mechanism to aid in the control of Ca^{2+} homeostasis. If Ca^{2+} levels go so awry in AD, it would follow that mid-channel proteolysis would try to compensate for the increased intracellular Ca^{2+}. Mid-channel proteolysis and AD are both strongly correlated to age. $Ca_V1.2$ is important

for memory and neuronal plasticity, two functions that APP also seems to be involved in and which AD disrupts. What's more, there seems to be a direct link between APP and $Ca_V1.2$, whereby APP levels augment Ca^{2+} influx through $Ca_V1.2$. Pharmacologically inhibiting $Ca_V1.2$ also reverses toxic effects of Aβ and slows the progression of AD in patients. Therefore, a reasonable hypothesis would be that $Ca_V1.2$ plays a role in AD and that mid-channel proteolysis would occur as a protective mechanism for the neuron.

5.2 RESULTS

5.2.1 APP decreases L-type channel current and changes its biophysical properties

Based on reported observations (Yang et al., 2009), I wanted to confirm that APP causes a decrease in L-type channel current. Using *Xenopus* oocytes, I microinjected the human $Ca_V1.2$ channel, along with β_3 and $\alpha_2\delta$, with or without APP. I recorded peak currents 4 days post-injection between -10 mV and 0 mV. There was a dramatic decrease in peak current (~70%) when APP was coexpressed, indicating that APP inhibits the channel (Figure 5.3).

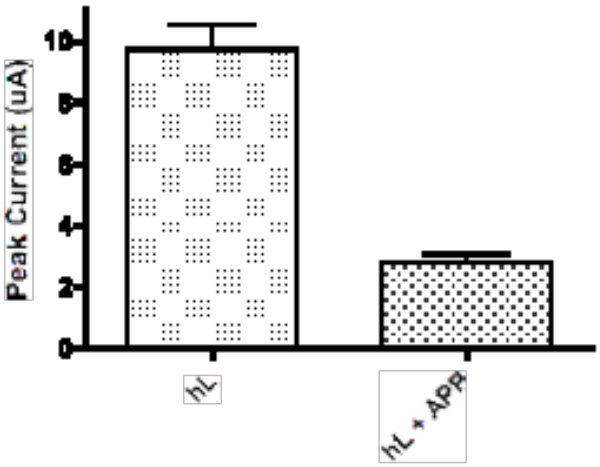

Figure 5.3 APP inhibits $Ca_V1.2$ peak current. Peak Ba^{2+} currents of human $Ca_V1.2$, β_3 and $\alpha_2\delta$ without (hL, N = 11) and with APP (hL + APP, N = 13). Currents were recorded at +10 mV in whole oocytes and averaged. Error bars represent SE.

There was also a +10 mV shift in the current-voltage relationship when APP was present (Figure 5.4 a). This indicates that APP makes the channel harder to open,

positively shifting the activation voltage. There was also a +10 mV shift in the inactivation curve (Figure 5.4 b), revealing that APP decreased inactivation of the channel. Interestingly, the same +10 mV shift in both the inactivation and I-V curve was seen when complimentary pairs of fragment channels were coexpressed (Chapter 4, Figure 4.2).

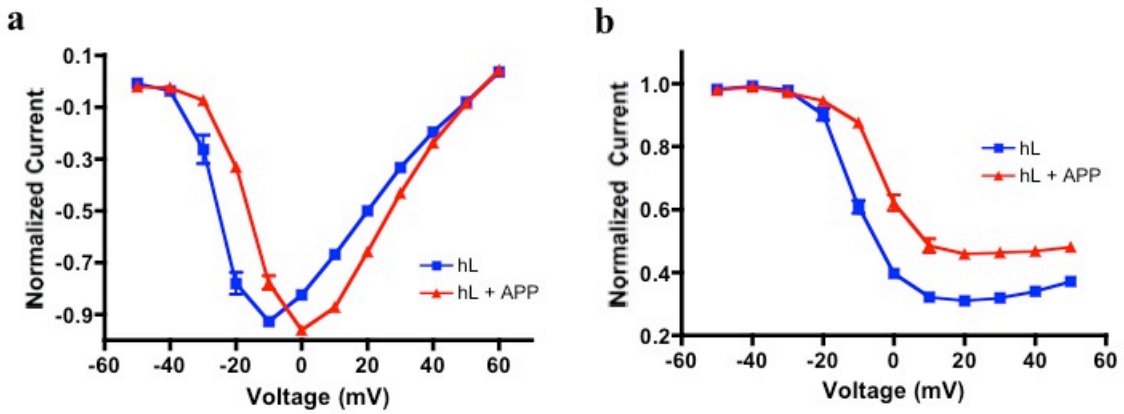

Figure 5.4 Biophysical changes to $Ca_V1.2$ in the presence of APP. (a) I-V curve of hL (blue ■, N = 49) and hL + APP (red Δ, N = 48). A +10 mV shift occurs when APP is present. (b) Inactivation curve of hL (blue ■, N = 10) and hL + APP (red Δ, N = 9). APP causes a decrease in channel inactivation.

Due to the similarity in biophysical properties to the fragment channels, perhaps the decrease in peak current could be caused by proteolysis of the channel. APP is itself robustly proteolyzed by three different proteases. One of these proteases, γ-secretase, is known to be highly expressed in oocytes (Tsujimura et al., 1997), because it is involved

in Notch processing and the polarization of the oocyte. A western of the oocytes confirmed that presenilin-1 is indeed endogenously expressed (data not shown).

5.2.2 A ~100kD band appears in westerns when APP is coexpressed with $Ca_V1.2$

To investigate whether the channel was being proteolyzed in the presence of APP, a Western was done on oocytes (N = ~40/group) injected with human $Ca_V1.2$ (hL), β_3, and $\alpha_2\delta$ with or without APP. Oocytes were biotinylated 4 days post-injection and both the surface proteins and cytosolic proteins were collected. Each group of oocytes showed the predicted 240 kD band indicating full-length $Ca_V1.2$. However, in the group of oocytes also expressing APP, a ~100 kD band appeared in both the surface and cytosolic preparations (Figure 5.5). It appeared that the channel was being cut when APP was present. Perhaps APP was colocalizing with the channel and targeting one of the secretases to the channel. A likely candidate for a protease is γ-secretase for reasons previously mentioned. I wanted to test if inhibiting γ-secretase would change the occurrence of this ~100 kD band.

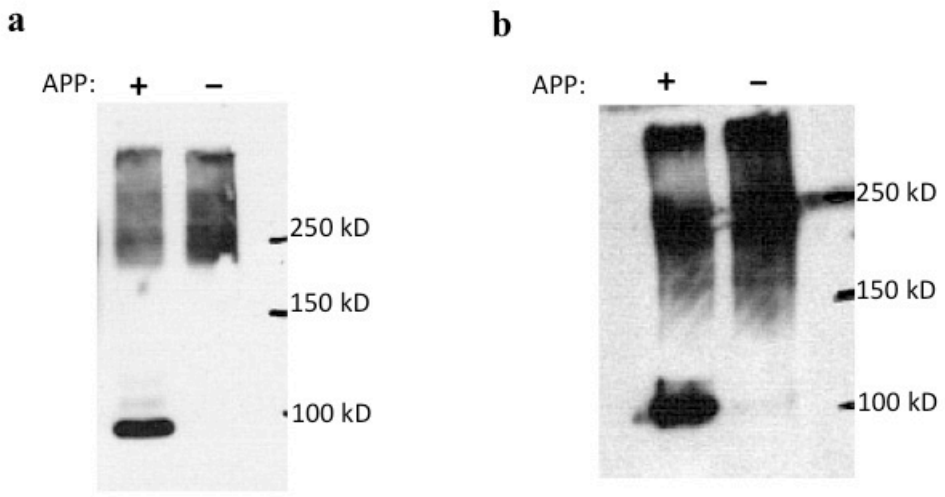

Figure 5.5 APP causes the appearance of a ~100 kD band in Western blots. Western blots of oocyte lysates stained with anti-$Ca_V1.2$ II-III loop antibody (Sigma). (a) Membrane proteins from oocytes injected with hL, β_3 and $\alpha_2\delta$ with or without APP. Membrane proteins were separated using ultracentrifugation. N = ~ 40 oocytes. (b) Total cell lysate from oocytes injected with hL, β_3 and $\alpha_2\delta$ with or without APP. N = ~ 40 oocytes.

5.2.3 DAPT reverses the effect on current and proteolysis

DAPT, N-[N-(3,5-Difluorophenyl)-L-alanyl]-D-phenylglycine t-butyl ester, is a potent and specific γ-secretase inhibitor that blocks the catalytic site in presenilin. I added DAPT to the oocyte media two days post-injection (two days pre-recording/ isolation) for a final concentration of 10 μM. If APP is needed to target γ-secretase to the channel for cleavage, thus causing a decrease in channel function, then the addition of DAPT should reverse the currents to levels seen when APP is not expressed. This is indeed what I observed. DAPT was applied to the media of oocytes injected with hL and oocytes injected with both hL and APP. Without DAPT, the decrease in current was observed when APP was coexpressed (Figure 5.6 a). This effect was completely reversed when

DAPT was applied to oocytes expressing both hL and APP (Figure 5.6 a). There was a small effect of DAPT on L-type currents when APP was not coexpressed. This result is consistent with the hypothesis that γ-secretase is being targeted to $Ca_V1.2$ by APP and then cutting the channel, since inhibition of γ-secretase prevents the APP-induced decrease in peak current amplitude.

DAPT did not have as dramatic an effect on the I-V curve. While APP still shifted the I-V curve +10 mV, DAPT only partially reversed this to ~+5 mV (Figure 5.6 b). DAPT applied to oocytes that only expressed hL had the same +5 mV shift however, indicating that DAPT itself has an effect on the current-voltage relationship of the channel. It is not clear if this is due to an inhibition of proteolysis, or if it is a pharmacological effect on the channel itself. Interestingly, DAPT had a huge effect on the inactivation properties of $Ca_V1.2$ coexpressed with APP. As seen before, the addition of APP slowed down inactivation (Figure 5.6 c), shifting the inactivation curve by approximately +10 mV. DAPT treatment reversed this effect, and actually increased inactivation beyond that of hL expressed alone (Figure 5.6 c). The addition of DAPT caused 80% of channels to inactivate compared to ~60% of channels observed previously at the same voltages. If γ-secretase is cutting the channel and decreasing channel inactivation, it is possible that even without APP present there is a basal level of proteolysis by γ-secretase that is abolished by DAPT.

To confirm that DAPT was preventing the proteolysis of the channel, I ran a Western on the oocytes treated with DAPT to see if the presence of the ~100 kD was abolished. In two independent experiments, the addition of DAPT to the media of oocytes injected with both hL and APP resulted in the complete absence of the ~100 kD band

(Figure 5.6 d). There were a few new bands that appeared in these gels (at ~130 kD and ~200 kD), but the ~100 kD band was only present in the oocytes expressing APP without DAPT treatment.

It now seems likely that γ-secretase cleaves $Ca_V1.2$, which results in a current decrease as well as a slower and decreased inactivation. APP, a known γ-secretase substrate, might somehow interact with or colocalize with the channel, targeting γ-secretase to $Ca_V1.2$ to increase the chances of this proteolysis. This result leads to the question of whether this is a L-type channel specific effect, or if APP would induce this cleavage on any calcium channel.

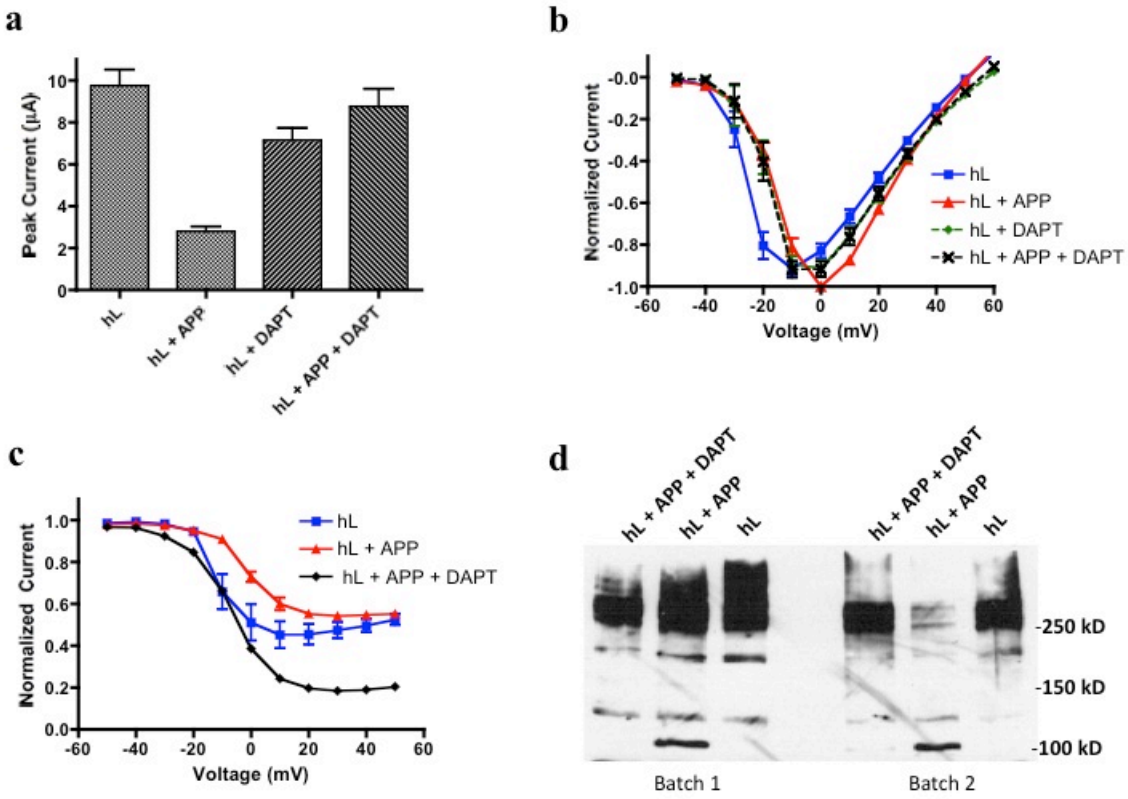

Figure 5.6 DAPT reverses the effect APP has on $Ca_V1.2$. (a) Peak Ba^{2+} currents of hL, β_3 and $\alpha_2\delta$ without (hL, N = 11), with APP (hL + APP, N = 13), with DAPT (hL + DAPT, N= 10) and with APP and DAPT (hL + APP + DAPT, N = 12). Currents were recorded at +10 mV in whole oocytes and averaged. (b) I-V curve of hL (blue, ■, N = 15), hL + APP (red, Δ, N = 13), hL + DAPT (green, ◆, N = 10) and hL + APP + DAPT (black, ✕, N = 12). A +10 mV shift occurs when APP is present. 24 hour DAPT treatment with or without APP have the same + 5 mV shift on the channel's current-voltage relationship. All error bars represent SE. (c) Inactivation curve of hL (blue ■, N = 10), hL + APP (red Δ, N = 9), and hL + APP + 24 hour DAPT treatment (black, ◆, N= 4). APP slows the inactivation of the channel, while DAPT markedly reverses this, beyond untreated hL. All error bars represent SE. (d) Western blots of membrane fractionated lysates taken from two batches of oocytes injected with hL, hL + APP, and hL + APP treated with 10 μM DAPT for 24 hours. The ~100 kD band only appears when APP is coexpressed with $Ca_V1.2$ and disappears when oocytes are treated with DAPT.

5.2.4 The ~100kD band occurs with rat $Ca_V1.2$ but not PQ channel

If γ-secretase cleaves the human $Ca_V1.2$, and this is a L-type channel specific phenomenon, it should also cleave $Ca_V1.2$ channels from other species. To test this, rat $Ca_V1.2$ (ratL) was injected into oocytes with or without APP and four days later oocytes were isolated for Western blot analysis. The same ~100 kD band that was produced when hL was expressed was also seen with ratL (Figure 5.7 a). Therefore, this APP-induced proteolysis seems to happen to $Ca_V1.2$ channels in general. Next, I wanted to determine if APP-induced γ-secretase proteolysis is specific to L-type calcium channels. Does co-expression of APP with another type of voltage-gated calcium channel cause the same proteolysis pattern? I injected oocytes with rabbit P/Q-type channel with and without APP and isolated the oocytes four days later for Western blot analysis. No difference in band patterns was seen between the two groups (Figure 5.7 b) and there was no band visible around 100 kD. It therefore seems likely that this is a L-type specific effect.

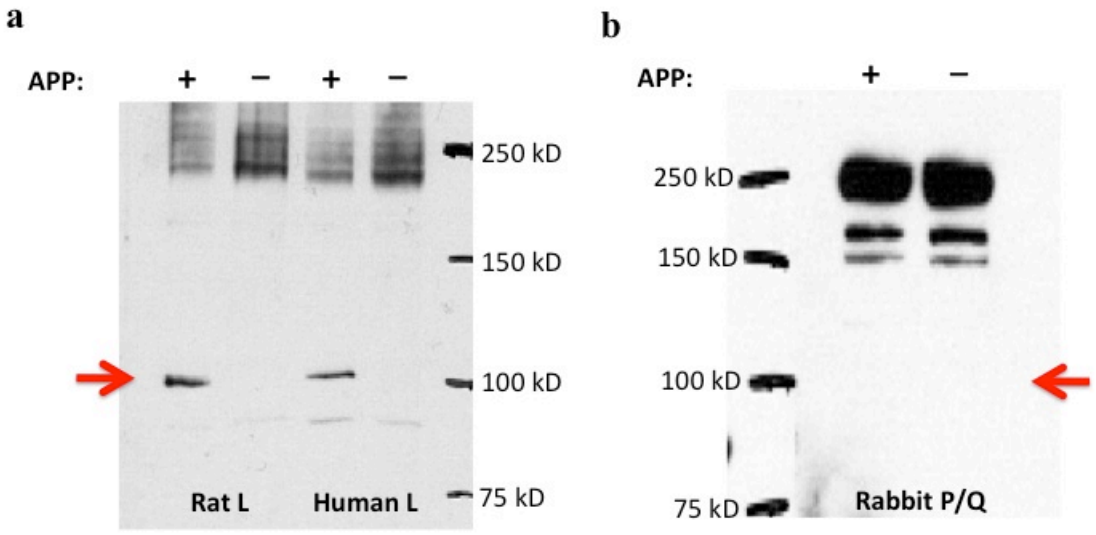

Figure 5.7 The ~100 kD band is L-type specific. (a) Western blots stained with anti-$Ca_V1.2$ II-III loop antibody (Sigma). Membrane fractionated lysates from oocytes injected with Rat L (ratL) or Human L (hL) with (+) out without (-) APP. The ~100 kD band appears (arrow) with both the rat and human L-type channel when APP is present. (b) Membrane fractionated lysates from oocytes injected with rabbit P/Q-type channel with (+) out without (-) APP. The ~100 kD band does not appear (arrow) when APP is present.

5.2.5 Potential cut sites on the channel – mutations change cleavage pattern

As mentioned in the introduction, presenilin is a promiscuous protease, not having a particular "cut site". The location that it cuts APP however, is well characterized and contains the residues TVIVIT. I aligned the sequence of many $Ca_V1.2$ channels and found they all contain the residues IVIVT within a well-conserved region of the channel (Figure 5.8 a). These residues mirror the APP γ-secretase cut site. Moreover, this site is not conserved in any other of the voltage-gated calcium channels, strengthening the possibility that this is a $Ca_V1.2$ specific effect. These residues also occur in a region of

the channel that, if cut, would produce a band with the predicted molecular weight of 115 kD (Figure 5.8 b), close to the observed ~100 kD band in my Western blots.

Mutating these residues could determine whether this is the region presenilin cuts $Ca_V1.2$. I first mutated all four residues to alanine (hL 4xAla) and expressed the mutant channel with APP in oocytes, along with the controls of wild-type hL with and without APP. The protein was isolated four days later for Western blot analysis. Surprisingly, the 4xAla mutation did not decrease proteolysis (Figure 5.8 c). It appeared that this was not the cut site, since changing the residues to alanines is a severe mutation to the cut site. However, the putative site was modeled after the APP γ-secretase site, and γ-secretase has other substrates. Notch, another well described γ-secretase substrate, is cut at a site containing four alanines (Selkoe and Kopan, 2003). This could explain why the hL 4xAla channel did not abolish proteolysis. Therefore, I decided to try different mutations to the same site, one changing the two isoleucines to valines (hL 4xVal) and the other changing the two valines to isoleucines (hL 4xIle). This time the band was completely missing in the valine and isoleucine substitution mutants (Figure 5.8 c). It now seems likely that this is the site presenilin is cutting the channel.

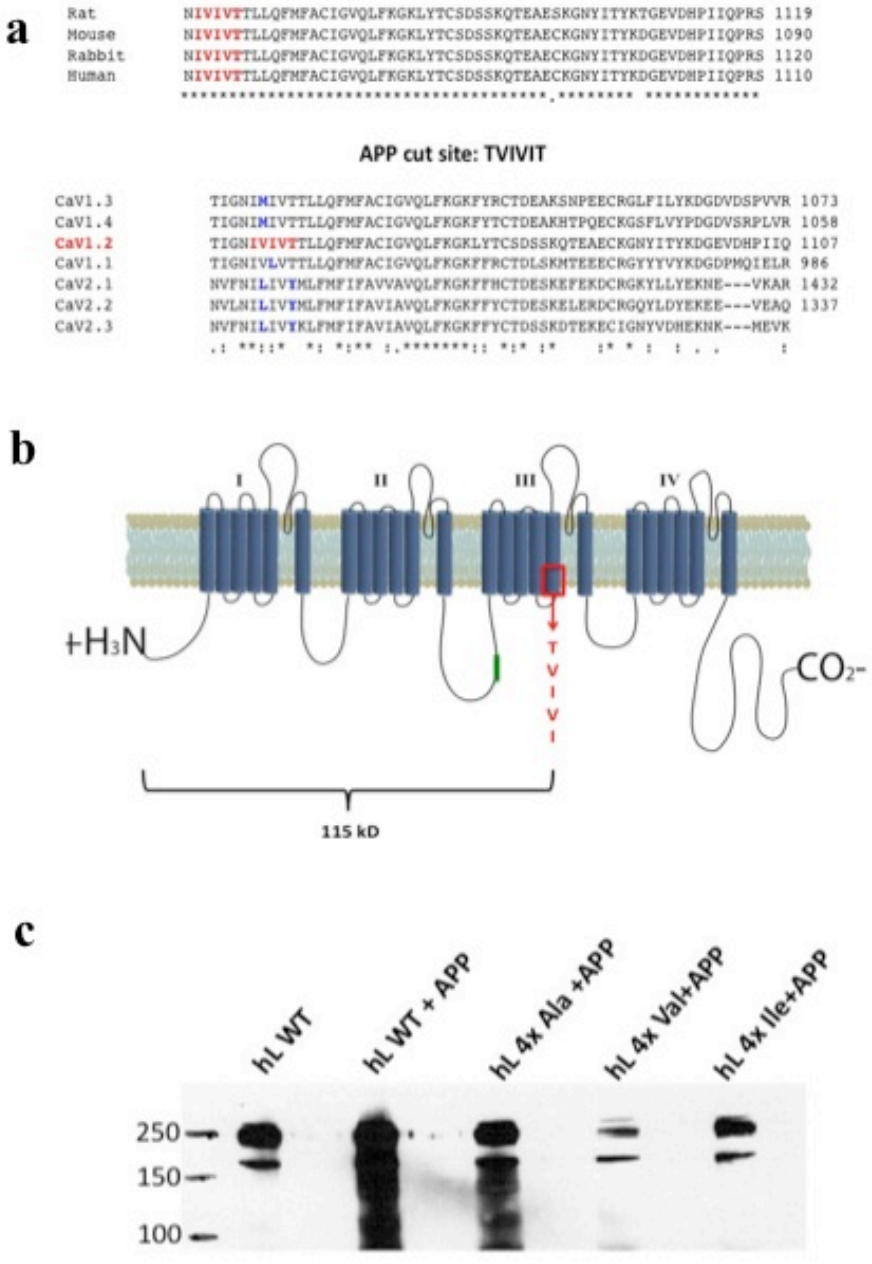

Figure 5.8 Mapping the potential cut site in $Ca_V1.2$. (a) Top: Amino acid alignment of $Ca_V1.2$ channel from rat, mouse, rabbit and human. Conserved residues shown (*) and residues comprising the putative cut site in red. Bottom: Amino acid alignment of different VGCCs from rat. Conserved residues shown (*). The putative cut site is only present in $Ca_V1.2$. (b) Topology of $Ca_V1.2$ and putative cute site region shown in red box. II-III loop antibody residues (green) and molecular weight of channel from N-terminus to putative cut site indicated. (c) Western blots stained with anti-$Ca_V1.2$ II-III loop antibody (Sigma). Membrane fractionated lysates from

oocytes injected with wild-type hL, β_3, $\alpha_2\delta$, +/- APP or with hL mutants + APP. The ~100 kD band only appears when wild-type hL and hL 4xAla are coexpressed with APP. hL 4xVal and hL 4x Ile do not produce the ~100 kD band, and look similar to hL without APP.

5.2.6 APP-induced proteolysis is not reproducible in neurons

Having demonstrated APP-induced proteolysis of $Ca_V1.2$ by γ-secretase in oocytes, I focused on reproducing the result in a more physiological relevant system. Since the interaction between APP and $Ca_V1.2$ has implications for Alzheimer's disease (AD), and AD is a disease affecting the brain, the next logical step was to move into neuronal models. An added benefit of this model is that $Ca_V1.2$, APP, and all of the components of γ-secretase are endogenously expressed in neurons. Therefore, I could observe what happens to endogenous channels in cortical slices and hippocampal neurons after treatment with DAPT.

Using rat cortical slices is an efficient way to see if the ~100 kD band is present under normal conditions and whether DAPT is able to reverse this effect. Cortical slices were collected from one adult rat (~6 weeks old) and split into three groups: control, KCl + BayK, and KCl + BayK + DAPT. In case APP-induced proteolysis is dependent on channel activity or calcium influx, 65 mM KCl and 14μM BayK8644 was added to the artificial cerebral spinal fluid (ACS) to activate the channel. The same condition plus the addition of 100 μM DAPT was used on another group of slices to block any activity-dependent APP-induced γ-secretase proteolysis of the channel. After 20 minutes of treatment, slices were biotinylated to label surface proteins. After cytosolic and surface

proteins were separated using streptavidin beads (Thermo), samples were analyzed by Western blot to see if the DAPT treatment prevented the proteolysis of the channel. Two bands were observed, one at ~140 kD and one at ~110 kD. There was not a significant DAPT effect on the ~110 kD band (Figure 5.9 a), as this band did not change considerably from the KCl + BayK group. This ~110 kD band was slightly larger than the ~100 kD band seen in oocytes, but this could be due to the change in model systems. There was, however, a decrease in the intensity of ~140 kD band after DAPT treatment. Surprisingly, the KCl + BayK treatment did not enhance 140 kD proteolysis in these samples. It is possible that a 20-minute DAPT treatment was not long enough to see an effect. After all, the oocytes were exposed to DAPT for 48 hours before they were lysed for Western blot analysis. If longer treatment is required to see a DAPT effect on $Ca_V1.2$ proteolysis, then it is not be possible to uses cortical slices because they do not live for longer than 8 hours after isolation. Cultured hippocampal neurons are a better choice.

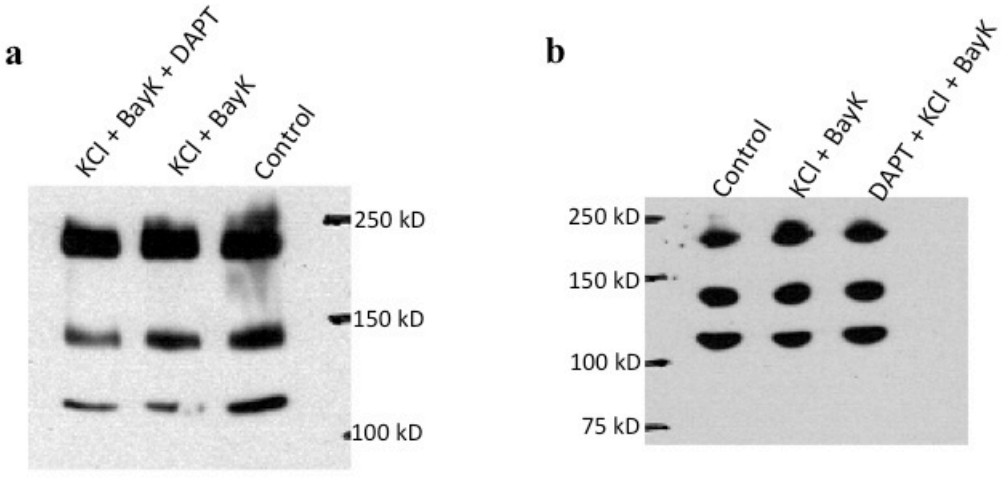

Figure 5.9 $Ca_V1.2$ proteolysis patterns in rat neurons. Western blots stained with anti-$Ca_V1.2$ II-III loop antibody (Sigma). (a) Slices from a 6-week old rat treated in parallel with DMSO (control), 65 mMKCl + BayK8644, or 65 mM KCl + BayK8644 + 50 μM DAPT for 30 minutes. Samples were biotinylated and surface proteins are shown. Proteolysis patterns look similar between all three treatment groups. (b) Cultured hippocampal neurons from E17-19 rats treated on DIV 14 in parallel with DMSO (control), 65 mMKCl + BayK8644, or 65 mM KCl + BayK8644 + 50 μM DAPT for 30 minutes. Samples were biotinylated and surface proteins are shown. Proteolysis patterns look similar between all three treatment groups.

Using the same strategy on embryonic rat hippocampal neuron cultures, it would be possible to see if this ~100 kD band appears under normal circumstances, and if so, whether it is abolished or reduced with DAPT treatment. Cultured neurons have the benefit of being able to be treated for any duration of time before isolating the protein. Neurons were cultured for 10 days according to normal conditions. On day 11, one plate was treated with DAPT (50 μM final concentration). 48 hours later, the DAPT treated plate and an untreated plate were treated with KCl and BayK for 20 minutes. A control plate was treated with DMSO. After this treatment, neurons were biotinylated and

collected for Western blot analysis. The same band pattern that appeared with the cortical slices was present in the hippocampal neurons (Figure 5.9 b). Unfortunately, there was not a significant change in any of the bands between treatment groups. Perhaps DAPT was degraded in the neuronal media after such a long time. This experiment was then repeated testing DAPT treatment at 12 and 24 hours, but the results were the same. DAPT treatment did not seem to change the amount of ~110 kD band that appeared. One explanation for the DAPT effect being observed in oocyte experiments is that APP was exogenously expressed. Perhaps the high level of endogenous APP present in neurons makes it difficult to observe a change.

5.2.7 APP-/- brain slices and neurons

If the co-localization of APP and $Ca_V1.2$ is necessary for targeting γ-secretase to the channel, APP knockout animals should have little to no proteolysis of $Ca_V1.2$. We therefore decided to compare WT and APP-/- mice brain homogenates. In very young mice (P7-9), there was no proteolysis of $Ca_V1.2$ in either the WT or the APP-/- mice (Figure 5.10 a). This came as a surprise, since a 150 kD band has always been seen in rat brain of all ages (Chapter 3 and Appendix). There was an equal amount of presenilin in both brains, and it was confirmed that there was no APP protein in the APP-/- brain (Figure 5.10 a).

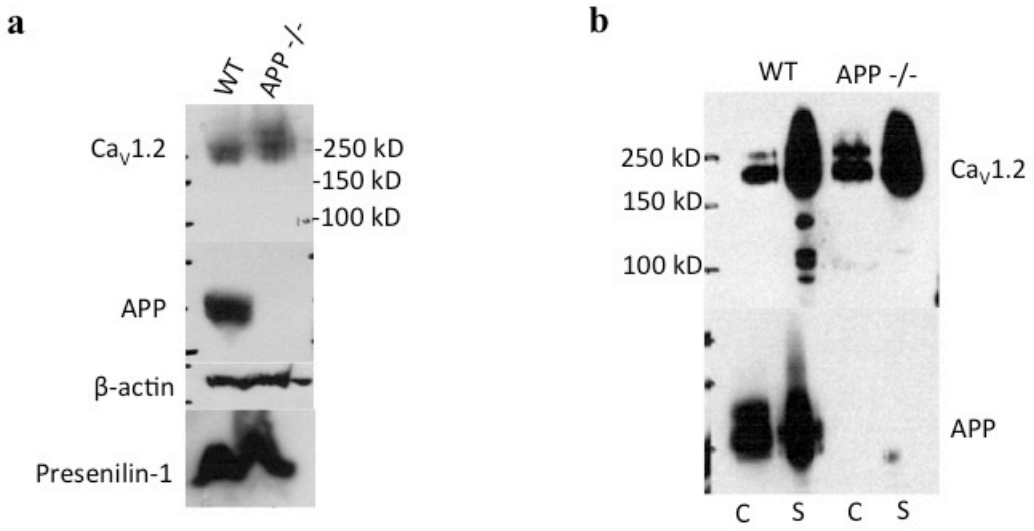

Figure 5.10 Comparing proteolysis patterns of $Ca_V1.2$ in wild-type (WT) and APP-/- mice. (a) Brain homogenate from mice (P7-9). Anti-$Ca_V1.2$ (top) only reveals full-length channel in both WT and APP samples. APP, β-actin and presenilin-1 levels indicated for both WT and APP-/- samples. (b) Hippocampal neuronal cultures (DIV 14) from WT and APP-/- mice. Samples were split into cytoplasmic (C) flow-through fractions and surface (S) biotinylated fractions. Anti-$Ca_V1.2$ reveals the ~100 kD band in surface fractions of WT neurons but not in APP-/- neurons. Anti-APP shows APP levels in both WT and APP-/- neurons.

I next wanted to see whether culturing these neurons *in vitro* would induce the proteolysis so often observed in rat hippocampal neurons. Performing side-by-side cultures of P0/P1 WT and APP-/- mice, I plated hippocampal neurons under normal culture conditions and let them grow for 14 days. At that point, neurons from both groups were biotinylated and processed for western blots. The cytosolic samples from both mice showed no difference in the proteolysis pattern of $Ca_V1.2$. Interestingly, the surface samples showed a dramatic difference. WT surface $Ca_V1.2$ was highly proteolyzed with distinct bands at ~140 kD and ~100 kD (Figure 5.10 b). These bands were completely

absent in the APP-/- surface sample. Consistent with this observation, there appeared to be slightly more full-length $Ca_V1.2$ in the APP-/- mice. As expected, there was no APP present in the APP-/- neurons.

Why these bands would be so heavily expressed on the surface, but not present at all in the cytoplasmic pool could be explained by a protein concentration issue. Only 1% of the total cytoplasmic sample was loaded onto the gel, whereas 10% of the surface sample was loaded. Regardless, the protein levels between the two different mice were equal, so the difference in surface fragments is significant. Having observed APP-induced proteolysis of $Ca_V1.2$ in mouse cultures, APP-/- neurons can be used to transfect different forms of APP and measure endogenous $Ca_V1.2$ proteolysis patterns.

5.2.8 There is no proteolysis in HEK 293 cells

Hippocampal neurons have only a 5-10% transfection efficiency and are therefore not suitable for Westerns on transfected proteins. Therefore, in order to perform co-immunoprecipitations (co-IPs) to test the association between APP and $Ca_V1.2$, as well as Westerns to look at differences in $Ca_V1.2$ proteolysis in response to different APPs, a heterologous system must be used. Due to the seasonality of oocytes as a model system, a more reliable model system is the HEK293-$\beta_3\alpha_2\delta$ stable line.

Cells were either untransfected, transfected with hL, or transfected with both hL and APP. In all cases, cytoplasmic and surface protein samples were collected. There did not appear to be any marked proteolysis of hL in the cytoplasmic (flow-thru) samples and there were no proteolysis products detected in the surface protein samples regardless of

whether APP was coexpressed (Figure 5.11). It appears that the proteolysis that occurs in neurons and oocytes does not occur in HEK 293 cells. Perhaps the necessary, and unknown, proteases and auxiliary proteins are not endogenously expressed.

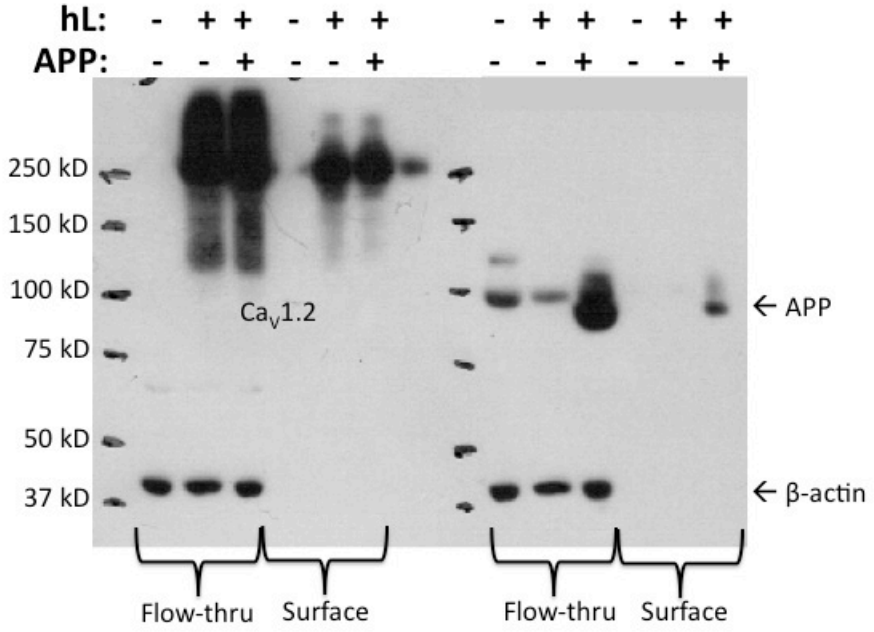

Figure 5.11 $Ca_V1.2$ proteolysis is absent in the HEK293 β_3-$\alpha_2\delta$ stable line. Western on biotinylated samples collected from cells transfected with hL with or without APP. Cytosolic (flow-thru) and surface proteins stained with anti-$Ca_V1.2$ II-III loop antibody, anti-APP antibody, and anti-β-actin antibody. There is little to no proteolysis of hL and no difference in hL proteolysis patterns when APP is coexpressed. HEK293 cells have a small amount of endogenous APP found in cytosolic fractions, which is absent in surface fractions. Only transfected HEK293 cells have surface APP.

5.2.9 APP and hL do not co-IP in HEK cells or oocytes

Based on observations that APP and $Ca_V1.2$ co-immunoprecipitate from HEK 293 cells and mouse brain (Yang et al., 2009), and that APP induces a change in channel current, there is a strong possibility that APP and $Ca_V1.2$ are directly interacting. To test this hypothesis, I tagged hL with a flag tag on the N-terminus (Flag-hL) and tagged APP with a HA tag on the N-terminus (HA-APP) and both were transfected into the HEK293-$\beta_3\alpha_2\delta$ stable cell line. Even if $Ca_V1.2$ proteolysis does not occur in HEK 293 cells, APP and hL may still interact in this system. Using Flag or HA beads (Sigma) I was able to purify the transfected proteins from the cell lysates. If there was any interaction between the two proteins, HA-APP should be pulled down with the Flag beads and Flag-hL pulled down with the HA beads. Strangely, when HA-APP was coexpressed with Flag-hL, it was no longer pulled down by HA beads (Figure 5.12 a and b). This also happened in a repeat experiment, suggesting that the presence of the channel either impeded the HA tag from binding to the beads or induced proteolysis of the N-terminus off APP. Flag-hL was not pulled down with HA-APP, most likely for one of the same reasons.

To circumvent this issue, I moved the HA tag to the C-terminus of APP. In this case, HA-APP was pulled down by the HA beads, however Flag-hL was not pulled down with it in HEK293-$\beta_3\alpha_2\delta$ cells (Figure 5.12 c). Because APP had such a robust effect on hL current in oocytes, they might serve as a better model system for looking at interactions between the proteins. Surprisingly, the same result was observed in oocytes (Figure 5.12 d). Therefore, it appears that the two proteins do not directly interact.

However, this does not rule out an indirect interaction, since HEK293 cells and oocytes may not express the other proteins necessary for an interaction to occur.

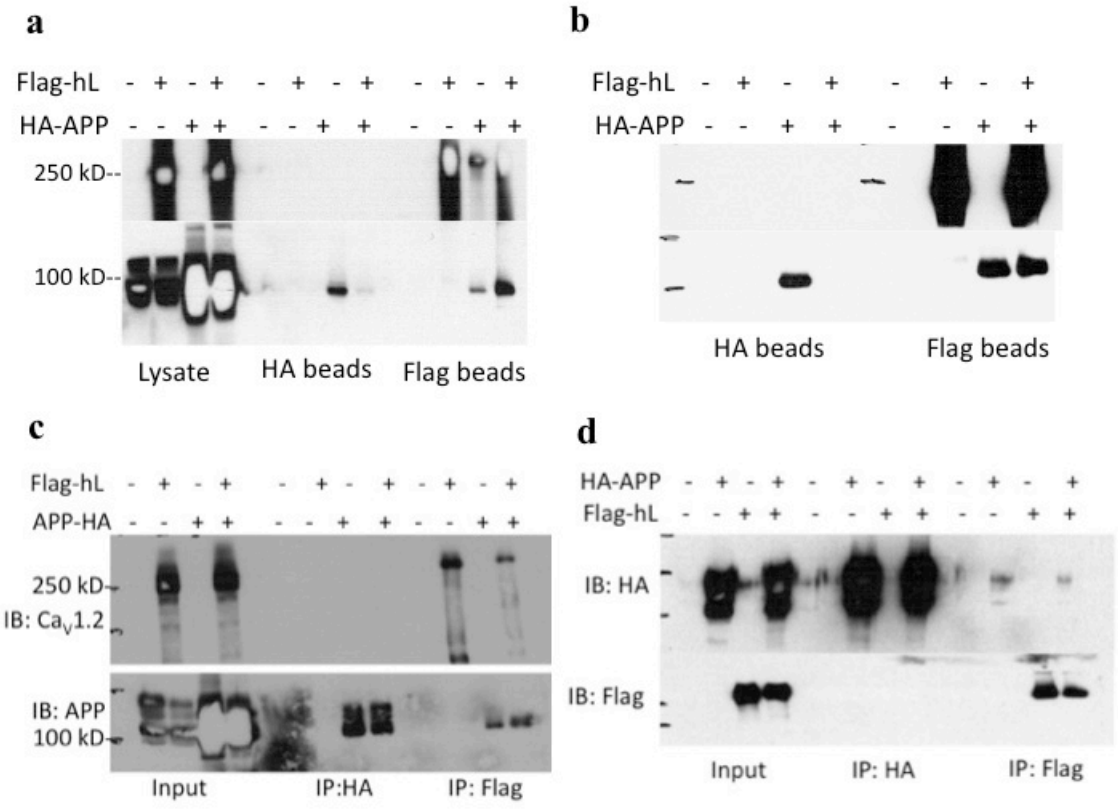

Figure 5.12 There is no apparent association between hL and APP. (a and b) Co-IPs with N-terminally HA tagged APP in HEK293 β_3-$\alpha_2\delta$ stable line. When Flag-hL is coexpressed with HA-APP, HA-APP can no longer be pulled down with HA beads. Flag-hL is not pulled down with HA-APP using HA beads. HA-APP appears to be pulled down with Flag-hL, but is pulled down at the same rate with Flag beads and no Flag-hL present, indocating this is background APP. (c) Co-IP with C-terminally HA tagged APP in HEK293 β3-α2δ stable line. HA beads pull down APP-HA when alone or coexpressed with Flag-hL. Flag-hL is not pulled down with APP-HA by HA beads. APP-HA is pulled down by Flag beads when Flag-hL is not expressed indicating this is background binding. APP and hL do not appear to associate in HEK293 cells. (d) Co-IP of C-terminally HA tagged APP and Flag-hL isolated from injected *Xenopus* oocytes. Flag-hL is not pulled down with APP-HA by HA beads. APP-HA is not pulled down by Flag-hL with Flag beads. APP and hL do not appear to associate in oocytes.

5.2.10 Effect of APP mutants on $Ca_V1.2$ current in oocytes

Many different mutations in APP are linked to Familial Alzheimer's disease (FAD). One particularly well studied FAD APP mutant has a valine to phenylalanine (V642F) mutation in the γ-secretase cut site (Goate et al., 1991). This mutation causes γ-secretase to cut APP at a site that releases more of the toxic Aβ42, eventually causing more Aβ plaques. On the other hand, the APP mutation that seems to have a protective effect against Alzheimer's disease (Jonsson et al., 2012) forces APP to undergo the non-amlyoidogenic pathway of proteolytic processing by α-secretase. Since wild-type APP has such a dramatic effect on $Ca_V1.2$ current, I wanted to investigate whether mutations to APP altered this effect. Indeed, the FAD mutant APP_V642F further decreased hL current when coexpressed in oocytes (Figure 5.13 a). Even more interesting was that this decrease in peak current amplitude was partially rescued when hL was coexpressed with the protective mutant, APP_A598T (Figure 5.13 a). While the FAD mutant shifted the I-V curve to the right, the protective mutant did not reverse the effect wild-type APP had on the current-voltage relationship of hL (Figure 5.13 b).

If the decrease in hL peak current when APP is present is due to the channel being cut, and the FAD mutant enhances this effect while the protective mutant dampens it, one would expect that the amount of ~100 kD band would vary accordingly. However, when a Western was performed on the lysates of oocytes injected with hL and APP, APP_A598T, or APP_V642F, no difference was seen in the intensity of the ~100 kD band in any of the groups injected with APP variations (Figure 5.13 c). Of greater concern was the observation that when samples are stained with an antibody against APP, the band appears at the same ~100 kD molecular weight. Is it possible that the $Ca_V1.2$ II-

III loop Sigma antibody is somehow recognizing APP? The antibody epitope shares four consecutive residues in common with APP, not usually enough to elicit a reaction. To test this possibility, oocytes were injected with just APP and run on a Western against samples injected with both the channel and APP variations. Indeed, the ~100 kD band appeared in the sample where no channel was present and only APP was expressed (Figure 5.13 d). This raises the possibility that the ~100 kD band observed in oocytes is actually APP.

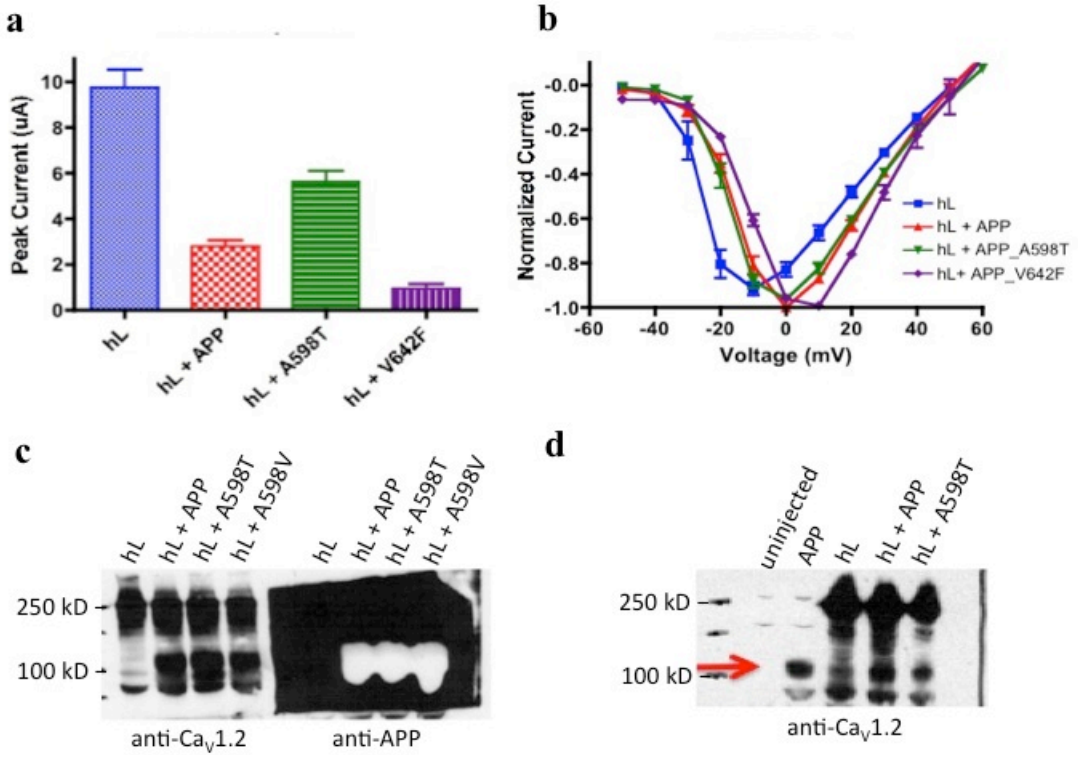

Figure 5.13 APP mutants' effect on current and proteolysis of hL. (a) Peak Ba^{2+} currents of hL, β_3 and $\alpha_2\delta$ without (hL, blue, N = 11), with APP (hL + APP, red, N = 13), with protective APP (hL + A598T, green, N= 17) and with FAD APP (hL + V642F, purple, N = 10). Currents were recorded at +10 mV in whole oocytes and averaged. Error bars represent SE. Peak current of hL was reduced by the presence of wild-type (WT) APP and dramatically reduced by the presence of FAD APP mutant (V642F). The protective APP mutant, while still reducing current, partially rescued the effect of WT APP. (b) I-V curve of hL (blue, N = 15), hL + APP (red, N = 13), hL + APP_A598T (green, N = 10) and hL + APP_V642F (purple, N = 12). A +10 mV shift occurs when WT APP is present and a +20 mV shift occurs with FAD APP mutant (V642F). The protective APP mutant (A598T) has the same effect as WT APP. All error bars represent SE. (c) Western blot of membrane fractionated lysates taken from oocytes injected with hL, hL + WT APP, hL + APP protective mutant (A598T) and hL + APP FAD mutant (A598V). The ~100 kD band appears with equal intensity when any version of APP is coexpressed with $Ca_V1.2$. APPs are expressed at equal levels in all samples (white blotches on black background). (d) Western blots of membrane fractionated lysates taken from uninjected oocytes, oocytes injected with just hL, just APP, hL + APP, and hL + protective mutant APP (A598T) stained with anti-$Ca_V1.2$ II-III loop antibody (Sigma). The ~100 kD band appears when APP is expressed, regardless of whether hL is expressed.

5.2.11 Imaging reveals APP-dependent proteolysis of $Ca_V1.2$ in neurons

While Western blots from cortical slices, neurons, HEK 293 cells and oocytes remain inconclusive, the functional data points to possible proteolysis of the channel. Another way to examine this is using the imaging method described in Chapter 3. Transfecting LGH3 (Chapter 3, Figure 3.2 a) into neurons along with different forms of APP would allow visualization of the channel separating on the membrane if it is indeed cut. The channel is tagged with an intracellular GFP on the N-terminus, so LGH3 in the cytosol and on the membrane will glow green (Figure 5.14 a left). Only channel that is on the plasma membrane will be stained with the HA antibody, and therefore red signal represents surface LGH3 (Figure 5.14 a middle). Quantifying the overlay of signals (Figure 5.14 a right) would give a non-colocalization index (NCI) for each group of neurons. This method also does not require the use of the Sigma II-III loop antibody, so there is limited risk in non-specifically staining APP.

When LGH3 was coexpressed with wild-type APP, there was no significant shift in the NCI from when LGH3 was expressed alone (Figure 5.14 b). This is not surprising, since neurons have a high level of endogenous APP expression, the LGH3 expressed alone could still be interacting with native APP. Interestingly, when LGH3 was coexpressed with the protective mutant of APP, APP_A598T, the NCI shifted to the left (Figure 5.14 b), indicating less red/green separation on the membrane, and hence less proteolysis. The same effect was seen in another batch of neurons (Figure 5.14 c). Even more striking was the NCI shift when LGH3 was coexpressed with an FAD mutant, APP_A598V. This mutant caused a dramatic NCI shift to the right, indicating greater proteolysis of the channel (Figure 5.14 c).

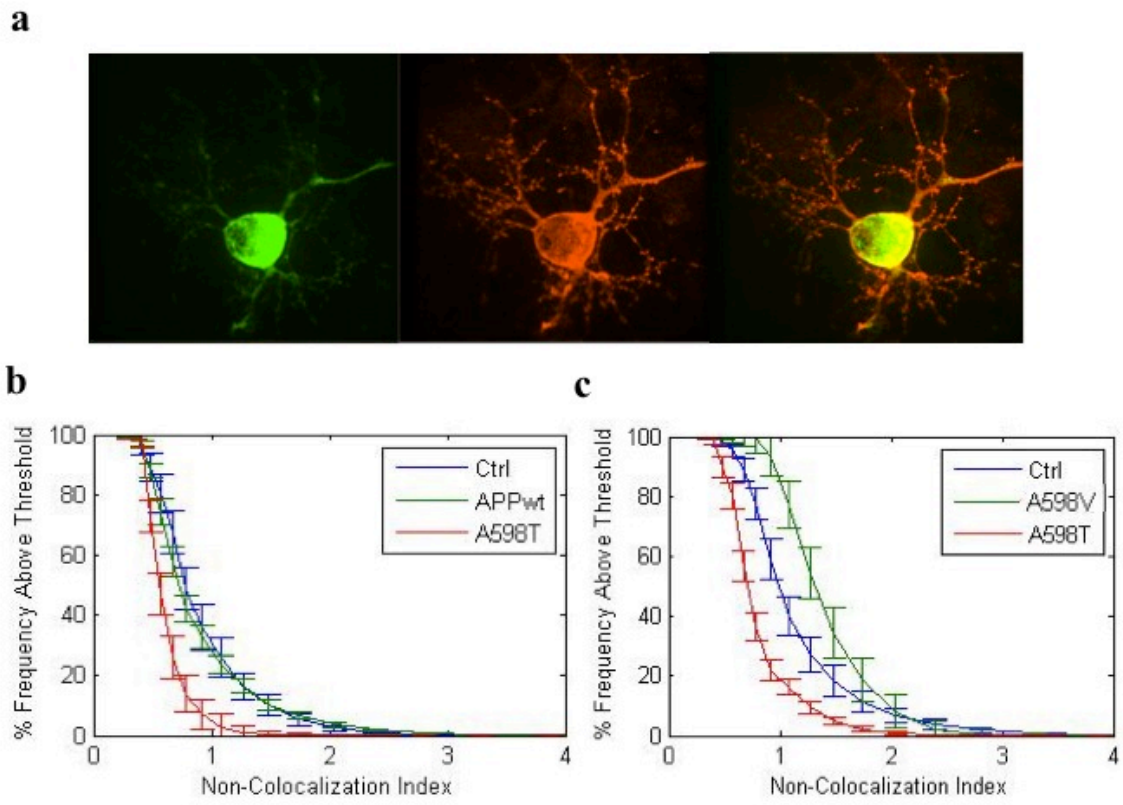

Figure 5.14 APP FAD and protective mutant effects on the separation of surface LGH3. (a) Representative hippocampal neuron expressing LGH3 and APP. Left: GFP representing total LGH3. Middle: HA-Alexa 594 representing surface LGH3. Right: Overlay, yellow representing surface channels containing GFP and red representing surface channels without associated GFP. (b) Graph displaying the red/green ratio of LGH3 in transfected neurons alone (Ctrl), with wild-type APP (APPwt), with the APP protective mutant (A598T) or a FAD APP mutant (A598V). Values greater than 1 represent increased separation of red and green, signifying mid-channel proteolysis.

5.3 DISCUSSION

My studies show that APP has an effect on $Ca_V1.2$ current (Figure 5.3-4). Reduction of Ca^{2+} current from L-type VGCCs when APP is present has previously been shown in mouse neurons (Yang et al., 2009), however the shift in the current-voltage relationship and inactivation properties is a new finding. Even more interesting, I found that the FAD APP mutants further enhance APP's effect on channel current (Figure 5.13). Astonishingly, the recently discovered APP protective mutant (APP_A598T) partially reversed the inhibition APP induced on the channel, displaying a restorative effect on channel function (Figure 5.13). Another very interesting observation was that inhibiting presenilin-1 has a dramatic effect on $Ca_V1.2$ current, as DAPT completely reversed the APP-induced current inhibition (Figure 5.6 a). While the APP_A598T effect could be considered incompatible with the DAPT effect, it shouldn't be. Perhaps decreasing β-secretase cleavage leads to a decrease in γ-secretase recruitment, since γ-secretase prefers to cut proteins that have already shed their ectodomians. The amount of soluble Aβ released could also be what is inhibiting channel function since DAPT and the protective mutant prevent Aβ from being released, however after applying conditioned media containing Aβ no change was found in peak current (data not shown).

That I was unable to show an association between APP and $Ca_V1.2$ is disappointing (Figure 5.12). However, negative data is never conclusive. One reason could have been that the system I used prevented me from being able to observe an interaction. For example, the HA- and Flag- tags tethered to the proteins could have interfered in their interaction. I did show that the placement of the tag on APP was very important to be able to pull down APP. The two proteins could also interact in a more

transient manner, or could perhaps interact through auxiliary proteins. Perhaps it is one of the many APP fragments (Figure 5.2) that interacts with the channel to inhibit current, and that fragment was not tagged. Additionally, APP could be interacting with another protein that in turn affects the channel current. It has been reported that APP and $Ca_V1.2$ directly interact since they were able to be co-precipitated in HEK 293 cells and whole brain lysate (Yang et al., 2009). However, an important detail to note is that the authors of this paper pulled down the channel with an antibody against the same epitope as the II-III loop Sigma antibody, an antibody I found to non-specifically stain APP. If APP can be stained by the antibody, the antibody must bind to APP, and therefore would pull APP down regardless of the channel being present. The authors did not do the proper control experiment of a co-IP using the $Ca_V1.2$ II-III loop antibody on cells only transfected with APP. Therefore, the notion that these two proteins interact, while plausible, is still not substantiated by experimental evidence.

Unfortunately, no conclusive evidence of proteolysis besides the separation in imaging experiments (Figure 5.14) could be gained. While the I-V curve and inactivation profile of $Ca_V1.2$ in the presence of APP looks very similar to that of the fragment channels (Chapter 4, Figure 4.1), more experiments need to be done to see whether APP is stimulating proteolysis of the channel. APP at first seemed to induce the proteolysis of $Ca_V1.2$ in oocytes, causing the appearance of a ~100 kD band in Western blots (Figure 5.5). Unfortunately, it was later found that APP is a non-specific target of the $Ca_V1.2$ II-III loop Sigma antibody (Figure 5.13 d), and therefore the ~100 kD band in Western blots could possibly be APP. Strangely, DAPT reversed the appearance of this band in oocytes (Figure 5.6 d), while APP levels remained similar. Also puzzling was the effect of the

cut-site mutants on the appearance of the ~100 kD band (Figure 5.8 c), considering all mutants were coexpressed with the same levels of APP. Therefore, this band could still be the channel and more experiments should be done with different antibodies to determine this. If this band is actually full-length APP, its disappearance with DAPT and the channel mutants could signify that the channel is somehow regulating the expression of APP. The inability to generate this ~100 kD band in HEK 293 cells was not surprising. Other, unknown proteins not endogenously expressed in HEK 293 cells could be needed for proteolysis to take place. Primary neurons and cortical slices did show a ~110 kD band, however it was not as easily manipulated with DAPT treatment (Figure 5.9). Optimal DAPT concentration and treatment time can vary in neurons, so perhaps more experimental variations should have been tested. This band was absent in APP-/- neurons (Figure 5.10) suggesting it is APP induced, but this could also be due to nonspecific antibody staining.

Mid-channel proteolysis of $Ca_V1.2$ changes with age and happens in response to channel activity and increased intracellular Ca^{2+}. AD is an age-dependent disease that is characterized by disrupted Ca^{2+} homeostasis. Both processes involve multiple proteases. It is a rational hypothesis to investigate whether there is a link between the two. Clearly, APP and presenilin exert an inhibitory effect on the L-type channel, however the mechanism remains to be uncovered. Whether or not APP induces proteolysis of the channel or presenilin cleaves the channel remains to be resolved. More experiments are necessary, in different model systems, to identify what other proteins could be involved and how APP, presenilin and $Ca_V1.2$ interact with each other to change channel function.

Chapter 6

Concluding Remarks and Future Prospects

6.1 Mid-channel Proteolysis of $Ca_V1.2$

Our lab has uncovered a new form of L-type channel regulation that involves the proteolysis of the channel in the main body of the α_1 subunit in response to increased intracellular calcium, channel activity and age of the animal. In Chapter 3, I addressed the effect this proteolysis has on the function of the channel. I found that the immediate effect of a protease cutting the channel in the intracellular loops is a shift in gating properties, however over a longer time scale, proteolysis dramatically decreased channel current. This is possibly due to a separation of the fragments on the membrane, since it was determined that fragment channels can still traffic to the membrane and function. One caveat to these experiments was they measured a channel that was engineered with a cut site for the protease of my choice. Therefore, many questions remain about the functional effect of the actual endogenous protease responsible for $Ca_V1.2$ mid-channel proteolysis. Proteolysis was reduced, but not abolished, when calpains were inhibited, signaling another protease must be involved. More experiments are necessary to decipher the protease(s) responsible for mid-channel proteolysis and to uncover the precise cleavage site on the α_1 subunit.

Mid-channel proteolysis appears to be a novel form of $Ca_V1.2$ regulation. It will be interesting to see whether other channels, such as voltage-gated sodium channels, are regulated in the same manner. There are also a myriad of co-factors yet to be discovered

that aid in this regulation. We have already shown that ubiquitin and the PEST sequences on α_1 are involved. The Ca_V1 C-terminal proteolysis involved in β-adrenergic regulation was discovered in 1991 (Catterall, 1991), and papers are still being published today parsing out the details of this complicated mechanism. Perhaps we have only scratched the surface of how mid-channel proteolysis is initiated and how it ultimately regulates intracellular Ca^{2+} levels.

6.2 The Fate and Function of Fragment Channels

Mid-channel proteolysis creates fragment channels that can remain on the plasma membrane. In Chapter 4, I was able to show that fragment channels formed from cuts in any of the three intracellular loops can still function when properly paired with one another. Moreover, one set of improperly paired fragment channels produced current, albeit very little. Intriguingly, all three sets of fragment channel exhibited the same shift in inactivation and their current-voltage relationship. Some fragments were also able to impact the function of the full-length channel and almost all fragments interacted with either the channel complex or α_1 itself. These results are not entirely consistent with work done on other constructed channel fragments (Raghib et al., 2001), however those N-type fragments were less physiologically relevant considering they were modeled after P/Q-type channel disease truncations. In contrast, we have shown that the L-type channel undergoes mid-channel proteolysis under normal conditions *in vivo*, and therefore the fragment channels that result are physiologically relevant. To my knowledge, these are the first experiments done to assess the functionality of L-type fragment channels.

The dominant negative effect of fragment C2 leaves many unanswered questions. What is the nature of C2's inhibitory effect? It binds to the channel complex, but does this decrease surface expression by interfering with trafficking? Perhaps it binds to the full-length channel in the ER and triggers the unfolded protein response causing degradation (Page et al., 2004). It could also bind to the channel on the cell surface and prevent it from opening. Is the inhibition a result of the C-terminus or the entire C2 fragment? It is known that the distal C-terminus binds to the proximal C-terminus and inhibits the channel (Hulme et al., 2006). Recently it was reported that the distal C-terminus interferes with full-length channel transcription and overall protein expression (Bannister et al., 2013). These questions can be answered by looking at the surface expression of the full-length channel in the presence of C2. To narrow down the region on C2 responsible for $Ca_V1.2$ inhibition, C2 can be further truncated. Full-length channel function and surface expression can then be measured when the channel is coexpressed with these new variations of C2.

Collectively, my results demonstrate how the result of mid-channel proteolysis can impact $Ca_V1.2$ functionality and intracellular Ca^{2+} levels. While the ultimate fate of these fragments is still uncertain, their temporary existence allows them to form functional channels and interact with full-length channels on the membrane to alter gating properties. It remains to be determined whether fragment channels are the first step in protein degradation, or if they are created as a way to modulate calcium influx. Live cell imaging experiments could reveal the fate of these fragments after mid-channel proteolysis occurs, perhaps by visualizing them entering lysosomes below the surface.

6.3 The Effect of Amyloid-β Precursor Protein and Presenilin on $Ca_V1.2$

In Chapter 5, I investigated the role AD related proteins might play in mid-channel proteolysis. I was able to show that coexpression of APP with $Ca_V1.2$ in *Xenopus* oocytes decreases channel current and shifts inactivation and the current-voltage relationship in the same manner as fragment channels. FAD APP mutants exasperated this effect. Interestingly, an AD protective APP mutant had the opposite effect, increasing $Ca_V1.2$ currents towards levels seen in the absence of wild-type APP. Furthermore, I was able to reverse APP-induced inhibition by adding a γ-secretase inhibitor to the oocyte media. γ-secretase is a multimeric complex consisting of presenilin, PEN-2, nicastrin, and APH-1 (Selkoe and Wolfe, 2007) of which presenilin is the catalytic component. These data suggest that presenilin is inhibiting $Ca_V1.2$ and that APP acts to target γ-secretase to the channel. Another experiment that could be done to further solidify these results would be to activate γ-secretase by coexpressing GASP in the absence of APP and see whether this decreases $Ca_V1.2$ current (He et al., 2010). Presenilin has high endogenous expression in oocytes, therefore coinjecting a siRNA against presenilin should have the same effect as DAPT if presenilin were specifically responsible for the decrease in channel current. All of the above experiments were performed using *Xenopus* oocytes. Therefore, it would be ideal to confirm these results using another model system such as a HEK 293 stable cell line expressing $Ca_V1.2$, $\alpha_2\delta$ and β_3. Whole cell recordings could then be performed after transient transfection of APP or after DAPT treatment to measure $Ca_V1.2$ current.

Due to γ-secretase being a protease and the channel displaying the same biophysical properties as fragment channels when in the presence of APP, I wanted to

determine whether the channel was being cleaved by presenilin. Western blots stained with an antibody against the II-III loop of $Ca_V1.2$ confirmed that a ~100 kD band appeared when APP was coexpressed. This band was completely absent when APP injected oocytes were treated with DAPT. Surprisingly, $Ca_V1.2$ harbors a consensus site that mirrors that of the APP γ-secretase cut site in a region of the channel that would produce a ~115 kD fragment. When this site on the channel was mutated, the ~100 kD band did not appear in Western blots. Unfortunately, when APP was injected without $Ca_V1.2$ the ~100 kD band also appeared. This posed a major setback to my research, since the L-type II-III loop antibody I had been so faithfully using was cross-reacting with APP. I tried to repeat the experiments using a HA-tagged APP and incubating the lysate with HA beads to remove the APP protein. However, this method did not work since APP still appeared in Western blots. This could have been caused by a saturation of the HA beads or because the HA tag was cleaved from APP, something I found to happen during co-immunoprecipitation experiments. A similar method could be used by tagging the channel in a region close to the II-III loop epitope. The tagged channel could then be pulled down and stained with II-III loop antibody, and the samples would presumably be rid of APP. Another option would be to affinity purify the antibody against APP. It is however very possible that the II-III loop antibody is staining a $Ca_V1.2$ fragment that happens to be of a similar size to APP.

It is critical that the effect of APP and presenilin on $Ca_V1.2$ be observable in primary neurons. While the DAPT effect in rat hippocampal neurons was not reproducible, there are some modifications that could be made to optimize the experiment. For example, lower concentrations of DAPT could be tried, since it is known

that DAPT concentrations can have differing effects on presenilin stability and rate of activity (Barthet et al., 2011). My experiments were all performed in hippocampal neurons, however another type of neuron, such as striatal neurons (Yang et al., 2009), might be more susceptible to DAPT treatment. There were some promising results using the APP-/- hippocampal cultures and these will be a very useful model system for future experiments. These neurons can be used to transfect various forms of APP and assess the effect on $Ca_V1.2$. Lastly, imaging experiments performed on neurons showed that APP mutants had an effect on channel separation on the plasma membrane. The co-localization index of the channel coexpressed with these APP mutants trended with the effect the mutants had on channel current.

Alzheimer's disease research has focused so heavily on the amyloid hypothesis over the years, however the mechanism of disease is likely to be far more convoluted. First, no one is certain what role APP plays in the normal physiology of the cell. Knockout models provide clues to processes it is involved in, but most mechanistic studies are focused on APP in the disease state. AD is likely to involve many molecular pathways. Aβ could just be a small part of a larger signaling cascade that ultimately causes AD, and $Ca_V1.2$ could be a part of that cascade. It is not unlikely that AD would eventually increase mid-channel proteolysis, since the cell would try to regain control over Ca^{2+} levels. Further experiments are necessary to determine if there is a link between mid-channel proteolysis and this devastating aging disease.

References

Abele, K., and Yang, J. (2012). Regulation of voltage-gated calcium channels by proteolysis. Sheng Li Xue Bao *64*, 504-514.

Albert, M.S. (2011). Changes in cognition. Neurobiol Aging *32 Suppl 1*, S58-63.

Altier, C., Dale, C.S., Kisilevsky, A.E., Chapman, K., Castiglioni, A.J., Matthews, E.A., Evans, R.M., Dickenson, A.H., Lipscombe, D., Vergnolle, N.*, et al.* (2007). Differential role of N-type calcium channel splice isoforms in pain. J Neurosci *27*, 6363-6373.

Anekonda, T.S., Quinn, J.F., Harris, C., Frahler, K., Wadsworth, T.L., and Woltjer, R.L. (2011). L-type voltage-gated calcium channel blockade with isradipine as a therapeutic strategy for Alzheimer's disease. Neurobiol Dis *41*, 62-70.

Arispe, N., Rojas, E., and Pollard, H.B. (1993). Alzheimer disease amyloid beta protein forms calcium channels in bilayer membranes: blockade by tromethamine and aluminum. Proc Natl Acad Sci U S A *90*, 567-571.

Bajjalieh, S.M., and Scheller, R.H. (1995). The biochemistry of neurotransmitter secretion. The Journal of biological chemistry *270*, 1971-1974.

Bangalore, R., Mehrke, G., Gingrich, K., Hofmann, F., and Kass, R.S. (1996). Influence of L-type Ca channel alpha 2/delta-subunit on ionic and gating current in transiently transfected HEK 293 cells. The American journal of physiology *270*, H1521-1528.

Bannister, J.P., Leo, M.D., Narayanan, D., Jangsangthong, W., Nair, A., Evanson, K.W., Pachuau, J., Gabrick, K.S., Boop, F.A., and Jaggar, J.H. (2013). The voltage-dependent L-type Ca2+ (CaV1.2) channel C-terminus fragment is a bi-modal vasodilator. The Journal of physiology *591*, 2987-2998.

Baroudi, G., Qu, Y., Ramadan, O., Chahine, M., and Boutjdir, M. (2006). Protein kinase C activation inhibits Cav1.3 calcium channel at NH2-terminal serine 81 phosphorylation site. Am J Physiol Heart Circ Physiol *291*, H1614-1622.

Barrett, C.F., and Tsien, R.W. (2008). The Timothy syndrome mutation differentially affects voltage- and calcium-dependent inactivation of CaV1.2 L-type calcium channels. Proceedings of the National Academy of Sciences of the United States of America *105*, 2157-2162.

Barthet, G., Shioi, J., Shao, Z., Ren, Y., Georgakopoulos, A., and Robakis, N.K. (2011). Inhibitors of gamma-secretase stabilize the complex and differentially affect processing of amyloid precursor protein and other substrates. FASEB J *25*, 2937-2946.

Bean, B.P. (1989). Classes of calcium channels in vertebrate cells. Annual review of physiology *51*, 367-384.

Bech-Hansen, N.T., Naylor, M.J., Maybaum, T.A., Pearce, W.G., Koop, B., Fishman, G.A., Mets, M., Musarella, M.A., and Boycott, K.M. (1998). Loss-of-function mutations in a calcium-channel alpha1-subunit gene in Xp11.23 cause incomplete X-linked congenital stationary night blindness. Nature genetics *19*, 264-267.

Beguin, P., Ng, Y.J., Krause, C., Mahalakshmi, R.N., Ng, M.Y., and Hunziker, W. (2007). RGK small GTP-binding proteins interact with the nucleotide kinase domain of Ca2+-channel beta-subunits via an uncommon effector binding domain. The Journal of biological chemistry *282*, 11509-11520.

Bell, T.J., Thaler, C., Castiglioni, A.J., Helton, T.D., and Lipscombe, D. (2004). Cell-specific alternative splicing increases calcium channel current density in the pain pathway. Neuron *41*, 127-138.

Ben Johny, M., Yang, P.S., Bazzazi, H., and Yue, D.T. (2013). Dynamic switching of calmodulin interactions underlies Ca2+ regulation of CaV1.3 channels. Nat Commun *4*, 1717.

Bernstein, G.M., and Jones, O.T. (2007). Kinetics of internalization and degradation of N-type voltage-gated calcium channels: role of the alpha2/delta subunit. Cell calcium *41*, 27-40.

Berridge, M.J. (2010). Calcium hypothesis of Alzheimer's disease. Pflugers Arch *459*, 441-449.

Bers, D.M. (2002). Cardiac excitation-contraction coupling. Nature *415*, 198-205.

Bezanilla, F. (2002). Voltage sensor movements. The Journal of general physiology *120*, 465-473.

Bezprozvanny, I., Scheller, R.H., and Tsien, R.W. (1995). Functional impact of syntaxin on gating of N-type and Q-type calcium channels. Nature *378*, 623-626.

Bi, X., Chang, V., Molnar, E., McIlhinney, R.A., and Baudry, M. (1996). The C-terminal domain of glutamate receptor subunit 1 is a target for calpain-mediated proteolysis. Neuroscience *73*, 903-906.

Bichet, D., Cornet, V., Geib, S., Carlier, E., Volsen, S., Hoshi, T., Mori, Y., and De Waard, M. (2000). The I-II loop of the Ca2+ channel alpha1 subunit contains an endoplasmic reticulum retention signal antagonized by the beta subunit. Neuron *25*, 177-190.

Birnbaumer, L., Qin, N., Olcese, R., Tareilus, E., Platano, D., Costantin, J., and Stefani, E. (1998). Structures and functions of calcium channel beta subunits. Journal of bioenergetics and biomembranes *30*, 357-375.

Black, J.L., 3rd (2003). The voltage-gated calcium channel gamma subunits: a review of the literature. Journal of bioenergetics and biomembranes *35*, 649-660.

Bourinet, E., Soong, T.W., Sutton, K., Slaymaker, S., Mathews, E., Monteil, A., Zamponi, G.W., Nargeot, J., and Snutch, T.P. (1999). Splicing of alpha 1A subunit gene generates phenotypic variants of P- and Q-type calcium channels. Nature neuroscience *2*, 407-415.

Buraei, Z., and Yang, J. (2010). The beta subunit of voltage-gated Ca2+ channels. Physiological reviews *90*, 1461-1506.

Cao, X., and Sudhof, T.C. (2001). A transcriptionally [correction of transcriptively] active complex of APP with Fe65 and histone acetyltransferase Tip60. Science *293*, 115-120.

Carbone, E., and Lux, H.D. (1984). A low voltage-activated, fully inactivating Ca channel in vertebrate sensory neurones. Nature *310*, 501-502.

Catalucci, D., Zhang, D.H., DeSantiago, J., Aimond, F., Barbara, G., Chemin, J., Bonci, D., Picht, E., Rusconi, F., Dalton, N.D., *et al.* (2009). Akt regulates L-type Ca2+ channel activity by modulating Cavalpha1 protein stability. J Cell Biol *184*, 923-933.

Catterall, W.A. (1991). Excitation-contraction coupling in vertebrate skeletal muscle: a tale of two calcium channels. Cell *64*, 871-874.

Catterall, W.A. (2000). Structure and regulation of voltage-gated Ca2+ channels. Annual review of cell and developmental biology *16*, 521-555.

Catterall, W.A. (2011). Voltage-gated calcium channels. Cold Spring Harb Perspect Biol *3*, a003947.

Catterall, W.A., and Few, A.P. (2008). Calcium channel regulation and presynaptic plasticity. Neuron *59*, 882-901.

Catterall, W.A., Leal, K., and Nanou, E. (2013). Calcium channels and short-term synaptic plasticity. The Journal of biological chemistry *288*, 10742-10749.

Chan, S.L., Mayne, M., Holden, C.P., Geiger, J.D., and Mattson, M.P. (2000). Presenilin-1 mutations increase levels of ryanodine receptors and calcium release in PC12 cells and cortical neurons. J Biol Chem *275*, 18195-18200.

Chen, Y.H., Li, M.H., Zhang, Y., He, L.L., Yamada, Y., Fitzmaurice, A., Shen, Y., Zhang, H., Tong, L., and Yang, J. (2004). Structural basis of the alpha1-beta subunit interaction of voltage-gated Ca2+ channels. Nature *429*, 675-680.

Cheung, K.H., Shineman, D., Muller, M., Cardenas, C., Mei, L., Yang, J., Tomita, T., Iwatsubo, T., Lee, V.M., and Foskett, J.K. (2008). Mechanism of Ca2+ disruption in Alzheimer's disease by presenilin regulation of InsP3 receptor channel gating. Neuron *58*, 871-883.

Cook, D.G., Li, X., Cherry, S.D., and Cantrell, A.R. (2005). Presenilin 1 deficiency alters the activity of voltage-gated Ca2+ channels in cultured cortical neurons. J Neurophysiol *94*, 4421-4429.

Coon, A.L., Wallace, D.R., Mactutus, C.F., and Booze, R.M. (1999). L-type calcium channels in the hippocampus and cerebellum of Alzheimer's disease brain tissue. Neurobiol Aging *20*, 597-603.

Correll, R.N., Botzet, G.J., Satin, J., Andres, D.A., and Finlin, B.S. (2008a). Analysis of the Rem2 - voltage dependant calcium channel beta subunit interaction and Rem2 interaction with phosphorylated phosphatidylinositide lipids. Cellular signalling *20*, 400-408.

Correll, R.N., Pang, C., Niedowicz, D.M., Finlin, B.S., and Andres, D.A. (2008b). The RGK family of GTP-binding proteins: regulators of voltage-dependent calcium channels and cytoskeleton remodeling. Cellular signalling *20*, 292-300.

Coulson, E.J., Paliga, K., Beyreuther, K., and Masters, C.L. (2000). What the evolution of the amyloid protein precursor supergene family tells us about its function. Neurochem Int *36*, 175-184.

Cox, R.H., and Fromme, S.J. (2013). A naturally occurring truncated Cav1.2 alpha1-subunit inhibits Ca2+ current in A7r5 cells. Am J Physiol Cell Physiol *305*, C896-905.

Cueni, L., Canepari, M., Adelman, J.P., and Luthi, A. (2009). Ca(2+) signaling by T-type Ca(2+) channels in neurons. Pflugers Arch *457*, 1161-1172.

Dai, S., Hall, D.D., and Hell, J.W. (2009). Supramolecular assemblies and localized regulation of voltage-gated ion channels. Physiological reviews *89*, 411-452.

Dalton, S., Takahashi, S.X., Miriyala, J., and Colecraft, H.M. (2005). A single CaVbeta can reconstitute both trafficking and macroscopic conductance of voltage-dependent calcium channels. The Journal of physiology *567*, 757-769.

De Jongh, K.S., Warner, C., and Catterall, W.A. (1990). Subunits of purified calcium channels. Alpha 2 and delta are encoded by the same gene. The Journal of biological chemistry *265*, 14738-14741.

De Jongh, K.S., Warner, C., Colvin, A.A., and Catterall, W.A. (1991). Characterization of the two size forms of the alpha 1 subunit of skeletal muscle L-type calcium channels. Proceedings of the National Academy of Sciences of the United States of America *88*, 10778-10782.

De Strooper, B. (2010). Proteases and proteolysis in Alzheimer disease: a multifactorial view on the disease process. Physiol Rev *90*, 465-494.

DeMaria, C.D., Soong, T.W., Alseikhan, B.A., Alvania, R.S., and Yue, D.T. (2001). Calmodulin bifurcates the local Ca2+ signal that modulates P/Q-type Ca2+ channels. Nature *411*, 484-489.

Dolphin, A.C. (2003). Beta subunits of voltage-gated calcium channels. Journal of bioenergetics and biomembranes *35*, 599-620.

Dolphin, A.C. (2012). Calcium channel auxiliary alpha(2)delta and beta subunits: trafficking and one step beyond. Nat Rev Neurosci *13*, 542-555.

Eberst, R., Dai, S., Klugbauer, N., and Hofmann, F. (1997). Identification and functional characterization of a calcium channel gamma subunit. Pflugers Arch *433*, 633-637.

Emrick, M.A., Sadilek, M., Konoki, K., and Catterall, W.A. (2010). Beta-adrenergic-regulated phosphorylation of the skeletal muscle Ca(V)1.1 channel in the fight-or-flight response. Proceedings of the National Academy of Sciences of the United States of America *107*, 18712-18717.

Esler, W.P., and Wolfe, M.S. (2001). A portrait of Alzheimer secretases--new features and familiar faces. Science *293*, 1449-1454.

Evans, R.M., and Zamponi, G.W. (2006). Presynaptic Ca2+ channels--integration centers for neuronal signaling pathways. Trends in neurosciences *29*, 617-624.

Fan, M., Buraei, Z., Luo, H.R., Levenson-Palmer, R., and Yang, J. Direct inhibition of P/Q-type voltage-gated Ca2+ channels by Gem does not require a direct Gem/Cavbeta interaction. Proceedings of the National Academy of Sciences of the United States of America *107*, 14887-14892.

Fan, M., Zhang, W.K., Buraei, Z., and Yang, J. (2012). Molecular determinants of Gem protein inhibition of P/Q-type Ca2+ channels. The Journal of biological chemistry *287*, 22749-22758.

Fletcher, C.F., Lutz, C.M., O'Sullivan, T.N., Shaughnessy, J.D., Jr., Hawkes, R., Frankel, W.N., Copeland, N.G., and Jenkins, N.A. (1996). Absence epilepsy in tottering mutant mice is associated with calcium channel defects. Cell *87*, 607-617.

Freir, D.B., Costello, D.A., and Herron, C.E. (2003). A beta 25-35-induced depression of long-term potentiation in area CA1 in vivo and in vitro is attenuated by verapamil. J Neurophysiol *89*, 3061-3069.

Friedrich, O., von Wegner, F., Chamberlain, J.S., Fink, R.H., and Rohrbach, P. (2008). L-type Ca2+ channel function is linked to dystrophin expression in mammalian muscle. PLoS ONE *3*, e1762.

Fu, Y., Westenbroek, R.E., Yu, F.H., Clark, J.P., 3rd, Marshall, M.R., Scheuer, T., and Catterall, W.A. (2011). Deletion of the distal C terminus of CaV1.2 channels leads to loss of beta-adrenergic regulation and heart failure in vivo. The Journal of biological chemistry *286*, 12617-12626.

Fukuda, K., Kaneko, S., Yada, N., Kikuwaka, M., Akaike, A., and Satoh, M. (1996). Cyclic AMP-dependent modulation of N- and Q-type Ca2+ channels expressed in Xenopus oocytes. Neurosci Lett *217*, 13-16.

Fuller, M.D., Emrick, M.A., Sadilek, M., Scheuer, T., and Catterall, W.A. (2010). Molecular mechanism of calcium channel regulation in the fight-or-flight response. Sci Signal *3*, ra70.

Gao, T., Bunemann, M., Gerhardstein, B.L., Ma, H., and Hosey, M.M. (2000). Role of the C terminus of the alpha 1C (CaV1.2) subunit in membrane targeting of cardiac L-type calcium channels. The Journal of biological chemistry *275*, 25436-25444.

Gao, T., Cuadra, A.E., Ma, H., Bunemann, M., Gerhardstein, B.L., Cheng, T., Eick, R.T., and Hosey, M.M. (2001). C-terminal fragments of the alpha 1C (CaV1.2) subunit associate with and regulate L-type calcium channels containing C-terminal-truncated alpha 1C subunits. The Journal of biological chemistry *276*, 21089-21097.

Gao, T., Puri, T.S., Gerhardstein, B.L., Chien, A.J., Green, R.D., and Hosey, M.M. (1997). Identification and subcellular localization of the subunits of L-type calcium channels and adenylyl cyclase in cardiac myocytes. The Journal of biological chemistry *272*, 19401-19407.

Garcia, A.G., Garcia-De-Diego, A.M., Gandia, L., Borges, R., and Garcia-Sancho, J. (2006). Calcium signaling and exocytosis in adrenal chromaffin cells. Physiological reviews *86*, 1093-1131.

Gargus, J.J. (2006). Ion channel functional candidate genes in multigenic neuropsychiatric disease. Biological psychiatry *60*, 177-185.

Gerhardstein, B.L., Gao, T., Bunemann, M., Puri, T.S., Adair, A., Ma, H., and Hosey, M.M. (2000). Proteolytic processing of the C terminus of the alpha(1C) subunit of L-type calcium channels and the role of a proline-rich domain in membrane tethering of proteolytic fragments. The Journal of biological chemistry *275*, 8556-8563.

Goate, A., Chartier-Harlin, M.C., Mullan, M., Brown, J., Crawford, F., Fidani, L., Giuffra, L., Haynes, A., Irving, N., James, L.*, et al.* (1991). Segregation of a missense mutation in the amyloid precursor protein gene with familial Alzheimer's disease. Nature *349*, 704-706.

Gomez-Ospina, N., Panagiotakos, G., Portmann, T., Pasca, S.P., Rabah, D., Budzillo, A., Kinet, J.P., and Dolmetsch, R.E. (2013). A promoter in the coding region of the calcium channel gene CACNA1C generates the transcription factor CCAT. PLoS ONE *8*, e60526.

Gomez-Ospina, N., Tsuruta, F., Barreto-Chang, O., Hu, L., and Dolmetsch, R. (2006). The C terminus of the L-type voltage-gated calcium channel Ca(V)1.2 encodes a transcription factor. Cell *127*, 591-606.

Gray, A.C., Raingo, J., and Lipscombe, D. (2007). Neuronal calcium channels: splicing for optimal performance. Cell calcium *42*, 409-417.

Gray, P.C., Johnson, B.D., Westenbroek, R.E., Hays, L.G., Yates, J.R., 3rd, Scheuer, T., Catterall, W.A., and Murphy, B.J. (1998). Primary structure and function of an A kinase anchoring protein associated with calcium channels. Neuron *20*, 1017-1026.

Gray, P.C., Tibbs, V.C., Catterall, W.A., and Murphy, B.J. (1997). Identification of a 15-kDa cAMP-dependent protein kinase-anchoring protein associated with skeletal muscle L-type calcium channels. The Journal of biological chemistry *272*, 6297-6302.

Green, K.N., Demuro, A., Akbari, Y., Hitt, B.D., Smith, I.F., Parker, I., and LaFerla, F.M. (2008). SERCA pump activity is physiologically regulated by presenilin and regulates amyloid beta production. J Cell Biol *181*, 1107-1116.

Green, K.N., and LaFerla, F.M. (2008). Linking calcium to Abeta and Alzheimer's disease. Neuron *59*, 190-194.

Hall, D.D., Dai, S., Tseng, P.Y., Malik, Z., Nguyen, M., Matt, L., Schnizler, K., Shephard, A., Mohapatra, D.P., Tsuruta, F.*, et al.* (2013). Competition between alpha-actinin and Ca(2)(+)-calmodulin controls surface retention of the L-type Ca(2)(+) channel Ca(V)1.2. Neuron *78*, 483-497.

Hatakeyama, S., Wakamori, M., Ino, M., Miyamoto, N., Takahashi, E., Yoshinaga, T., Sawada, K., Imoto, K., Tanaka, I., Yoshizawa, T.*, et al.* (2001). Differential nociceptive responses in mice lacking the alpha(1B) subunit of N-type Ca(2+) channels. Neuroreport *12*, 2423-2427.

He, G., Luo, W., Li, P., Remmers, C., Netzer, W.J., Hendrick, J., Bettayeb, K., Flajolet, M., Gorelick, F., Wennogle, L.P.*, et al.* (2010). Gamma-secretase activating protein is a therapeutic target for Alzheimer's disease. Nature *467*, 95-98.

He, L.L., Zhang, Y., Chen, Y.H., Yamada, Y., and Yang, J. (2007). Functional modularity of the beta-subunit of voltage-gated Ca2+ channels. Biophysical journal *93*, 834-845.

Helguera, G., Olcese, R., Song, M., Toro, L., and Stefani, E. (2002). Tissue-specific regulation of Ca(2+) channel protein expression by sex hormones. Biochim Biophys Acta *1569*, 59-66.

Hell, J.W., Westenbroek, R.E., Breeze, L.J., Wang, K.K., Chavkin, C., and Catterall, W.A. (1996). N-methyl-D-aspartate receptor-induced proteolytic conversion of postsynaptic class C L-type calcium channels in hippocampal neurons. Proceedings of the National Academy of Sciences of the United States of America *93*, 3362-3367.

Herlitze, S., Garcia, D.E., Mackie, K., Hille, B., Scheuer, T., and Catterall, W.A. (1996). Modulation of Ca2+ channels by G-protein beta gamma subunits. Nature *380*, 258-262.

Hershko, A., and Ciechanover, A. (1998). The ubiquitin system. Annu Rev Biochem *67*, 425-479.

Hulme, J.T., Ahn, M., Hauschka, S.D., Scheuer, T., and Catterall, W.A. (2002). A novel leucine zipper targets AKAP15 and cyclic AMP-dependent protein kinase to the C terminus of the skeletal muscle Ca2+ channel and modulates its function. The Journal of biological chemistry *277*, 4079-4087.

Hulme, J.T., Konoki, K., Lin, T.W., Gritsenko, M.A., Camp, D.G., 2nd, Bigelow, D.J., and Catterall, W.A. (2005). Sites of proteolytic processing and noncovalent association of

the distal C-terminal domain of CaV1.1 channels in skeletal muscle. Proceedings of the National Academy of Sciences of the United States of America *102*, 5274-5279.

Hulme, J.T., Yarov-Yarovoy, V., Lin, T.W., Scheuer, T., and Catterall, W.A. (2006). Autoinhibitory control of the CaV1.2 channel by its proteolytically processed distal C-terminal domain. The Journal of physiology *576*, 87-102.

Ikeda, S.R. (1996). Voltage-dependent modulation of N-type calcium channels by G-protein beta gamma subunits. Nature *380*, 255-258.

Iwatsubo, T., Odaka, A., Suzuki, N., Mizusawa, H., Nukina, N., and Ihara, Y. (1994). Visualization of A beta 42(43) and A beta 40 in senile plaques with end-specific A beta monoclonals: evidence that an initially deposited species is A beta 42(43). Neuron *13*, 45-53.

Jacobsen, K.T., and Iverfeldt, K. (2009). Amyloid precursor protein and its homologues: a family of proteolysis-dependent receptors. Cell Mol Life Sci *66*, 2299-2318.

Jarvis, S.E., and Zamponi, G.W. (2001). Distinct molecular determinants govern syntaxin 1A-mediated inactivation and G-protein inhibition of N-type calcium channels. J Neurosci *21*, 2939-2948.

Jay, S.D., Sharp, A.H., Kahl, S.D., Vedvick, T.S., Harpold, M.M., and Campbell, K.P. (1991). Structural characterization of the dihydropyridine-sensitive calcium channel alpha 2-subunit and the associated delta peptides. The Journal of biological chemistry *266*, 3287-3293.

Jeng, C.J., Sun, M.C., Chen, Y.W., and Tang, C.Y. (2008). Dominant-negative effects of episodic ataxia type 2 mutations involve disruption of membrane trafficking of human P/Q-type Ca2+ channels. Journal of cellular physiology *214*, 422-433.

Jeziorski, M.C., Greenberg, R.M., and Anderson, P.A. (2000). The molecular biology of invertebrate voltage-gated Ca(2+) channels. J Exp Biol *203*, 841-856.

Johnson, B.D., Brousal, J.P., Peterson, B.Z., Gallombardo, P.A., Hockerman, G.H., Lai, Y., Scheuer, T., and Catterall, W.A. (1997). Modulation of the cloned skeletal muscle L-type Ca2+ channel by anchored cAMP-dependent protein kinase. J Neurosci *17*, 1243-1255.

Johnson, B.D., Scheuer, T., and Catterall, W.A. (1994). Voltage-dependent potentiation of L-type Ca2+ channels in skeletal muscle cells requires anchored cAMP-dependent protein kinase. Proceedings of the National Academy of Sciences of the United States of America *91*, 11492-11496.

Jonsson, T., Atwal, J.K., Steinberg, S., Snaedal, J., Jonsson, P.V., Bjornsson, S., Stefansson, H., Sulem, P., Gudbjartsson, D., Maloney, J.*, et al.* (2012). A mutation in APP protects against Alzheimer's disease and age-related cognitive decline. Nature *488*, 96-99.

Jouvenceau, A., Eunson, L.H., Spauschus, A., Ramesh, V., Zuberi, S.M., Kullmann, D.M., and Hanna, M.G. (2001). Human epilepsy associated with dysfunction of the brain P/Q-type calcium channel. Lancet *358*, 801-807.

Jun, K., Piedras-Renteria, E.S., Smith, S.M., Wheeler, D.B., Lee, S.B., Lee, T.G., Chin, H., Adams, M.E., Scheller, R.H., Tsien, R.W.*, et al.* (1999). Ablation of P/Q-type Ca(2+) channel currents, altered synaptic transmission, and progressive ataxia in mice lacking the alpha(1A)-subunit. Proceedings of the National Academy of Sciences of the United States of America *96*, 15245-15250.

Jurkat-Rott, K., and Lehmann-Horn, F. (2004). The impact of splice isoforms on voltage-gated calcium channel alpha1 subunits. The Journal of physiology *554*, 609-619.

Kang, J., Lemaire, H.G., Unterbeck, A., Salbaum, J.M., Masters, C.L., Grzeschik, K.H., Multhaup, G., Beyreuther, K., and Muller-Hill, B. (1987). The precursor of Alzheimer's disease amyloid A4 protein resembles a cell-surface receptor. Nature *325*, 733-736.

Kero, M., Paetau, A., Polvikoski, T., Tanskanen, M., Sulkava, R., Jansson, L., Myllykangas, L., and Tienari, P.J. (2013). Amyloid precursor protein (APP) A673T mutation in the elderly Finnish population. Neurobiol Aging *34*, 1518 e1511-1513.

Kim, D.Y., Ingano, L.A., Carey, B.W., Pettingell, W.H., and Kovacs, D.M. (2005). Presenilin/gamma-secretase-mediated cleavage of the voltage-gated sodium channel beta2-subunit regulates cell adhesion and migration. J Biol Chem *280*, 23251-23261.

Kleyman, T.R., Carattino, M.D., and Hughey, R.P. (2009). ENaC at the cutting edge: regulation of epithelial sodium channels by proteases. The Journal of biological chemistry *284*, 20447-20451.

Klugbauer, N., Marais, E., and Hofmann, F. (2003). Calcium channel alpha2delta subunits: differential expression, function, and drug binding. Journal of bioenergetics and biomembranes *35*, 639-647.

Kopan, R., and Ilagan, M.X. (2004). Gamma-secretase: proteasome of the membrane? Nat Rev Mol Cell Biol *5*, 499-504.

Kordasiewicz, H.B., Thompson, R.M., Clark, H.B., and Gomez, C.M. (2006). C-termini of P/Q-type Ca2+ channel alpha1A subunits translocate to nuclei and promote polyglutamine-mediated toxicity. Hum Mol Genet *15*, 1587-1599.

Kovacs, D.M., Gersbacher, M.T., and Kim, D.Y. (2010). Alzheimer's secretases regulate voltage-gated sodium channels. Neurosci Lett *486*, 68-72.

Kubodera, T., Yokota, T., Ohwada, K., Ishikawa, K., Miura, H., Matsuoka, T., and Mizusawa, H. (2003). Proteolytic cleavage and cellular toxicity of the human alpha1A calcium channel in spinocerebellar ataxia type 6. Neurosci Lett *341*, 74-78.

Kuchibhotla, K.V., Goldman, S.T., Lattarulo, C.R., Wu, H.Y., Hyman, B.T., and Bacskai, B.J. (2008). Abeta plaques lead to aberrant regulation of calcium homeostasis in vivo resulting in structural and functional disruption of neuronal networks. Neuron *59*, 214-225.

LaFerla, F.M. (2002). Calcium dyshomeostasis and intracellular signalling in Alzheimer's disease. Nat Rev Neurosci *3*, 862-872.

Lathia, J.D., Mattson, M.P., and Cheng, A. (2008). Notch: from neural development to neurological disorders. J Neurochem *107*, 1471-1481.

Lee, K.S., Marban, E., and Tsien, R.W. (1985). Inactivation of calcium channels in mammalian heart cells: joint dependence on membrane potential and intracellular calcium. The Journal of physiology *364*, 395-411.

Leitch, B., Szostek, A., Lin, R., and Shevtsova, O. (2009). Subcellular distribution of L-type calcium channel subtypes in rat hippocampal neurons. Neuroscience *164*, 641-657.

Li, X., Dang, S., Yan, C., Gong, X., Wang, J., and Shi, Y. (2013). Structure of a presenilin family intramembrane aspartate protease. Nature *493*, 56-61.

Lin, Z., Haus, S., Edgerton, J., and Lipscombe, D. (1997). Identification of functionally distinct isoforms of the N-type Ca2+ channel in rat sympathetic ganglia and brain. Neuron *18*, 153-166.

Lipscombe, D., Andrade, A., and Allen, S.E. (2013). Alternative splicing: functional diversity among voltage-gated calcium channels and behavioral consequences. Biochim Biophys Acta *1828*, 1522-1529.

Lopez-Arrieta, J.M., and Birks, J. (2002). Nimodipine for primary degenerative, mixed and vascular dementia. Cochrane Database Syst Rev, CD000147.

Ma, H., Cohen, S., Li, B., and Tsien, R.W. (2012). Exploring the dominant role of Cav1 channels in signalling to the nucleus. Biosci Rep *33*, 97-101.

Ma, Q.H., Futagawa, T., Yang, W.L., Jiang, X.D., Zeng, L., Takeda, Y., Xu, R.X., Bagnard, D., Schachner, M., Furley, A.J.*, et al.* (2008). A TAG1-APP signalling pathway through Fe65 negatively modulates neurogenesis. Nat Cell Biol *10*, 283-294.

MacKinnon, R. (2003). Potassium channels. FEBS letters *555*, 62-65.

Mahapatra, S., Calorio, C., Vandael, D.H., Marcantoni, A., Carabelli, V., and Carbone, E. (2012). Calcium channel types contributing to chromaffin cell excitability, exocytosis and endocytosis. Cell calcium *51*, 321-330.

Manczak, M., Anekonda, T.S., Henson, E., Park, B.S., Quinn, J., and Reddy, P.H. (2006). Mitochondria are a direct site of A beta accumulation in Alzheimer's disease neurons: implications for free radical generation and oxidative damage in disease progression. Hum Mol Genet *15*, 1437-1449.

Matthews, E.A., and Dickenson, A.H. (2001). Effects of spinally delivered N- and P-type voltage-dependent calcium channel antagonists on dorsal horn neuronal responses in a rat model of neuropathy. Pain *92*, 235-246.

Mattson, M.P. (2007). Calcium and neurodegeneration. Aging Cell *6*, 337-350.

McHugh, D., Sharp, E.M., Scheuer, T., and Catterall, W.A. (2000). Inhibition of cardiac L-type calcium channels by protein kinase C phosphorylation of two sites in the N-terminal domain. Proceedings of the National Academy of Sciences of the United States of America *97*, 12334-12338.

Meyer, E.L., Strutz, N., Gahring, L.C., and Rogers, S.W. (2003). Glutamate receptor subunit 3 is modified by site-specific limited proteolysis including cleavage by gamma-secretase. J Biol Chem *278*, 23786-23796.

Mezghrani, A., Monteil, A., Watschinger, K., Sinnegger-Brauns, M.J., Barrere, C., Bourinet, E., Nargeot, J., Striessnig, J., and Lory, P. (2008). A destructive interaction mechanism accounts for dominant-negative effects of misfolded mutants of voltage-gated calcium channels. J Neurosci *28*, 4501-4511.

Michailidis, I.E., Zhang, Y., and Yang, J. (2007). The lipid connection-regulation of voltage-gated Ca(2+) channels by phosphoinositides. Pflugers Arch *455*, 147-155.

Milani, D., Malgaroli, A., Guidolin, D., Fasolato, C., Skaper, S.D., Meldolesi, J., and Pozzan, T. (1990). Ca2+ channels and intracellular Ca2+ stores in neuronal and neuroendocrine cells. Cell calcium *11*, 191-199.

Mintz, I.M., Venema, V.J., Adams, M.E., and Bean, B.P. (1991). Inhibition of N- and L-type Ca2+ channels by the spider venom toxin omega-Aga-IIIA. Proceedings of the National Academy of Sciences of the United States of America *88*, 6628-6631.

Moyer, J.R., Jr., Thompson, L.T., Black, J.P., and Disterhoft, J.F. (1992). Nimodipine increases excitability of rabbit CA1 pyramidal neurons in an age- and concentration-dependent manner. J Neurophysiol *68*, 2100-2109.

Nixon, R.A., Saito, K.I., Grynspan, F., Griffin, W.R., Katayama, S., Honda, T., Mohan, P.S., Shea, T.B., and Beermann, M. (1994). Calcium-activated neutral proteinase (calpain) system in aging and Alzheimer's disease. Ann N Y Acad Sci *747*, 77-91.

Okagaki, R., Izumi, H., Okada, T., Nagahora, H., Nakajo, K., and Okamura, Y. (2001). The maternal transcript for truncated voltage-dependent Ca2+ channels in the ascidian embryo: a potential suppressive role in Ca2+ channel expression. Dev Biol *230*, 258-277.

Page, K.M., Heblich, F., Davies, A., Butcher, A.J., Leroy, J., Bertaso, F., Pratt, W.S., and Dolphin, A.C. (2004). Dominant-negative calcium channel suppression by truncated constructs involves a kinase implicated in the unfolded protein response. J Neurosci *24*, 5400-5409.

Page, K.M., Heblich, F., Margas, W., Pratt, W.S., Nieto-Rostro, M., Chaggar, K., Sandhu, K., Davies, A., and Dolphin, A.C. (2010). N terminus is key to the dominant

negative suppression of Ca(V)2 calcium channels: implications for episodic ataxia type 2. The Journal of biological chemistry *285*, 835-844.

Palop, J.J., Jones, B., Kekonius, L., Chin, J., Yu, G.Q., Raber, J., Masliah, E., and Mucke, L. (2003). Neuronal depletion of calcium-dependent proteins in the dentate gyrus is tightly linked to Alzheimer's disease-related cognitive deficits. Proc Natl Acad Sci U S A *100*, 9572-9577.

Perez-Reyes, E. (2003). Molecular physiology of low-voltage-activated t-type calcium channels. Physiological reviews *83*, 117-161.

Perez-Reyes, E., and Schneider, T. (1995). Molecular biology of calcium channels. Kidney international *48*, 1111-1124.

Perret, D., and Luo, Z.D. (2009). Targeting voltage-gated calcium channels for neuropathic pain management. Neurotherapeutics *6*, 679-692.

Pierrot, N., Ghisdal, P., Caumont, A.S., and Octave, J.N. (2004). Intraneuronal amyloid-beta1-42 production triggered by sustained increase of cytosolic calcium concentration induces neuronal death. J Neurochem *88*, 1140-1150.

Pietrobon, D. (2005a). Function and dysfunction of synaptic calcium channels: insights from mouse models. Current opinion in neurobiology *15*, 257-265.

Pietrobon, D. (2005b). Migraine: new molecular mechanisms. Neuroscientist *11*, 373-386.

Pietrobon, D. (2010). CaV2.1 channelopathies. Pflugers Arch *460*, 375-393.

Pietrobon, D., and Striessnig, J. (2003). Neurobiology of migraine. Nat Rev Neurosci *4*, 386-398.

Platzer, J., Engel, J., Schrott-Fischer, A., Stephan, K., Bova, S., Chen, H., Zheng, H., and Striessnig, J. (2000). Congenital deafness and sinoatrial node dysfunction in mice lacking class D L-type Ca2+ channels. Cell *102*, 89-97.

Plummer, M.R., Logothetis, D.E., and Hess, P. (1989). Elementary properties and pharmacological sensitivities of calcium channels in mammalian peripheral neurons. Neuron *2*, 1453-1463.

Postina, R. (2012). Activation of alpha-secretase cleavage. J Neurochem *120 Suppl 1*, 46-54.

Pratt, K.G., Zhu, P., Watari, H., Cook, D.G., and Sullivan, J.M. (2011). A novel role for {gamma}-secretase: selective regulation of spontaneous neurotransmitter release from hippocampal neurons. J Neurosci *31*, 899-906.

Raghib, A., Bertaso, F., Davies, A., Page, K.M., Meir, A., Bogdanov, Y., and Dolphin, A.C. (2001). Dominant-negative synthesis suppression of voltage-gated calcium channel Cav2.2 induced by truncated constructs. J Neurosci *21*, 8495-8504.

Randall, A., and Tsien, R.W. (1995). Pharmacological dissection of multiple types of Ca2+ channel currents in rat cerebellar granule neurons. J Neurosci *15*, 2995-3012.

Rechsteiner, M., and Rogers, S.W. (1996). PEST sequences and regulation by proteolysis. Trends Biochem Sci *21*, 267-271.

Reimer, D., Huber, I.G., Garcia, M.L., Haase, H., and Striessnig, J. (2000). beta subunit heterogeneity of L-type Ca(2+) channels in smooth muscle tissues. FEBS letters *467*, 65-69.

Restituito, S., Khatri, L., Ninan, I., Mathews, P.M., Liu, X., Weinberg, R.J., and Ziff, E.B. (2011). Synaptic autoregulation by metalloproteases and gamma-secretase. J Neurosci *31*, 12083-12093.

Reuter, H. (1983). Calcium channel modulation by neurotransmitters, enzymes and drugs. Nature *301*, 569-574.

Roehm, P.C., Xu, N., Woodson, E.A., Green, S.H., and Hansen, M.R. (2008). Membrane depolarization inhibits spiral ganglion neurite growth via activation of multiple types of voltage sensitive calcium channels and calpain. Mol Cell Neurosci *37*, 376-387.

Rousset, M., Cens, T., Gouin-Charnet, A., Scamps, F., and Charnet, P. (2004). Ca2+ and phosphatidylinositol 4,5-bisphosphate stabilize a Gbeta gamma-sensitive state of Ca V2 Ca 2+ channels. The Journal of biological chemistry *279*, 14619-14630.

Sabo, S.L., Ikin, A.F., Buxbaum, J.D., and Greengard, P. (2001). The Alzheimer amyloid precursor protein (APP) and FE65, an APP-binding protein, regulate cell movement. J Cell Biol *153*, 1403-1414.

Sabo, S.L., Ikin, A.F., Buxbaum, J.D., and Greengard, P. (2003). The amyloid precursor protein and its regulatory protein, FE65, in growth cones and synapses in vitro and in vivo. J Neurosci *23*, 5407-5415.

Sachse, C.C., Kim, Y.H., Agsten, M., Huth, T., Alzheimer, C., Kovacs, D.M., and Kim, D.Y. (2013). BACE1 and presenilin/gamma-secretase regulate proteolytic processing of KCNE1 and 2, auxiliary subunits of voltage-gated potassium channels. FASEB J *27*, 2458-2467.

Sakurai, T., Hell, J.W., Woppmann, A., Miljanich, G.P., and Catterall, W.A. (1995). Immunochemical identification and differential phosphorylation of alternatively spliced forms of the alpha 1A subunit of brain calcium channels. The Journal of biological chemistry *270*, 21234-21242.

Schroder, E., Byse, M., and Satin, J. (2009). L-type calcium channel C terminus autoregulates transcription. Circulation research *104*, 1373-1381.

Scott, V.E., Felix, R., Arikkath, J., and Campbell, K.P. (1998). Evidence for a 95 kDa short form of the alpha1A subunit associated with the omega-conotoxin MVIIC receptor of the P/Q-type Ca2+ channels. J Neurosci *18*, 641-647.

Sculptoreanu, A., Scheuer, T., and Catterall, W.A. (1993). Voltage-dependent potentiation of L-type Ca2+ channels due to phosphorylation by cAMP-dependent protein kinase. Nature *364*, 240-243.

Seisenberger, C., Specht, V., Welling, A., Platzer, J., Pfeifer, A., Kuhbandner, S., Striessnig, J., Klugbauer, N., Feil, R., and Hofmann, F. (2000). Functional embryonic cardiomyocytes after disruption of the L-type alpha1C (Cav1.2) calcium channel gene in the mouse. J Biol Chem *275*, 39193-39199.

Selkoe, D., and Kopan, R. (2003). Notch and Presenilin: regulated intramembrane proteolysis links development and degeneration. Annu Rev Neurosci *26*, 565-597.

Selkoe, D.J., and Wolfe, M.S. (2007). Presenilin: running with scissors in the membrane. Cell *131*, 215-221.

Sharp, A.H., and Campbell, K.P. (1989). Characterization of the 1,4-dihydropyridine receptor using subunit-specific polyclonal antibodies. Evidence for a 32,000-Da subunit. The Journal of biological chemistry *264*, 2816-2825.

Sheng, Z.H., Westenbroek, R.E., and Catterall, W.A. (1998). Physical link and functional coupling of presynaptic calcium channels and the synaptic vesicle docking/fusion machinery. Journal of bioenergetics and biomembranes *30*, 335-345.

Simms, B.A., Souza, I.A., and Zamponi, G.W. (2013). A novel calmodulin site in the Cav1.2 N-terminus regulates calcium-dependent inactivation. Pflugers Arch.

Singh, A., Gebhart, M., Fritsch, R., Sinnegger-Brauns, M.J., Poggiani, C., Hoda, J.C., Engel, J., Romanin, C., Striessnig, J., and Koschak, A. (2008). Modulation of voltage- and Ca2+-dependent gating of CaV1.3 L-type calcium channels by alternative splicing of a C-terminal regulatory domain. The Journal of biological chemistry *283*, 20733-20744.

Snutch, T.P. (2005). Targeting chronic and neuropathic pain: the N-type calcium channel comes of age. NeuroRx *2*, 662-670.

Soong, T.W., DeMaria, C.D., Alvania, R.S., Zweifel, L.S., Liang, M.C., Mittman, S., Agnew, W.S., and Yue, D.T. (2002). Systematic identification of splice variants in human P/Q-type channel alpha1(2.1) subunits: implications for current density and Ca2+-dependent inactivation. J Neurosci *22*, 10142-10152.

Stotz, S.C., Jarvis, S.E., and Zamponi, G.W. (2004). Functional roles of cytoplasmic loops and pore lining transmembrane helices in the voltage-dependent inactivation of HVA calcium channels. The Journal of physiology *554*, 263-273.

Striessnig, J., Hoda, J.C., Koschak, A., Zaghetto, F., Mullner, C., Sinnegger-Brauns, M.J., Wild, C., Watschinger, K., Trockenbacher, A., and Pelster, G. (2004). L-type Ca2+ channels in Ca2+ channelopathies. Biochemical and biophysical research communications *322*, 1341-1346.

Struhl, G., and Adachi, A. (2000). Requirements for presenilin-dependent cleavage of notch and other transmembrane proteins. Mol Cell *6*, 625-636.

Stutzmann, G.E., Smith, I., Caccamo, A., Oddo, S., Laferla, F.M., and Parker, I. (2006). Enhanced ryanodine receptor recruitment contributes to Ca2+ disruptions in young, adult, and aged Alzheimer's disease mice. J Neurosci *26*, 5180-5189.

Supnet, C., and Bezprozvanny, I. (2010). The dysregulation of intracellular calcium in Alzheimer disease. Cell Calcium *47*, 183-189.

Takahashi, T., and Momiyama, A. (1993). Different types of calcium channels mediate central synaptic transmission. Nature *366*, 156-158.

Tamse, C.T., Xu, Y., Song, H., Nie, L., and Yamoah, E.N. (2003). Protein kinase A mediates voltage-dependent facilitation of Ca2+ current in presynaptic hair cells in Hermissenda crassicornis. Journal of neurophysiology *89*, 1718-1726.

Tedford, H.W., and Zamponi, G.W. (2006). Direct G protein modulation of Cav2 calcium channels. Pharmacological reviews *58*, 837-862.

Thibault, O., and Landfield, P.W. (1996). Increase in single L-type calcium channels in hippocampal neurons during aging. Science *272*, 1017-1020.

Thibault, O., Pancani, T., Landfield, P.W., and Norris, C.M. (2012). Reduction in neuronal L-type calcium channel activity in a double knock-in mouse model of Alzheimer's disease. Biochim Biophys Acta *1822*, 546-549.

Thibault, O., Porter, N.M., Chen, K.C., Blalock, E.M., Kaminker, P.G., Clodfelter, G.V., Brewer, L.D., and Landfield, P.W. (1998). Calcium dysregulation in neuronal aging and Alzheimer's disease: history and new directions. Cell Calcium *24*, 417-433.

Timmermann, D.B., Westenbroek, R.E., Schousboe, A., and Catterall, W.A. (2002). Distribution of high-voltage-activated calcium channels in cultured gamma-aminobutyric acidergic neurons from mouse cerebral cortex. J Neurosci Res *67*, 48-61.

Tollefson, G.D. (1990). Short-term effects of the calcium channel blocker nimodipine (Bay-e-9736) in the management of primary degenerative dementia. Biol Psychiatry *27*, 1133-1142.

Toman, J., and Fiskum, G. (2011). Influence of aging on membrane permeability transition in brain mitochondria. J Bioenerg Biomembr *43*, 3-10.

Tremml, P., Lipp, H.P., Muller, U., Ricceri, L., and Wolfer, D.P. (1998). Neurobehavioral development, adult openfield exploration and swimming navigation learning in mice with a modified beta-amyloid precursor protein gene. Behav Brain Res *95*, 65-76.

Triggle, D.J. (2006). L-type calcium channels. Current pharmaceutical design *12*, 443-457.

Tsujimura, A., Yasojima, K., and Hashimoto-Gotoh, T. (1997). Cloning of Xenopus presenilin-alpha and -beta cDNAs and their differential expression in oogenesis and embryogenesis. Biochem Biophys Res Commun *231*, 392-396.

Tu, H., Nelson, O., Bezprozvanny, A., Wang, Z., Lee, S.F., Hao, Y.H., Serneels, L., De Strooper, B., Yu, G., and Bezprozvanny, I. (2006). Presenilins form ER Ca2+ leak channels, a function disrupted by familial Alzheimer's disease-linked mutations. Cell *126*, 981-993.

Vassar, R., Bennett, B.D., Babu-Khan, S., Kahn, S., Mendiaz, E.A., Denis, P., Teplow, D.B., Ross, S., Amarante, P., Loeloff, R.*, et al.* (1999). Beta-secretase cleavage of Alzheimer's amyloid precursor protein by the transmembrane aspartic protease BACE. Science *286*, 735-741.

Viard, P., Butcher, A.J., Halet, G., Davies, A., Nurnberg, B., Heblich, F., and Dolphin, A.C. (2004). PI3K promotes voltage-dependent calcium channel trafficking to the plasma membrane. Nature neuroscience *7*, 939-946.

von Reyn, C.R., Spaethling, J.M., Mesfin, M.N., Ma, M., Neumar, R.W., Smith, D.H., Siman, R., and Meaney, D.F. (2009). Calpain mediates proteolysis of the voltage-gated sodium channel alpha-subunit. J Neurosci *29*, 10350-10356.

Waithe, D., Ferron, L., Page, K.M., Chaggar, K., and Dolphin, A.C. (2011). Beta-subunits promote the expression of Ca(V)2.2 channels by reducing their proteasomal degradation. The Journal of biological chemistry *286*, 9598-9611.

Wakamori, M., Mikala, G., and Mori, Y. (1999). Auxiliary subunits operate as a molecular switch in determining gating behaviour of the unitary N-type Ca2+ channel current in Xenopus oocytes. The Journal of physiology *517 (Pt 3)*, 659-672.

Wei, X., Neely, A., Lacerda, A.E., Olcese, R., Stefani, E., Perez-Reyes, E., and Birnbaumer, L. (1994). Modification of Ca2+ channel activity by deletions at the carboxyl terminus of the cardiac alpha 1 subunit. The Journal of biological chemistry *269*, 1635-1640.

Westenbroek, R.E., Hell, J.W., Warner, C., Dubel, S.J., Snutch, T.P., and Catterall, W.A. (1992). Biochemical properties and subcellular distribution of an N-type calcium channel alpha 1 subunit. Neuron *9*, 1099-1115.

Westenbroek, R.E., Sakurai, T., Elliott, E.M., Hell, J.W., Starr, T.V., Snutch, T.P., and Catterall, W.A. (1995). Immunochemical identification and subcellular distribution of the alpha 1A subunits of brain calcium channels. J Neurosci *15*, 6403-6418.

Wielowieyski, P.A., Wigle, J.T., Salih, M., Hum, P., and Tuana, B.S. (2001). Alternative splicing in intracellular loop connecting domains II and III of the alpha 1 subunit of Cav1.2 Ca2+ channels predicts two-domain polypeptides with unique C-terminal tails. The Journal of biological chemistry *276*, 1398-1406.

Willis, M., Kaufmann, W.A., Wietzorrek, G., Hutter-Paier, B., Moosmang, S., Humpel, C., Hofmann, F., Windisch, M., Knaus, H.G., and Marksteiner, J. (2010). L-type calcium channel CaV 1.2 in transgenic mice overexpressing human AbetaPP751 with the London (V717I) and Swedish (K670M/N671L) mutations. J Alzheimers Dis *20*, 1167-1180.

Wittemann, S., Mark, M.D., Rettig, J., and Herlitze, S. (2000). Synaptic localization and presynaptic function of calcium channel beta 4-subunits in cultured hippocampal neurons. The Journal of biological chemistry *275*, 37807-37814.

Wolfe, M.S. (2012). Processive proteolysis by gamma-secretase and the mechanism of Alzheimer's disease. Biol Chem *393*, 899-905.

Wu, L., Bauer, C.S., Zhen, X.G., Xie, C., and Yang, J. (2002). Dual regulation of voltage-gated calcium channels by PtdIns(4,5)P2. Nature *419*, 947-952.

Yagami, T., Ueda, K., Sakaeda, T., Itoh, N., Sakaguchi, G., Okamura, N., Hori, Y., and Fujimoto, M. (2004). Protective effects of a selective L-type voltage-sensitive calcium channel blocker, S-312-d, on neuronal cell death. Biochem Pharmacol *67*, 1153-1165.

Yang, J., Ellinor, P.T., Sather, W.A., Zhang, J.F., and Tsien, R.W. (1993). Molecular determinants of Ca2+ selectivity and ion permeation in L-type Ca2+ channels. Nature *366*, 158-161.

Yang, L., Katchman, A., Morrow, J.P., Doshi, D., and Marx, S.O. (2011). Cardiac L-type calcium channel (Cav1.2) associates with gamma subunits. Faseb J *25*, 928-936.

Yang, L., Katchman, A., Samad, T., Morrow, J.P., Weinberg, R.L., and Marx, S.O. (2013). beta-adrenergic regulation of the L-type Ca2+ channel does not require phosphorylation of alpha1C Ser1700. Circulation research *113*, 871-880.

Yang, L., Liu, G., Zakharov, S.I., Morrow, J.P., Rybin, V.O., Steinberg, S.F., and Marx, S.O. (2005). Ser1928 is a common site for Cav1.2 phosphorylation by protein kinase C isoforms. The Journal of biological chemistry *280*, 207-214.

Yang, L., Wang, Z., Wang, B., Justice, N.J., and Zheng, H. (2009). Amyloid precursor protein regulates Cav1.2 L-type calcium channel levels and function to influence GABAergic short-term plasticity. J Neurosci *29*, 15660-15668.

Yang, T., and Colecraft, H.M. (2013). Regulation of voltage-dependent calcium channels by RGK proteins. Biochim Biophys Acta *1828*, 1644-1654.

Ye, C., Walsh, D.M., Selkoe, D.J., and Hartley, D.M. (2004). Amyloid beta-protein induced electrophysiological changes are dependent on aggregation state: N-methyl-D-aspartate (NMDA) versus non-NMDA receptor/channel activation. Neurosci Lett *366*, 320-325.

Young-Pearse, T.L., Bai, J., Chang, R., Zheng, J.B., LoTurco, J.J., and Selkoe, D.J. (2007). A critical function for beta-amyloid precursor protein in neuronal migration revealed by in utero RNA interference. J Neurosci *27*, 14459-14469.

Zamponi, G.W., Bourinet, E., Nelson, D., Nargeot, J., and Snutch, T.P. (1997). Crosstalk between G proteins and protein kinase C mediated by the calcium channel alpha1 subunit. Nature *385*, 442-446.

Zamponi, G.W., and Currie, K.P. (2013). Regulation of Ca(V)2 calcium channels by G protein coupled receptors. Biochim Biophys Acta *1828*, 1629-1643.

Zamponi, G.W., Lory, P., and Perez-Reyes, E. (2009). Role of voltage-gated calcium channels in epilepsy. Pflugers Arch.

Zamponi, G.W., and Snutch, T.P. (1998). Decay of prepulse facilitation of N type calcium channels during G protein inhibition is consistent with binding of a single Gbeta subunit. Proceedings of the National Academy of Sciences of the United States of America *95*, 4035-4039.

Zhang, Y., Chen, Y.H., Bangaru, S.D., He, L., Abele, K., Tanabe, S., Kozasa, T., and Yang, J. (2008). Origin of the voltage dependence of G-protein regulation of P/Q-type Ca2+ channels. J Neurosci *28*, 14176-14188.

Zhong, H., Yokoyama, C.T., Scheuer, T., and Catterall, W.A. (1999). Reciprocal regulation of P/Q-type Ca2+ channels by SNAP-25, syntaxin and synaptotagmin. Nature neuroscience *2*, 939-941.

Zuhlke, R.D., and Reuter, H. (1998). Ca2+-sensitive inactivation of L-type Ca2+ channels depends on multiple cytoplasmic amino acid sequences of the alpha1C subunit. Proceedings of the National Academy of Sciences of the United States of America *95*, 3287-3294.

Appendix

Age-related homeostatic mid-channel proteolysis of neuronal L-type voltage-gated Ca^{2+} channels

Ioannis E. Michailidis[1], Kathryn Abele-Henckels[1], Wei K. Zhang[1], Bochao Lin[1], Yong Yu[1], Larry Geyman[1], Michael D. Ehlers[2], Eftychios A. Pnevmatikakis[3], Jian Yang[1,4 *]

[1]Department of Biological Sciences, Columbia University, New York, NY 10027

[2]Pfizer Worldwide Research and Development, Neuroscience Research Unit, Cambridge, MA 02139

[3]Department of Statistics, Columbia University, New York, NY 10027

[4]Ion Channel Research and Drug Development Center, Kunming Institute of Zoology, Chinese Academy of Sciences, Kunming 650223, Yunnan, China

*Correspondence:

Jian Yang

Department of Biological Sciences, 917 Fairchild Center, MC2462, Columbia University, New York, NY 10027

Phone: (212)-854-6161; Fax: (212)-531-0425 Email: jy160@columbia.edu

SUMMARY

Neural circuitry and brain activity depend critically on proper function of voltage-gated calcium channels (VGCCs), whose activity must be tightly controlled. We show that the main body of the pore-forming α_1 subunit of neuronal L-type VGCCs, $Ca_v1.2$, is proteolytically cleaved, resulting in $Ca_v1.2$ fragment-channels that separate but remain on the plasma membrane. This "mid-channel" proteolysis is regulated by channel activity, involves the Ca^{2+}-dependent protease calpain and the ubiquitin-proteasome system, and causes attenuation and biophysical alterations of VGCC currents. Recombinant $Ca_v1.2$ fragment-channels mimicking the products of mid-channel proteolysis do not form active channels on their own, but when properly paired, produce currents with distinct biophysical properties. Mid-channel proteolysis increases dramatically with age and can be attenuated with an L-type VGCC blocker *in vivo*. Mid-channel proteolysis represents a novel form of homeostatic negative-feedback processing of VGCCs that could profoundly affect neuronal excitability, neurotransmission, neuroprotection, and calcium signaling in physiological and disease states.

HIGHLIGHTS

► The core of L-type VGCC pore-forming subunit $Ca_v1.2$ undergoes regulated cleavage

► Cleaved $Ca_v1.2$ fragments stay on the plasma membrane but can dissociate

► Aging, channel activity, calpain and PEST sequences play a role in $Ca_v1.2$ proteolysis

► $Ca_v1.2$ core cleavage greatly changes L-type VGCC properties and currents

INTRODUCTION

VGCCs (L-, N-, P/Q-, R-, and T-types) control a plethora of physiological processes, from muscle contraction, heartbeat, neural communication and hormone secretion to cell differentiation, motility, growth and apoptosis (Catterall, 2000). Their mutations and dysfunction are linked to diverse disorders such as epilepsy, migraine, ataxia, hypertension, arrhythmia, and autism (Cain and Snutch, 2011; Liao and Soong, 2010; Pietrobon, 2010; Striessnig et al., 2010; Zamponi et al., 2010). In neurons, L-type VGCCs regulate membrane excitability, Ca^{2+} signaling, and gene transcription (Catterall, 2000; Deisseroth et al., 2003; Dolmetsch, 2003; Wheeler et al., 2012). Changes in L-type VGCC activity are linked to aging and age-related neurodegenerative diseases (Moyer et al., 1992; Thibault and Landfield, 1996; Thibault et al., 1998), and variations in L-type VGCC genes are linked to neuropsychiatric diseases including schizophrenia, bipolar disorder, autism spectrum disorder, major depressive disorder, and attention deficit-hyperactivity disorder (Smoller et al., 2013).

To serve their vital and varying roles, VGCCs are subject to tight regulation by diverse pathways and mechanisms (Catterall, 2000; Zamponi and Currie, 2013). One form of regulation is proteolytic processing of the cytosolic C-terminus (Ct) of the α_1 subunit ($Ca_v\alpha_1$) of L-type VGCCs (Brawley and Hosey, 1992; De Jongh et al., 1994; De Jongh et al., 1991; Gao et al., 2001; Gerhardstein et al., 2000; Hell et al., 1993; Hulme et al., 2005; Hulme et al., 2006; Lai et al., 1990). This proteolysis produces a 30-45 kDa distal C-terminal fragment, which acts as an auto-inhibitory domain (Hulme et al., 2006). Relief of this autoinhibition is believed to underlie the sympathetic nerve stimulation-induced increase of cardiac and skeletal muscle calcium currents, part of the "fight or flight" response (Fuller et al., 2010). In addition to this Ct fragment, a spectrum of other fragments has been observed in Western blots of L-, N- and P/Q-type $Ca_v\alpha_1$ (Kordasiewicz et al., 2006; Leenders et al., 2008; Leenders et al., 2002; Ramakrishnan et al., 2006; Sakurai et al., 1995; Schiff et al., 2000; Scott et al., 1998; Westenbroek et al., 1995; Woppmann et al., 1994); the most consistent and prominent include a 90-kDa, a 150-kDa, and a 170-kDa fragment. These fragments have generally been thought to be non-specific degradation products. Intriguingly, however, short isoforms of L- and P/Q-type $Ca_v\alpha_1$ have been found in neurons and muscle cells (Malouf et al., 1992; Okagaki et al., 2001; Scott et al., 1998). Moreover, truncated P/Q-type $Ca_v\alpha_1$, generated by disease-causing mutations, are present in neurons (Jeng et al., 2008; Mezghrani et al., 2008; Page et al., 2004; Pietrobon, 2010; Scott et al., 1998; Wappl et al., 2002).

VGCCs are typically composed of a pore-forming $Ca_v\alpha_1$ and auxiliary $\alpha_2\delta$ and β ($Ca_v\beta$) subunits. Full length $Ca_v\alpha_1$ is a large protein (with a predicted molecular mass of 190-280 kDa) consisting of four homologous repeats, each containing six transmembrane

segments; the four repeats are connected by cytoplasmic loops termed I-II loop, II-III loop, and III-IV loop. The aforementioned findings motivated us to investigate the existence and functional importance of proteolytic cleavage in the core (i.e., the four repeats and the tethering cytosolic loops) of $Ca_v\alpha_1$. We find that indeed the core of native brain L-type $Ca_v\alpha_1$, $Ca_v1.2$, undergoes extensive regulated proteolysis, generating $Ca_v1.2$ fragments on the plasma membrane and greatly influencing channel activity. We further find that this proteolysis is age-dependent and can be reversed in vivo by reducing L-type channel activity. To distinguish this proteolytic event from C-terminal proteolysis, we refer to it as "mid-channel proteolysis".

RESULTS

Biochemical detection of mid-channel proteolysis of native L-type channels

We first studied mid-channel proteolysis of native L-type channels in cortical brain slices freshly isolated from 6-week old rats. Surface channels were biotinylated and analyzed by Western blot. When probed with an antibody against the $Ca_v1.2$ II-III loop (anti-L_{II-III}, epitope=T821-S838 of rat brain $Ca_v1.2$, Figure 1A), two prominent bands were routinely observed: 240 kDa (full-length $Ca_v1.2$) and 150 kDa (Figures 1B-1I). An 85-kDa band was also sometimes detected (Figures 1B-1G). The 150-kDa band was also recognized (Figure 1D, arrow) by an antibody against the distal C-terminus (anti-Ct, epitope=G2127-L2143, Figure 1A). Thus, this fragment appears to contain part of II-III loop, repeats III and IV, and the C-terminus (Figure 1A). Anti-Ct also labeled bands at 100 kDa and 70 kDa (Figure 1D, arrowheads). Probing with an antibody against the N-terminus (anti-Nt, epitope=V2-N14, Figure 1A) also revealed several low molecular

weight (MW) bands, including those at 175 kDa, 100 kDa, and 90 kDa (Figure 1E, arrowheads and arrow). These results suggest that native $Ca_v1.2$ in cortical neurons undergo extensive proteolysis *in vivo* and that the cleaved products reside in the plasma membrane as fragment-channels. The 150-kDa fragment detected by both anti-L_{II-III} and anti-Ct (Figures 1C, 1D, arrow) and the 90-kDa fragment detected by anti-Nt (Figure 1E, arrow) are complementary, adding up to 240 kDa (expected full-length $Ca_v1.2$ MW). As the 150-kDa fragment was the most robust, we focused subsequent studies on this fragment.

Mid-channel proteolysis is bidirectionally regulated

We next investigated whether $Ca_v1.2$ mid-channel proteolysis is a regulated event occurring *in vivo*. To minimize non-specific degradation, abundant protease inhibitors were added and all procedures were performed rapidly at 4°C. More critically, as non-specific degradation is an unregulated event, we investigated whether mid-channel proteolysis could instead be disrupted or enhanced. Agents that affect intracellular Ca^{2+}, L-type channel activity, and/or cell excitability were used to treat cortical slices prior to surface biotinylation. To quantify mid-channel proteolysis, densitometry was used to define a proteolysis index as the intensity ratio of the 150-kDa/240-kDa bands detected by anti-L_{II-III}. This index is unaffected by the total protein amount since it is the ratio of two bands from the same lane/sample. The non-normalized proteolysis index differed among preparations (Figures 1F-1I), reflecting intrinsic animal-to-animal variation. However, this variation does not affect pair-wise comparison of control and test results, which were obtained from parallel experiments from the same animal.

Mid-channel proteolysis was decreased by the L-type channel antagonist verapamil (Figure 1F), or by an activity-suppressing cocktail of nifedipine (another L-type channel antagonist) and the glutamate receptor inhibitor CNQX (Figure 1G). In contrast, mid-channel proteolysis was increased by the Ca^{2+}-ionophore ionomycin (Figure 1H), and by an activity-enhancing cocktail of high extracellular K^+ and L-type channel agonist BayK8644 (Figure 1I). Thus, mid-channel proteolysis correlated with L-type channel activity and intracellular Ca^{2+} levels. This *bidirectional* regulation suggests that $Ca_v1.2$ mid-channel proteolysis takes place *in vivo*.

Regulated mid-channel proteolysis of native $Ca_v1.2$ was also observed in cultured hippocampal neurons (Figure 2A and Figure S1A). After surface biotinylation and Western blot, anti-L_{II-III} robustly detected bands at 240 kDa and 150 kDa (Figure 2A, left, arrow). Both bands were also detected by anti-Ct (Figure 2A, middle, arrow), as were a 100-kDa band and a 70-kDa band (arrowheads), which were also present in cortical slices (Figure 1D, arrowheads). In the same samples, anti-Nt visualized the 240-kDa band and a 90-kDa band (Figure 2A, right, arrow). The detection of the complementary 150-kDa and 90-kDa bands in *both* cortical slices and cultured hippocampal neurons is consistent with proteolysis in the II-III loop of $Ca_v1.2$.

Visualization of mid-channel proteolysis reveals separation of cleaved fragment-channels

The above biochemical results indicate that the complementary 150-kDa and 90-kDa $Ca_v1.2$ fragments are present on the plasma membrane. Do these cleaved fragments remain associated on the cell surface? To address this question, we transfected cultured

hippocampal neurons with "LGH3", a $Ca_v1.2$ tagged with GFP on the N-terminus and HA on an extracelluar loop of repeat III (Figure S1B), and visualized the channels by confocal microscopy. LGH3 generated currents in *Xenopus* oocytes (Figure S1C) and expressed robustly in cultured hippocampal neurons (Figure S2). Labeling the HA tag with an anti-HA antibody and Alexa594 under *non-permeabilizing* conditions revealed LGH3 on the plasma membrane (Figure S2A, red). $Ca_v1.2$ with GFP but without HA tag (LGN) showed no surface labeling (Figure S2B), indicating that the anti-HA labeling was specific.

In optical sections, Alexa594-labeled dendrites of LGH3-expressing neurons often displayed a membrane-associated pattern (Figure 2B, middle), consistent with red labeling representing surface $Ca_v1.2$. Surface $Ca_v1.2$ channels tend to form clusters (Figures 2B and 2C), as has been reported (Di Biase et al., 2011). Intriguingly, in some locations green and red clustered separately (Figure 2B, left, and 2C). Green-only clusters likely represent intracellular LGH3 and are expected, but red-only clusters are anomalous - in theory, GFP and HA signals should colocalize since the two tags are on the same protein. The separation of red and green, however, is consistent with cleavage of $Ca_v1.2$ somewhere between the two tags. Furthermore, it suggests that the cleavage products on the plasma membrane dissociate from one another.

We developed an unbiased procedure to quantify red/green separation in imaging experiments: (1) A software routine scanned optical sections of dendrites and automatically detected red "voxels", each with a dimension of 0.211 x 0.211 x 0.211 μm (typical dendrites are <2 μm in diameter), and ~10,000 voxels were typically found per neuron; (2) The intensity of red and green for each voxel was measured; (3) The

red/green ratio, termed non-colocalization index (NCI), was calculated, binned, and graphed in a cumulative frequency (ordinate) vs. NCI (abscissa) plot (Figures 2D-2F).

Three conclusions apply to the results of this analysis protocol: (i) Voxels of high NCI are likely proteolysis hot spots and contain proteolytically cleaved, HA-containing fragment-channels, including the 150-kDa fragment; (ii) the higher the NCI, the more extensive the proteolysis; and (iii) a shift of the distribution curve to the right signifies greater proteolysis.

The above analysis protocol was calibrated in two dendritic segments selected for their different extent of red/green separation (Figure 2D). As expected, the segment displaying a higher number of visual red-only spots (segment y) showed a right-shifted NCI distribution (Figure 2D). In another critical test, LGH3-expressing neurons from the same culture randomly divided into two groups showed identical ensemble NCI distributions (Figure 2E), strongly validating the analysis protocol.

Visualization of mid-channel proteolysis suggests multiple cleavage sites

If red/green separation represents mid-channel proteolysis of $Ca_v1.2$, it should decrease when GFP and HA are closer together on the channel. Moreover, the appearance of multiple $Ca_v1.2$ fragments in Western blots (Figures 1D, 1E and 2A) suggests that there may be more than one cleavage site in the $Ca_v1.2$ core domain. To test these predictions, we constructed two additional GFP/HA double-tagged $Ca_v1.2$ subunits named LGH1 and LGH2 (HA positioned extracellularly on repeats I or II, respectively). LGH1 and LGH2 produced currents in oocytes (Figure S1C), confirming they traffic to the plasma membrane and are functional. Parallel imaging experiments showed markedly

reduced red/green separation as the two tags were moved closer together (Figure 2F). These results further validate the analysis protocol and support the notion that red/green separation is indicative of mid-channel proteolysis. They also suggest proteolysis not only in the II-III loop but also in the I-II loop.

Molecular determinants of mid-channel proteolysis

To examine the signaling pathways of mid-channel proteolysis, we first tested the role of calpain, a Ca^{2+}-sensitive protease likely responsible for the cleavage of $Ca_v1.2$ C-terminus (Hell et al., 1996; Hulme et al., 2006). A cocktail of calpain inhibitors significantly reduced mid-channel proteolysis in hippocampal neurons, detected by both Western blot and imaging (Figures 3A and 3B), supporting calpain's involvement. However, residual mid-channel proteolysis persisted (Figure 3A), suggesting additional proteases. We thus tested the role of the ubiquitin-proteasome system, a common route for protein degradation. The mid-channel proteolysis of LGH3 was markedly reduced by a cocktail of ubiquitin aldehyde, a general inhibitor of ubiquitination, and MG-132, a proteasome inhibitor (Figure 3C), and by mutating a putative ubiquitination motif on LGH3 (Figure 3D). Two PEST sequences have been found in $Ca_v1.2$, in the I-II and II-III loops (Catalucci et al., 2009) (named PEST1 and PEST3, respectively, Figure 3E); PEST sequences serve as signals for rapid proteolysis and possible degradation by the ubiquitin-proteasome system in various proteins (Rechsteiner and Rogers, 1996). Mid-channel proteolysis was greatly reduced by PEST3 deletion (Figure 3F) and was virtually abolished by PEST1 deletion (Figure 3G and Figure S3C). These results identify

structural elements regulating mid-channel proteolysis and suggest a compelling role for the ubiquitin-proteasome system.

Separation of fragment-channels is regulated by channel activity

Mid-channel proteolysis of LGH3, like that of endogenous $Ca_v1.2$, was regulated by L-type channel activity. Depolarizing neurons with high extracellular K^+, in the absence or presence of BayK8644, increased mid-channel proteolysis in both imaging and Western blot experiments (Figures 4A and 4B). On the other hand, treatment with nifedipine, even in the presence of high extracellular K^+, decreased it (Figures 4C, 4D and Figure S4). These results further support the notion that the red/green separation is a consequence and manifestation of mid-channel proteolysis.

Functional impact of mid-channel proteolysis

We next investigated the functional effect of mid-channel proteolysis on calcium channel currents in several ways. First, we tested the long-term effect of two treatments shown to differentially alter mid-channel proteolysis on native VGCC currents in hippocampal neurons. Incubating neurons with high K^+ and BayK8644 (followed by washout) increased mid-channel proteolysis (Figures 4A and 4B) and *reduced* VGCC currents (Figure 4E), whereas incubation with nifedipine (followed by washout) decreased mid-channel proteolysis (Figures 4C and 4D) and *enhanced* VGCC currents (Figure 4F). These results are consistent with a hypothesis that mid-channel proteolysis serves to homeostatically regulate VGCC activity, keeping at bay excessive Ca^{2+} influx that could have a potential deleterious effect to neurons.

Second, in another test of the long-term effect of mid-channel proteolysis, we inserted a cleavage motif for the tobacco etch virus protease (TEVp) in the II-III loop of LGH3 (between D815 and G816, upstream of the anti-L_{II-III} epitope T821-S838), generating LGH3_TEVp (Figure 5A). *Xenopus* oocytes expressing LGH3, LGH3_TEVp, or LGH3 with TEVp had comparable currents (Figure 5B, top), but those expressing LGH3_TEVp *with* TEVp had much smaller currents (Figure 5B, top). The latter group showed a prominent 150-kDa fragment detected by anti-L_{II-III} on the plasma membrane, with a drastic concomitant reduction of the 270-kDa ($Ca_v1.2$ + 27-kDa GFP) full-length band (Figure 5B, bottom). This 150-kDa fragment, largely absent in the three control groups, most likely represents the C-terminal product of specific TEVp cleavage of LGH3_TEVp. The decreased current of LGH3_TEVp by TEVp proteolysis validates the hypothesis that mid-channel proteolysis down-regulates VGCC currents.

Third, we examined the acute effect of mid-channel proteolysis. To accomplish this, we engineered TEVp cleavage sites in the I-II and II-III loops of $Ca_v2.1$ (this mutant is called $Ca_v2.1$_TEVp), and tested the effect of purified recombinant TEVp on $Ca_v2.1$_TEVp channels in inside-out membrane macro-patches excised from *Xenopus* oocytes. $Ca_v2.1$ was chosen because its currents run down much slower than $Ca_v1.2$ currents do. A 2-min application of TEVp did not abolish channel activity, but did produce an irreversible left shift of the activation curve of $Ca_v2.1$_TEVp, but not WT $Ca_v2.1$ channels (Figure 5C, bottom). A catalytically inactive TEVp (carrying the C151A mutation) had no effect (Figure 5C, bottom). These results indicate that mid-channel proteolysis alters VGCC gating, leaving a biophysical imprint.

Fourth, we constructed three pairs of complementary $Ca_v1.2$ fragment-channels, mimicking mid-channel proteolysis in loop I-II, II-III or III-IV (Figure 6A), and tested their activity in oocytes by two-electrode voltage clamp (TEVC). None of the six recombinant fragment-channels, named A1, A2, B1, B2, C1 and C2, produced currents when individually expressed in oocytes (Figure 6B). However, all three complementary pairs produced sizeable currents, albeit their amplitude was smaller than that of $Ca_V1.2$ currents (Figure 6C). Channels formed by all three complementary pairs displayed a right-shifted I-V curve (Figure 6D) and a change in the voltage-dependence of inactivation (Figure 6E). Thus, although individual fragment-channels do not conduct current, when properly paired they can assemble and reach the plasma membrane to form functional channels with distinct biophysical properties. We also examined expression of four non-complementary fragment pairs, A1+C2, A2+B1, A2+C1 and B2+C1, in oocytes. The first three pairs did not produce any currents while the last pair produced a small current (Figure S6B). These results suggest that all four repeats of $Ca_v\alpha_1$ are needed to form functional channels and that certain non-complementary $Ca_v\alpha_1$ fragments containing, altogether, more than four repeats may still assemble and form functional channels, albeit poorly.

Lastly, we examined whether the recombinant fragment-channels change the properties of full-length $Ca_v1.2$. Previous studies have shown that coexpression of $Ca_v\alpha_1$-fragments with full-length $Ca_v\alpha_1$ often suppresses WT channel currents in a dominant-negative manner and sometimes alters their biophysical properties (Ebihara et al., 2002; Jeng et al., 2008; Mezghrani et al., 2008; Page et al., 2004; Page et al., 2010; Raghib et al., 2001; Raike et al., 2007). We found that fragment C2 greatly dampened $Ca_v1.2$

current amplitude while other fragments did not have a significant dominant-negative effect (Figure 6F). Fragments A1 and A2 shifted the $Ca_v1.2$ I-V curve to the right (Figure 6G) and increased $Ca_v1.2$ inactivation (Figure 6H). Fragments B1 and B2 did not have a significant effect (Figures 6I and 6J). Fragment C1 shifted $Ca_v1.2$'s I-V curve to the left (Figure 6K) and markedly increased $Ca_v1.2$ inactivation (Figure 6L). Thus, $Ca_v1.2$ fragment-channels can have multifaceted effects on full-length $Ca_v1.2$ channels.

Mid-channel proteolysis is age-dependent and can be reversed *in vivo*

Because changes in L-type Ca^{2+} channel activity have been linked to normal aging (Moyer et al., 1992; Thibault and Landfield, 1996; Thibault et al., 1998), we examined whether mid-channel proteolysis of $Ca_v1.2$ is regulated across the life span. Cortical slices were freshly isolated, in strict parallel, from rats of four age groups (10 days, 6 weeks, 6 months and 16 months), and cell-surface $Ca_v1.2$ was examined by Western blot (Figure 7A). Mid-channel proteolysis increased steadily and significantly with age, being ~7 times more pronounced in 16-month old rats than in 10-day old rats (Figure 7A). Moreover, the elevated mid-channel proteolysis in the 16-month old rats could be partially reversed by a 3-5 week treatment with verapamil, a L-type VGCC blocker commonly used for hypertension, cardiac arrhythmia, cluster headache and bipolar disorder (Figure 7B), at a dosage equivalent to that used for human patients, adjusted for body weight and metabolic rate.

DISCUSSION

We have uncovered a new form of regulation of L-type VGCCs, namely, proteolytic cleavage of the main body of native $Ca_v1.2$ channels. Strikingly, cleaved fragment-channels are present on the plasma membrane and can dissociate from each other. This mid-channel proteolysis is not a result of non-specific protein degradation since it is *bidirectionally* regulated, is inversely correlated with Ca^{2+} channel activity, and is dependent on age. The finding that mid-channel proteolysis in freshly isolated cortical slices and cultured hippocampal neurons can be *reduced* by inhibiting L-type Ca^{2+} channel activity (Figures 1F, 1G, and 4C, 4D) suggests that it is an on-going physiological event occurring in native cells. This finding, together with the observation that mid-channel proteolysis can be enhanced by increased intracellular Ca^{2+} (Figure 1H and Figure S1A) or increased L-type Ca^{2+} channel activity (Figures 1I and 4A, 4B) suggests that mid-channel proteolysis is a homeostatic/neuroprotective mechanism to regulate intracellular Ca^{2+}. The dramatic increase of $Ca_v1.2$ mid-channel proteolysis with age *in vivo* is likely a manifestation of such a homeostatic/neuroprotective mechanism: as neurons age, their L-type Ca^{2+} channel currents increase (Moyer et al., 1992; Thibault and Landfield, 1996; Thibault et al., 1998), leading to an increased intracellular Ca^{2+} and a compensatory increase of $Ca_v1.2$ mid-channel proteolysis.

The conditions shown in this study that enhance $Ca_v1.2$ mid-channel proteolysis, such as increased intracellular Ca^{2+}, increased Ca^{2+} channel activity and increased age, did not change the levels of surface Na^+-K^+ ATPases and did not increase proteolysis of PARP (Figures S5A-S5D), an apoptotic protein marker whose proteolytic cleavage has been correlated with programmed cell death (Chaitanya et al., 2010), suggesting that mid-

channel proteolysis of $Ca_v1.2$ is not simply an early step of L-type VGCC degradation, is not due to cell damage, and is not a prelude to cell death. That mid-channel proteolysis is robustly detected in freshly isolated cortical slices and hippocampal neurons (Figures 1-4 and 7), is *bidirectionally* regulated (Figures 1F-1I and 4A-4D), is strongly linked to aging (Figure 7A), and is reversible in animals by a L-type VGCC blocker (Figure 7B), suggest that mid-channel proteolysis is a physiological mechanism of feedback regulation of L-type VGCCs in intact cells *in vivo*.

In our imaging experiments, we postulated that the red/green separation is indicative of mid-channel proteolysis of $Ca_v1.2$, and that the lateral shifts of the ensemble NCI plots represent changes in mid-channel proteolysis. Is it possible, however, that such shifts are due to changes in the relative expression level of $Ca_v1.2$ in the plasma membrane versus intracellular compartments? To examine this possibility, we plotted the ratio of total red over total green (i.e., surface plus intracellular) fluorescence for four drug treatments that produced shifts in the NCI: calpain inhibitors, proteasome inhibitors, 65 mM KCl or 65 mM KCl+BayK, and 65 mM KCl or 65 mM KCl + nifedipine. The exact same neurons used for the NCI plots were used in the total fluorescence plots. In each case, the drug treatment did not significantly change total red/total green fluorescence compared to its untreated control group (Figures S3A, S3B, and S4B, S4C). This analysis is consistent with the notion that NCI shifts reflect a redistribution of red and green in the plasma membrane rather than a change of intracellular GFP.

Mid-channel proteolysis is distinct from the well-studied C-terminal proteolysis (Brawley and Hosey, 1992; De Jongh et al., 1994; De Jongh et al., 1991; Gao et al., 2001; Gerhardstein et al., 2000; Hell et al., 1993; Hulme et al., 2005; Hulme et al., 2006; Lai et

al., 1990) in cleavage sites and consequences: the core of $Ca_v1.2$ remains intact after C-terminal proteolysis but is split following mid-channel proteolysis. Our biochemical and imaging experiments both suggest that mid-channel proteolysis takes place at several locations of $Ca_v1.2$ (Figures 1D, 1E, and 2A, 2F). As a result, $Ca_v1.2$ channels on the plasma membrane of native cells may be heterogeneous, with some being full-length $Ca_v1.2$ subunits and some being $Ca_v1.2$ fragments of various lengths. Our results from recombinant fragment-channels show that they display biophysical properties distinct from full-length channels (Figures 6C-6E). Furthermore, our results show that cleaved $Ca_v1.2$ fragments can dissociate from one another (Figures 2B, 2C and 2F), and while these fragments do not form functional channels on their own (Figure 6B), some of them can alter the biophysical properties of full-length channels (Figures 6F-6L). Thus, $Ca_v1.2$ currents in native cells could be produced by a highly heterogeneous population of channels. How fragment-channels change full-length $Ca_v1.2$ properties is unclear; possibilities include competition for the ancillary subunits (β and/or $\alpha_2\delta$) or a direct association with $Ca_v1.2$.

VGCCs are regulated by a host of Ca^{2+}-binding proteins and undergo Ca^{2+}-dependent inactivation (CDI) involving calmodulin (Christel and Lee, 2012). Why do neurons need yet another Ca^{2+}-dependent negative feedback mechanism, and one as drastic as mid-channel proteolysis? For neuroprotection, it is not surprising if neurons utilize multiple or even redundant means to diligently control the activity of channels as essential as VGCCs. There may also be significant differences between CDI and mid-channel proteolysis for neurons to exploit. For example, CDI can occur quickly to affect VGCC activity within milliseconds (Tadross et al., 2008, Christel, 2012 #197); mid-channel

proteolysis, on the other hand, takes longer and may affect not only VGCC activity but also intracellular Ca^{2+} homeostasis. Furthermore, while CDI mainly assists VGCC inactivation, the consequences of mid-channel proteolysis can involve Ca^{2+} current attenuation, channel biophysical property changes, and perhaps putative non-channel functions of the nascent fragments.

It has been shown that $Ca_v1.2$ and $Ca_v2.2$ undergo ubiquitination and proteasomal degradation, and that these events are regulated by $Ca_v\beta$ (Altier et al., 2011; Waithe et al., 2011). In the absence of $Ca_v\beta$, $Ca_v1.2$ is robustly ubiquitinated and is targeted to the proteasome for degradation; association of $Ca_v\beta$ attenuates $Ca_v1.2$ ubiquitination and prevents endoplasmic reticulum (ER)-associated protein degradation (ERAD), leading to an increased surface expression of $Ca_v1.2$ (Altier et al., 2011). It is unclear if and how mid-channel proteolysis relates to ERAD, but imaging experiments revealed that separation of proteolytically cleaved $Ca_v1.2$ fragments was unaltered by the overexpression of $\alpha_2\delta$ and β subunits (Figures S2C, S2D), suggesting that either these auxiliary subunits do not affect mid-channel proteolysis, or the channels undergoing mid-channel proteolysis already have associated endogenous $\alpha_2\delta$ and $Ca_v\beta$ subunits.

Where does $Ca_v1.2$ mid-channel proteolysis take place, on the plasma membrane or in an intracellular compartment? Although our results do not provide a definitive answer, they are consistent with the possibility that mid-channel proteolysis occurs on the plasma membrane: (1) Cleaved complementary $Ca_v1.2$ fragments are present on the plasma membrane (Figures 1C-1E and Figure 2A). (2) It is not affected by the overexpression of $\alpha_2\delta$ and β subunits (Figures S2C, S2D). (3) It is dependent on the ubiquitin-proteasome system, being greatly reduced by a cocktail of ubiquitination and proteasome inhibitors or

when a putative ubiquitination site on $Ca_v1.2$ is mutated (Figures 3C and 3D). (4) It is significantly reduced (Figure 3F) or virtually abolished (Figure 3G) when PEST sequences in $Ca_v1.2$ are deleted. PEST sequences serve as signals for rapid proteolysis by yet unknown proteases (with calpain as a candidate) or by proteasomal degradation, presumably by recruiting proper proteases to the target protein or directing the target protein to proteasomes (Rechsteiner and Rogers, 1996). It has been reported that the two PEST sequences in $Ca_v1.2$ are involved in Akt-mediated increase of calcium channel currents (Catalucci et al., 2009). Akt is thought to phosphorylate $Ca_v\beta_2$, resulting in the masking of the PEST sequences and, consequently, decreased degradation of surface $Ca_v1.2$. Consistent with this notion, deleting each PEST sequence individually increases the stability and current density of $Ca_v1.2$ channels expressed in COS-7 or tsA-201 cells (Catalucci et al., 2009). The precise role of the two PEST sequences and why PEST1 is more effective than PEST3 in aiding $Ca_v1.2$ mid-channel proteolysis remain to be investigated. These sequences are probably not the cleavage sites themselves. We speculate that PEST1, because of its location and/or conformation in the three-dimensional structure of $Ca_v1.2$, is more effective than PEST3 in recruiting calpain to $Ca_v1.2$.

Many other questions remain to be elucidated, including the kinetics of mid-channel proteolysis, additional proteases involved, the precise cleavage sites in $Ca_v\alpha_1$, and the fate and function of the resulting fragment-channels. It will be interesting to examine whether other types of VGCCs and other multi-repeat ion channels such as Na^+ channels also undergo mid-channel proteolysis. Truncated forms of $Ca_v\alpha_1$, generated by either alternative splicing or disease-causing mutations, are naturally present in muscles and

neurons (Jeng et al., 2008; Malouf et al., 1992; Mezghrani et al., 2008; Okagaki et al., 2001; Page et al., 2004; Pietrobon, 2010; Scott et al., 1998; Wappl et al., 2002). The fragment-channels produced by regulated mid-channel proteolysis, as well as these short forms of $Ca_v\alpha_1$, may play important roles in both physiological and pathological conditions.

EXPERIMENTAL PROCEDURES

Constructs

Rat (Rattus norvegicus) brain $Ca_v1.2$ was used for transfection in hippocampal neurons. GFP was linked to the N-terminus of $Ca_v1.2$ to generate LGN. HA epitopes were cloned on LGN at different extracellular locations to generate GFP- and HA-tagged LGH1, LGH2, and LGH3, in which the HA tag was placed, respectively, between residues T320-G321, Q683-T684, and G1136-P1137. A proteolytic motif (ENLYFQG) for TEVp was introduced on LGH3 between II-III loop residues D815-G816 (LGH3_TEVp). On LGH3_PY/AA, P1364 and Y1365 were each mutated to alanine. Residues 840-861 and 446-459 were deleted to generate LGH3_ΔPEST3 and LGH3_ΔPEST1, respectively. $Ca_v1.2$ fragment-channels were engineered to encompass the following channel regions: A1: M1-D449, A2: E450-L2143; B1: M1-S866, B2: M867-L2143; C1: M1-W1216, C2: Y1217-L2143. For oocyte macropatch recordings, rabbit $Ca_v2.1$ was used. $Ca_v2.1$_TEVp carried the TEVp cutting motif at three different locations: G419-A420 (loop I-II), L1096-S1097 and G1218-P1219 (loop II-III).

Cortical Slice Surface Protein Biotinylation

Neocortical slices (400-µm thick, cut horizontally) were obtained from 6-week old male rat brain and were incubated at 35-37°C in oxygenated artificial cerebrospinal fluid (ACF, in mM: NaCl 119, $NaHCO_3$ 26, NaH_2PO4 1.25, KCl 2.5, glucose 15, myo-inositol 1, pyruvate 2, ascorbic acid 0.4) for 20-60 min before any pharmacological treatments. For biotinylation of surface proteins, slices were rapidly collected into ice-cold bubbled ACF containing 1mg/ml sulfo-NHS-SS-biotin (Pierce) for 45 min. Quenching solution

was added for 5 min. Solubilization, incubation with neutravidin-agarose beads, washing and elution of surface proteins for SDS-PAGE and Western blot, were performed according to Pierce's instructions, with modifications for neocortical slices described in detail in Supplemental Experimental Procedures.

Cortical Slice Age Comparison

For the aging study of Figure 7A, the procedure described above was upgraded to handle 4 or more animals of different ages in strict parallel, as described in detail in Supplemental Experimental Procedures.

Verapamil Feeding of Aged Animals

Verapamil was used to medicate the drinking water of aged rats, at 12.5 mg per diem, for 3 to 5 weeks. Dosage calculation and details of verapamil administration are explained in Supplemental Experimental Procedures.

Hippocampal Neuron Culture, Transfection and Surface Biotinylation

Embryonic hippocampi were isolated and primary cultures were grown using standard procedures (Blanpied et al., 2002). 24 h after plating and then every 4 days, neurobasal medium containing B-27 and I-glutamax (Invitrogen) was used to replace 50% of the culture medium. Neurons were kept at 37°C in a 5% CO_2 humid atmosphere. Hippocampal neurons DIV10-13 were transfected with an optimized method using Lipofectamine 2000 (Invitrogen). 1.5 μg of DNA in 100 μl Opti-MEM (Invitrogen) were used to transfect each 12 mm (diameter) coverslip. Surface biotinylation was similar to that described for cortical slices.

Hippocampal Neuron Immunofluorescence and Imaging

Hippocampal neurons were fixed with 2% paraformaldehyde and immunostained 24-48 h post-transfection. To visualize surface HA tags, neurons were incubated with a mouse monoclonal anti-HA (Covance) for 1 h in PBS containing 0.5% fish gelatin and 10% goat serum, then washed with PBS 4 times. The goat anti-mouse secondary antibody conjugated with the Alexa594 fluorophore (Invitrogen) was added to the neurons for 1 h in the same buffer composition. The stained coverslips were washed and mounted on imaging slides using an anti-fade reagent (Biomeda). All procedures were done at room temperature.

Confocal imaging was performed using a spinning disc microscope. Optical slice thickness was 300 nm. Confocal images for each fluorophore in multi-labeling experiments were acquired separately (sequential scans). Images were analyzed using Volocity (PerkinElmer) and MatLab.

Imaging Data Quantification and Histogram Construction

A software routine was created to scan optical sections of dendrites and automatically select the red objects, which presumably represent surface $Ca_V1.2$. These objects vary in size and are divided into a volume unit called voxel, which has a dimension of 0.211x0.211x0.211μm and a volume of 0.00944 μm^3. Typically, ~10,000-15,000 voxels were generated for each neuron. The red and green intensity was measured for each voxel and the red/green ratio (i.e., non-colocalization index or NCI) was determined. The NCI of all the voxels was binned and plotted in a frequency (ordinate, Y-axis) vs. NCI

(abscissa, X-axis) graph. This resulting distribution (curve) shows the percentage of voxels that exhibit NCI *above* a threshold value.

In ensemble %Frequency-above-threshold vs. NCI curves using data pooled from multiple neurons, the X-axis consisted of step thresholds used to bin the entire population of NCI values. Typically, a group of ~15 neurons produced ~150,000-200,000 voxels. X-axis thresholds were a sequence of logarithmically spaced numbers generated by MatLab to represent values between 0.1 and 10 (listed in Supplemental Experimental Proceudures). Y-axis data points from all the neurons in any given group were averaged and plotted.

Xenopus Oocyte Preparation, Injection and Surface Biotinylation

Female oocyte-positive *Xenopus laevis* (African clawed) frogs were purchased from Xenopus I, Xenopus Express or Nasco, and stage V-VI oocytes were isolated. Briefly, frogs were anesthetized in a 0.3% tricaine solution. Ovarian lobes were excised in OR2 (Ca^{2+}-free) solution (mM: NaCl 82.4, KCl 2.5, $MgCl_2$ 1, HEPES 5) and digested in OR2 supplemented with collagenase A (0.2-0.5 mg/ml, Roche) for 2-3 h at room temperature. Oocytes were washed and recovered in ND96 solution (mM: NaCl 96, KCl 2.5, $MgCl_2$ 1, HEPES 5, $CaCl_2$ 1.8, supplemented with penicillin/streptomycin). mRNA injection and oocyte surface biotinylation protocol are presented in detail in Supplemental Experimental Procedures.

Electrophysiology

For whole-cell recording of hippocampal neurons, the pipette solution contained (in mM): CsCl 122, HEPES 10, EGTA 10, $MgCl_2$ 5, MgATP 4 and GTP 0.4, pH 7.2 with

CsOH. Recording electrodes had resistances of 2-4 MΩ. The bath solution contained (in mM): NaCl 115, TEA·OH 20, KCl 5, $MgCl_2$ 2, $BaCl_2$ 5, HEPES 10, D-glucose 10, pH 7.4 with NaOH. 1 μM TTX was added before recordings.

For two-electrode voltage-clamp recording of oocytes, the bath solution contained (in mM): $BaCl_2$ 10, KCl 5, tetraethyl ammonium hydroxide 60, NaOH 20, HEPES 5 (pH 7.4 adjusted with methanesulfonic acid).

For inside-out macropatch recordings from oocytes, $Ca_v2.1$ (P/Q-type) channels were used because of their slower rundown (Zhen et al., 2006). Electrodes had a diameter of 15-30 μm and a resistance of 0.2-0.4 MΩ when filled with a solution containing (in mM): $BaCl_2$ 45, KCl 80, HEPES 10, pH 7.3 with KOH. The bath solution contained (in mM): CsCl 125, NaCl 4, HEPES 10, EGTA 10, pH 7.3 with KOH. The purified WT or mutant TEV proteases were perfused in the bath solution for 2 min, followed by 1 min of wash.

Data were analyzed with Clampfit. All experiments were performed at 22-23°C.

Western Immunoblotting

Protein samples were run in 8% acrylamide (BioRad) gels or 4-12% precast gradient gels (Invitrogen). Electrical transfer to PVDF membranes (BioRad) was performed in a standard 25 mM Tris, 192 mM glycine, pH~8.3 buffer supplemented with 0.002% SDS for 90 min at 90 V, at 4°C. Membranes were handled in PBS containing 0.2% Tween-20 (PBST). Blocking buffer was 10% newborn calf serum (NCS, Gibco) plus 1% fish gelatin (Sigma) in PBST. Primary antibodies were used at 1:750-1:1000 dilutions, and were purchased from Sigma (anti-L_{II-III} and anti-Nt), Cell Signaling (anti-PARP), and

Abcam (anti-Na^+/K^+-ATPase). Anti-Ct, generated against residues 2155-2171 of the rabbit cardiac $Ca_v1.2$ (Hulme et al., 2006), was a courteous gift from Drs. W.A. Catterall and R. Westenbroek (University of Washington, Seattle). Secondary antibody (goat anti-rabbit, HRP-conjugated, SantaCruz Biotechnologies) was used at 1:2000 dilution. Protein bands were visualized using enhanced chemiluminescence reagents (Pierce) on X-ray film (Kodak). For stripping and reprobing of PVDF membranes, the stripping buffer was 100 mM β-mercaptoethanol, 2% SDS, 62.5 mM Tris-HCl, pH 6.8. Coomassie Blue staining was performed using Biosafe Coomassie (BioRad) according to the manufacturer's instructions, or using a stain consisting of 0.1% Coomassie Brilliant Blue R-250 in 40% MeOH and 1% acetic acid.

Purification of Tobacco etch virus protease

For protein synthesis in *E. coli*, DE3 bacteria were used for cDNA transformation and protein expression. The expressed recombinant tobacco etch virus protease (TEVp, Addgene Plasmid 8827: pRK793) construct contained an MBP molecule for enhanced expression, a TEVp self-cleavage recognition site (ENLYFQG), a His-tag, and finally TEVp itself. Ultimately, TEVp was isolated from transformed DE3 bacteria using a nickel-bead column system as described in Supplemental Experimental Procedures. Western blot with an antibody against TEVp (courtesy of Dr. Michael Ehrmann at University of Duisburg-Essen, Germany) revealed that the purified TEVp had the expected molecular mass of TEVp plus the His tag (27 kDa), indicating that the tagged MBP molecule had been removed from the parent construct by TEVp self-cleavage (Figure S6A). In contrast, the molecular mass of the purified C151A mutant protease was significantly higher (70 kDa) than that of WT TEVp (Figure S6A), as expected for the

original MBP-tagged parent construct, confirming the loss of catalytic activity caused by the C151A mutation.

Statistics

Data are represented as mean±s.e.m. and asterisks denote statistical differences throughout. For all statistical tests used and their resulting p-values, see Supplemental Experimental Procedures.

ACKNOWLEDGEMENTS

We thank Drs. William Catterall and Ruth Westenbroek of University of Washington for the anti-Ct antibody, Dr. Michael Ehrmann of University of Duisburg-Essen for the anti-TEVp antibody, Glynis Gordon and Rachel Schenkel for technical assistance, and Dr. Zafir Buraei of Pace University and members of Yang laboratory for commenting on the manuscript. This work was supported by National Institutes of Health Grants NS053494 and NS045383 (to J.Y), the Established Investigator Award of the American Heart Association (to J.Y), the Top Talents Program of Yunnan Province, China (to J.Y), and a Postdoctoral Fellowship (0625908T) from the American Heart Association (to I.E.M).

FIGURE LEGENDS

Figure 1. Mid-channel proteolysis of native $Ca_v1.2$ in cortical neurons and its dependence on channel activity

(A) Domain topology of $Ca_v1.2$. Indicated are epitope locations for three antibodies (anti-L_{II-III}, anti-Ct and anti-Nt) and predicted molecular masses for full-length $Ca_v1.2$ and two fragment-channels generated by a presumed proteolytic cut (scissors).

(B) Western blot with anti-L_{II-III} of native $Ca_v1.2$ in surface-biotinylated (+) and non-biotinylated (-) cortical slices from 6-week old rats, showing a 150-kDa band (arrow). (C-E) Western blot with anti-L_{II-III} (C), anti-Ct (D) or anti-Nt (E) of native $Ca_v1.2$ from the same sample of surface-biotinylated cortical slices.

(F-I) Channel activity-dependent regulation of mid-channel proteolysis. Left: representative Western blot with anti-L_{II-III} of $Ca_v1.2$ in cortical slices treated with either vehicle (control) or the indicated reagent(s) before surface biotinylation: (F) verapamil (VP, 65 μM, 2 hr); (G) nifedipine (Nif, 10 μM, 2 hr) and CNQX (21.5 μM, 2 hr); (H) ionomycin (Iono, 3 μM, 45 min); (I) BayK8644 (14 μM, 40 min) and 65 mM KCl (40 min). Middle: bar graph depicting the proteolysis index (intensity ratio of 150-kDa/240-kDa band) for the representative gel. Right: summary graph showing data pooled from the indicated number of independent experiments. In this and all subsequent figures, data in bar graphs are represented as mean±s.e.m. and asterisks denote statistical differences, with $P<0.01$, unless indicated otherwise. See also Figure S5.

Figure 2. Visualization of mid-channel proteolysis of $Ca_v1.2$ in the plasma membrane of cultured hippocampal neurons

(A) Western blot with the indicated antibodies of native $Ca_v1.2$ from the same preparation of surface-biotinylated neurons.

(B) Confocal images of a representative dendritic segment of a neuron expressing LGH3. Left: surface and intracellular LGH3 indicated by GFP. Middle: surface LGH3 indicated by anti-HA+Alexa594 secondary antibodies. Right: overlay. Exemplar clusters of red/green colocalization and non-colocalization are marked by yellow and white arrows, respectively. Scale bar: 5 μm.

(C) Fluorescence intensity profile (bottom) of another dendritic segment (top). Exemplar clusters of red/green colocalization and non-colocalization are marked by * and **, respectively.

(D) Quantification of red/green colocalization in two dendritic segments displaying visually different extents of mid-channel proteolysis. Left and middle: images of GFP (lane 1), HA-Alexa594 (lane 2), overlay (lane 3) and the "voxels" selected according to our analysis protocol (lane 4). Right: cumulative distribution of the non-colocalization index (NCI) for the two selected dendritic segments. Scale bar: 10 μm.

(E) Ensemble cumulative distribution of NCI from the dendrites of neurons expressing LGH3 randomly divided into two groups (n=15 each, same culture).

(F) Ensemble cumulative distribution of NCI from the dendrites of neurons expressing LGH1 (n=23), LGH2 (n=15) and LGH3 (n=13). All experiments were performed in parallel. The three distributions were significantly different. See also Figures S1 and S2.

Figure 3. Signaling pathways and molecular determinants of $Ca_v1.2$ mid-channel proteolysis.

(A) Role of calpain. Left: representative Western blot with anti-L_{II-III} in hippocampal neurons treated, before surface biotinylation, with a cocktail of calpain inhibitors (200 nM calpeptin, 1 μM ALLN, and 270 nM calpain inhibitor III) for 80 min at 37°C. Middle: proteolysis index for the representative gel. Right: summary graph showing data pooled from 4 independent experiments. $P<0.05$.

(B) Ensemble cumulative distribution of NCI from the dendrites of neurons expressing LGH3 treated with DMSO (control, n=24) or calpain inhibitors (n=19).

(C) Ensemble cumulative distribution of NCI from the dendrites of neurons expressing LGH3 (n=13) treated with DMSO (control) or a cocktail of MG-132 (7 μM) and ubiquitin aldehyde (1 μM) for 75 min at 37°C.

(D) Ensemble cumulative distribution of NCI from the dendrites of neurons expressing LGH3 (n=16) or LGH3_PY/AA (n=17), where residues P1364 and Y1365 of LGH3 were mutated to alanine.

(E) Schematic domain topology of LGH3, marking the positions and amino acid sequences of the PEST1 site, the PEST3 site, and the PY motif.

(F) Ensemble cumulative distribution of NCI from the dendrites of neurons expressing LGH3 (n=19) or LGH3_ΔPEST3 (n=17), where residues H840-R861 of LGH3 were deleted.

(G) Ensemble cumulative distribution of NCI from the dendrites of neurons expressing LGH3 (n=19) or LGH3_ΔPEST1 (n=15), where residues D446-D459 of LGH3 were deleted. Representative dendrites are shown in Figure S3C. In (B-D), (F) and (G), all

experiments in each panel were performed in parallel, and the two distributions were significantly different. See also Figure S3.

Figure 4. Channel activity-dependent regulation of $Ca_v1.2$ mid-channel proteolysis and Ca^{2+} channel currents in cultured hippocampal neurons.

(A and C) Ensemble cumulative distribution of NCI from the dendrites of neurons expressing LGH3. Neurons were treated for 30 min with DMSO (control), DMSO and 65 mM KCl, or 1.4 μM BayK8644 and 65 mM KCl (n=13 for all) in (A); or with DMSO (control) (n=19), DMSO and 65 mM KCl (n=14), or 20 μM nifedipine and 65 mM KCl (n=18) in (C). Representative dendrites for each condition are shown in Figure S4A. All experiments in each panel were performed in parallel. In (A), the two treated groups were significantly different from control but not from each other; in (C), all three distributions were significantly different. The same results were obtained from two other independent cultures.

(B and D) Channel activity-dependent regulation of mid-channel proteolysis. Left: representative Western blot with anti-$L_{II\text{-}III}$ in neurons treated (1hr) with DMSO (ctl) or BayK8644 (1.4 μM) (B), or nifedipine (10 μM) (D), before surface biotinylation. Middle: proteolysis index for the representative gel. Right: summary graph showing data pooled from the indicated number of independent experiments.

(E and F) Whole-cell Ca^{2+} channel currents from neurons blindly treated for 30 min with DMSO (ctl), or 65 mM KCl and 1.4 μM BayK8644 (E), or 10 μM nifedipine (F). Left: representative family of currents recorded from the indicated neuron. Right: summary

graph of the maximal current density for the indicated group of neurons. Number of blind recordings is indicated above the bar. $P<0.05$. See also Figure S4.

Figure 5. Functional effect of mid-channel cleavage at an engineered site on Ca^{2+} channel currents and properties.

(A) Schematic of LGH3_TEVp, which contains a TEVp cutting site (yellow circle) in the II-III loop between D815 and G816, upstream of the anti-L_{II-III} epitope T821-S838.

(B) Whole-cell currents (top) recorded at -10 mV from oocytes expressing the indicated constructs (middle). Currents were normalized to the mean value of the left-most control group. Number of measurements indicated above the bar. Bottom: Western blot with anti-L_{II-III} of surface-biotinylated oocytes from the exact same groups.

(C) Voltage-dependence of activation of currents recorded from inside-out macropatches excised from oocytes expressing $Ca_v2.1$_TEVp or WT $Ca_v2.1$, before (top) or after (bottom) bath application of 100 μM purified TEVp or TEVp(C151A). Standard error is smaller than the symbols (n=7-10). See also Figure S6A.

Figure 6. Functional properties and effects of fragment-channels.

(A) Schematic of three possible cuts (scissors) of $Ca_v1.2$ and three pairs of recombinant complementary fragment-channels.

(B and C) Whole-cell currents recorded at -10 mV from oocytes expressing the indicated recombinant fragment-channels (B) or proper pairs (C).

(D and E) Current-voltage relationship (D) and voltage-dependence of inactivation (E) of currents recorded from oocytes expressing the indicated constructs. Standard error is smaller than the symbols (n=6-18).

(F) Whole-cell currents recorded at -10 mV from oocytes expressing full-length $Ca_v1.2$, with or without the indicated recombinant fragment-channel coexpressed.

(G-L) Current-voltage (I-V) relationship (G, I, and K) and voltage-dependence of inactivation (H, J, and L) of currents recorded from oocytes expressing the indicated $Ca_v1.2$ constructs. Standard error is smaller than the symbols (n=3 for (L) and n=6-14 for other panels). The effect of C2 could not be assessed because the whole-cell current in those experiments was too small to allow accurate measurements (see (F), right-most bar). See also Figure S6B.

Figure 7. Mid-channel proteolysis is age-dependent and can be reversed by a L-type VGCC blocker *in vivo*.

(A) Progressive increase of mid-channel proteolysis with age. Left: representative Western blot with anti-L_{II-III} of native $Ca_v1.2$ in surface-biotinylated rat cortical slices from the indicated age groups. Middle: proteolysis index for the representative gel. Right: summary graph showing data pooled from the indicated number of independent experiments. Every independent experiment consisted of parallel dissections of the age groups involved (see Experimental Procedures).

(B) Reduction of mid-channel proteolysis by oral administration of verapamil. Left: representative Western blot with anti-L_{II-III} of native $Ca_v1.2$ in surface-biotinylated cortical slices from 16-month old rats fed with water, or water medicated with 12.5 mg

per day of verapamil for 3-5 weeks. Middle: proteolysis index for the representative gel. Right: summary graph showing data pooled from five independent experiments. See also Figure S7.

REFERENCES

Altier, C., Garcia-Caballero, A., Simms, B., You, H., Chen, L., Walcher, J., Tedford, H.W., Hermosilla, T., and Zamponi, G.W. (2011). The Cavbeta subunit prevents RFP2-mediated ubiquitination and proteasomal degradation of L-type channels. Nat Neurosci *14*, 173-180.

Blanpied, T.A., Scott, D.B., and Ehlers, M.D. (2002). Dynamics and regulation of clathrin coats at specialized endocytic zones of dendrites and spines. Neuron *36*, 435-449.

Brawley, R.M., and Hosey, M.M. (1992). Identification of two distinct proteins that are immunologically related to the alpha 1 subunit of the skeletal muscle dihydropyridine-sensitive calcium channel. J Biol Chem *267*, 18218-18223.

Cain, S.M., and Snutch, T.P. (2011). Voltage-gated calcium channels and disease. Biofactors *37*, 197-205.

Catalucci, D., Zhang, D.H., DeSantiago, J., Aimond, F., Barbara, G., Chemin, J., Bonci, D., Picht, E., Rusconi, F., Dalton, N.D.*, et al.* (2009). Akt regulates L-type Ca2+ channel activity by modulating Cavalpha1 protein stability. J Cell Biol *184*, 923-933.

Catterall, W.A. (2000). Structure and regulation of voltage-gated Ca2+ channels. Annu Rev Cell Dev Biol *16*, 521-555.

Chaitanya, G.V., Steven, A.J., and Babu, P.P. (2010). PARP-1 cleavage fragments: signatures of cell-death proteases in neurodegeneration. Cell Commun Signal *8*, 31.

Christel, C., and Lee, A. (2012). Ca2+-dependent modulation of voltage-gated Ca2+ channels. Biochim Biophys Acta *1820*, 1243-1252.

De Jongh, K.S., Colvin, A.A., Wang, K.K., and Catterall, W.A. (1994). Differential proteolysis of the full-length form of the L-type calcium channel alpha 1 subunit by calpain. J Neurochem *63*, 1558-1564.

De Jongh, K.S., Warner, C., Colvin, A.A., and Catterall, W.A. (1991). Characterization of the two size forms of the alpha 1 subunit of skeletal muscle L-type calcium channels. Proc Natl Acad Sci U S A *88*, 10778-10782.

Deisseroth, K., Mermelstein, P.G., Xia, H., and Tsien, R.W. (2003). Signaling from synapse to nucleus: the logic behind the mechanisms. Curr Opin Neurobiol *13*, 354-365.

Di Biase, V., Tuluc, P., Campiglio, M., Obermair, G.J., Heine, M., and Flucher, B.E. (2011). Surface traffic of dendritic CaV1.2 calcium channels in hippocampal neurons. J Neurosci *31*, 13682-13694.

Dolmetsch, R. (2003). Excitation-transcription coupling: signaling by ion channels to the nucleus. Sci STKE *2003*, PE4.

Ebihara, T., Komiya, Y., Izumi-Nakaseko, H., Adachi-Akahane, S., Okabe, S., and Okamura, Y. (2002). Coexpression of a Ca(v)1.2 protein lacking an N-terminus and the first domain specifically suppresses L-type calcium channel activity. FEBS Lett *529*, 203-207.

Fuller, M.D., Emrick, M.A., Sadilek, M., Scheuer, T., and Catterall, W.A. (2010). Molecular mechanism of calcium channel regulation in the fight-or-flight response. Sci Signal *3*, ra70.

Gao, T., Cuadra, A.E., Ma, H., Bunemann, M., Gerhardstein, B.L., Cheng, T., Eick, R.T., and Hosey, M.M. (2001). C-terminal fragments of the alpha 1C (CaV1.2) subunit associate with and regulate L-type calcium channels containing C-terminal-truncated alpha 1C subunits. J Biol Chem *276*, 21089-21097.

Gerhardstein, B.L., Gao, T., Bunemann, M., Puri, T.S., Adair, A., Ma, H., and Hosey, M.M. (2000). Proteolytic processing of the C terminus of the alpha(1C) subunit of L-type calcium channels and the role of a proline-rich domain in membrane tethering of proteolytic fragments. J Biol Chem *275*, 8556-8563.

Hell, J.W., Westenbroek, R.E., Breeze, L.J., Wang, K.K., Chavkin, C., and Catterall, W.A. (1996). N-methyl-D-aspartate receptor-induced proteolytic conversion of postsynaptic class C L-type calcium channels in hippocampal neurons. Proc Natl Acad Sci U S A *93*, 3362-3367.

Hell, J.W., Yokoyama, C.T., Wong, S.T., Warner, C., Snutch, T.P., and Catterall, W.A. (1993). Differential phosphorylation of two size forms of the neuronal class C L-type calcium channel alpha 1 subunit. J Biol Chem *268*, 19451-19457.

Hulme, J.T., Konoki, K., Lin, T.W., Gritsenko, M.A., Camp, D.G., 2nd, Bigelow, D.J., and Catterall, W.A. (2005). Sites of proteolytic processing and noncovalent association of

the distal C-terminal domain of CaV1.1 channels in skeletal muscle. Proc Natl Acad Sci U S A *102*, 5274-5279.

Hulme, J.T., Yarov-Yarovoy, V., Lin, T.W., Scheuer, T., and Catterall, W.A. (2006). Autoinhibitory control of the CaV1.2 channel by its proteolytically processed distal C-terminal domain. J Physiol *576*, 87-102.

Jeng, C.J., Sun, M.C., Chen, Y.W., and Tang, C.Y. (2008). Dominant-negative effects of episodic ataxia type 2 mutations involve disruption of membrane trafficking of human P/Q-type Ca2+ channels. J Cell Physiol *214*, 422-433.

Kordasiewicz, H.B., Thompson, R.M., Clark, H.B., and Gomez, C.M. (2006). C-termini of P/Q-type Ca2+ channel alpha1A subunits translocate to nuclei and promote polyglutamine-mediated toxicity. Hum Mol Genet *15*, 1587-1599.

Lai, Y., Seagar, M.J., Takahashi, M., and Catterall, W.A. (1990). Cyclic AMP-dependent phosphorylation of two size forms of alpha 1 subunits of L-type calcium channels in rat skeletal muscle cells. J Biol Chem *265*, 20839-20848.

Leenders, A.G., Lin, L., Huang, L.D., Gerwin, C., Lu, P.H., and Sheng, Z.H. (2008). The role of MAP1A light chain 2 in synaptic surface retention of Cav2.2 channels in hippocampal neurons. J Neurosci *28*, 11333-11346.

Leenders, A.G., van den Maagdenberg, A.M., Lopes da Silva, F.H., Sheng, Z.H., Molenaar, P.C., and Ghijsen, W.E. (2002). Neurotransmitter release from tottering mice nerve terminals with reduced expression of mutated P- and Q-type Ca2+-channels. Eur J Neurosci *15*, 13-18.

Liao, P., and Soong, T.W. (2010). CaV1.2 channelopathies: from arrhythmias to autism, bipolar disorder, and immunodeficiency. Pflugers Arch *460*, 353-359.

Malouf, N.N., McMahon, D.K., Hainsworth, C.N., and Kay, B.K. (1992). A two-motif isoform of the major calcium channel subunit in skeletal muscle. Neuron *8*, 899-906.

Mezghrani, A., Monteil, A., Watschinger, K., Sinnegger-Brauns, M.J., Barrere, C., Bourinet, E., Nargeot, J., Striessnig, J., and Lory, P. (2008). A destructive interaction mechanism accounts for dominant-negative effects of misfolded mutants of voltage-gated calcium channels. J Neurosci *28*, 4501-4511.

Moyer, J.R., Jr., Thompson, L.T., Black, J.P., and Disterhoft, J.F. (1992). Nimodipine increases excitability of rabbit CA1 pyramidal neurons in an age- and concentration-dependent manner. J Neurophysiol *68*, 2100-2109.

Okagaki, R., Izumi, H., Okada, T., Nagahora, H., Nakajo, K., and Okamura, Y. (2001). The maternal transcript for truncated voltage-dependent Ca2+ channels in the ascidian embryo: a potential suppressive role in Ca2+ channel expression. Dev Biol *230*, 258-277.

Page, K.M., Heblich, F., Davies, A., Butcher, A.J., Leroy, J., Bertaso, F., Pratt, W.S., and Dolphin, A.C. (2004). Dominant-negative calcium channel suppression by truncated constructs involves a kinase implicated in the unfolded protein response. J Neurosci *24*, 5400-5409.

Page, K.M., Heblich, F., Margas, W., Pratt, W.S., Nieto-Rostro, M., Chaggar, K., Sandhu, K., Davies, A., and Dolphin, A.C. (2010). N terminus is key to the dominant negative suppression of Ca(V)2 calcium channels: implications for episodic ataxia type 2. J Biol Chem *285*, 835-844.

Pietrobon, D. (2010). CaV2.1 channelopathies. Pflugers Arch *460*, 375-393.

Raghib, A., Bertaso, F., Davies, A., Page, K.M., Meir, A., Bogdanov, Y., and Dolphin, A.C. (2001). Dominant-negative synthesis suppression of voltage-gated calcium channel Cav2.2 induced by truncated constructs. J Neurosci *21*, 8495-8504.

Raike, R.S., Kordasiewicz, H.B., Thompson, R.M., and Gomez, C.M. (2007). Dominant-negative suppression of Cav2.1 currents by alpha(1)2.1 truncations requires the conserved interaction domain for beta subunits. Mol Cell Neurosci *34*, 168-177.

Ramakrishnan, N.A., Drescher, M.J., Sheikhali, S.A., Khan, K.M., Hatfield, J.S., Dickson, M.J., and Drescher, D.G. (2006). Molecular identification of an N-type Ca2+ channel in saccular hair cells. Neuroscience *139*, 1417-1434.

Rechsteiner, M., and Rogers, S.W. (1996). PEST sequences and regulation by proteolysis. Trends Biochem Sci *21*, 267-271.

Sakurai, T., Hell, J.W., Woppmann, A., Miljanich, G.P., and Catterall, W.A. (1995). Immunochemical identification and differential phosphorylation of alternatively spliced forms of the alpha 1A subunit of brain calcium channels. J Biol Chem *270*, 21234-21242.

Schiff, M.L., Siderovski, D.P., Jordan, J.D., Brothers, G., Snow, B., De Vries, L., Ortiz, D.F., and Diverse-Pierluissi, M. (2000). Tyrosine-kinase-dependent recruitment of RGS12 to the N-type calcium channel. Nature *408*, 723-727.

Scott, V.E., Felix, R., Arikkath, J., and Campbell, K.P. (1998). Evidence for a 95 kDa short form of the alpha1A subunit associated with the omega-conotoxin MVIIC receptor of the P/Q-type Ca2+ channels. J Neurosci *18*, 641-647.

Smoller, J.W., Craddock, N., Kendler, K., Lee, P.H., Neale, B.M., Nurnberger, J.I., Ripke, S., Santangelo, S., and Sullivan, P.F. (2013). Identification of risk loci with shared effects on five major psychiatric disorders: a genome-wide analysis. Lancet *381*, 1371-1379.

Striessnig, J., Bolz, H.J., and Koschak, A. (2010). Channelopathies in Cav1.1, Cav1.3, and Cav1.4 voltage-gated L-type Ca2+ channels. Pflugers Arch *460*, 361-374.

Tadross, M.R., Dick, I.E., and Yue, D.T. (2008). Mechanism of local and global Ca2+ sensing by calmodulin in complex with a Ca2+ channel. Cell *133*, 1228-1240.

Thibault, O., and Landfield, P.W. (1996). Increase in single L-type calcium channels in hippocampal neurons during aging. Science *272*, 1017-1020.

Thibault, O., Porter, N.M., Chen, K.C., Blalock, E.M., Kaminker, P.G., Clodfelter, G.V., Brewer, L.D., and Landfield, P.W. (1998). Calcium dysregulation in neuronal aging and Alzheimer's disease: history and new directions. Cell Calcium *24*, 417-433.

Waithe, D., Ferron, L., Page, K.M., Chaggar, K., and Dolphin, A.C. (2011). Beta-subunits promote the expression of Ca(V)2.2 channels by reducing their proteasomal degradation. J Biol Chem *286*, 9598-9611.

Wappl, E., Koschak, A., Poteser, M., Sinnegger, M.J., Walter, D., Eberhart, A., Groschner, K., Glossmann, H., Kraus, R.L., Grabner, M.*, et al.* (2002). Functional consequences of P/Q-type Ca2+ channel Cav2.1 missense mutations associated with episodic ataxia type 2 and progressive ataxia. J Biol Chem *277*, 6960-6966.

Westenbroek, R.E., Sakurai, T., Elliott, E.M., Hell, J.W., Starr, T.V., Snutch, T.P., and Catterall, W.A. (1995). Immunochemical identification and subcellular distribution of the alpha 1A subunits of brain calcium channels. J Neurosci *15*, 6403-6418.

Wheeler, D.G., Groth, R.D., Ma, H., Barrett, C.F., Owen, S.F., Safa, P., and Tsien, R.W. (2012). Ca(V)1 and Ca(V)2 channels engage distinct modes of Ca(2+) signaling to control CREB-dependent gene expression. Cell *149*, 1112-1124.

Woppmann, A., Ramachandran, J., and Miljanich, G.P. (1994). Calcium channel subtypes in rat brain: biochemical characterization of the high-affinity receptors for omega-conopeptides SNX-230 (synthetic MVIIC), SNX-183 (SVIB), and SNX-111 (MVIIA). Mol Cell Neurosci *5*, 350-357.

Zamponi, G.W., and Currie, K.P. (2013). Regulation of Ca(V)2 calcium channels by G protein coupled receptors. Biochim Biophys Acta *1828*, 1629-1643.

Zamponi, G.W., Lory, P., and Perez-Reyes, E. (2010). Role of voltage-gated calcium channels in epilepsy. Pflugers Arch *460*, 395-403.

Zhen, X.G., Xie, C., Yamada, Y., Zhang, Y., Doyle, C., and Yang, J. (2006). A single amino acid mutation attenuates rundown of voltage-gated calcium channels. FEBS Lett *580*, 5733-5738.

Figure 1

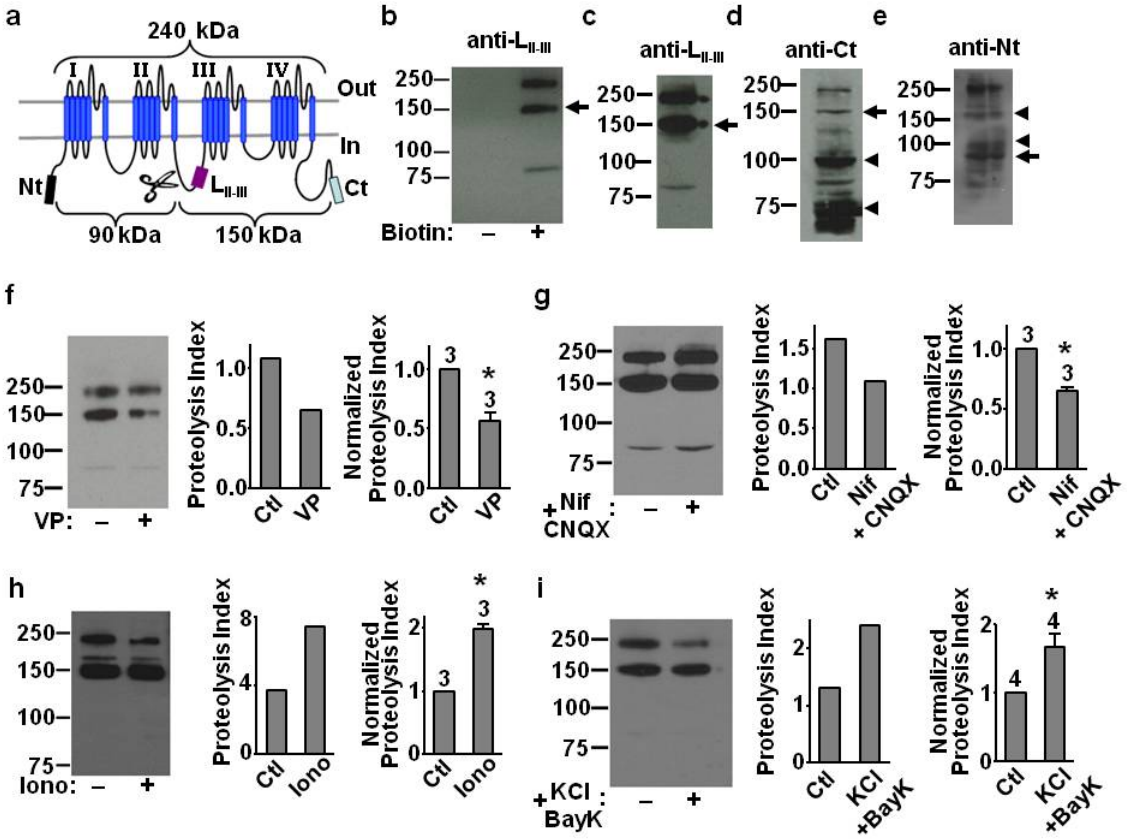

Figure 2

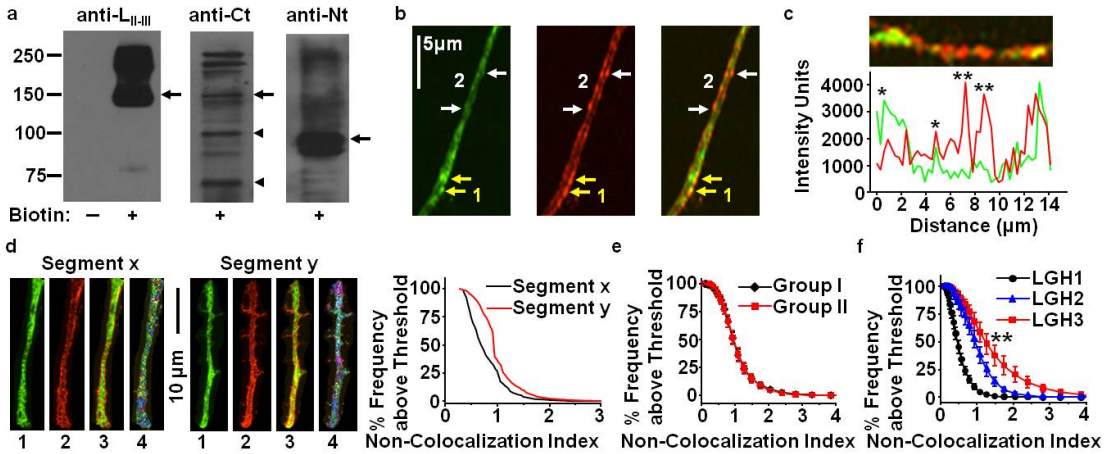

Figure 3

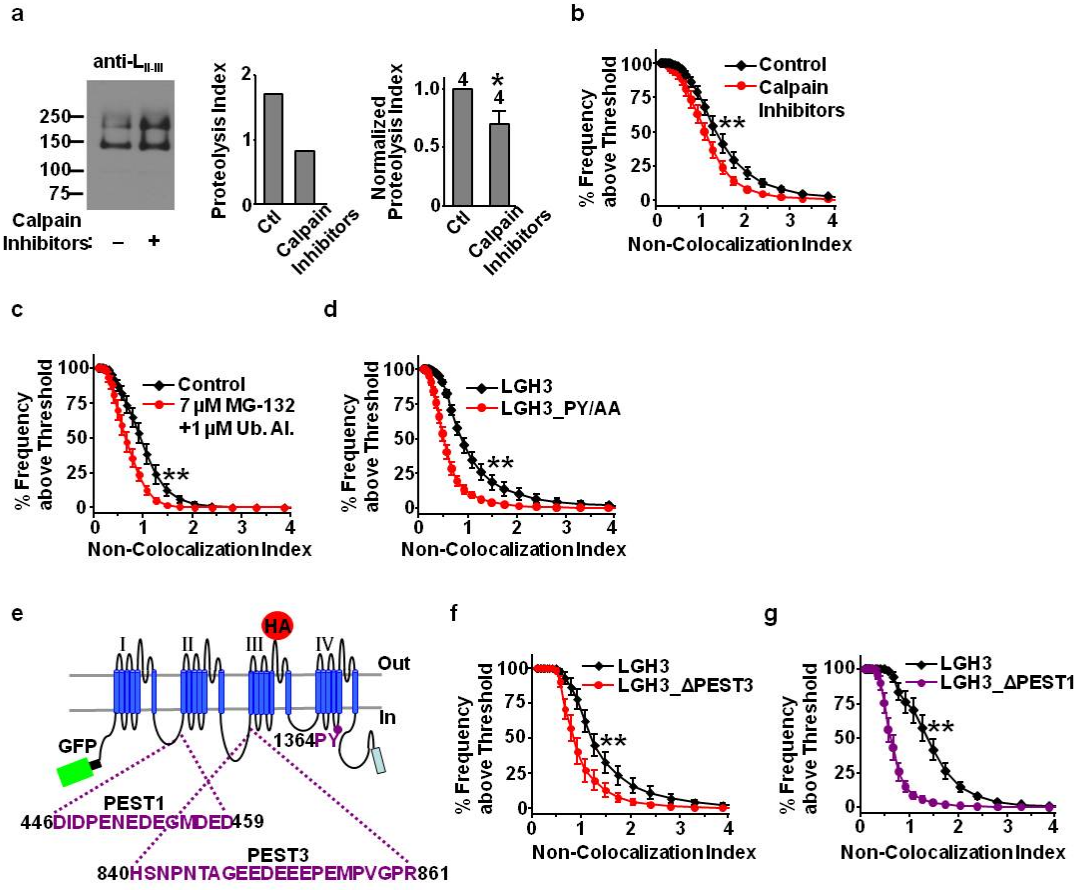
a
anti-L II-III
250
150
100
75
Calpain Inhibitors: – +
Proteolysis Index
Ctl
Calpain Inhibitors
Normalized Proteolysis Index
4
4
*
b
Control
Calpain Inhibitors
% Frequency above Threshold
Non-Colocalization Index
**
c
Control
7 µM MG-132
+1 µM Ub. Al.
d
LGH3
LGH3_PY/AA
e
HA
I
II
III
IV
Out
In
GFP
1364PY
PEST1
446DIDPENEDEGMDED459
PEST3
840HSNPNTAGEEDEEEPEMPVGPR861
f
LGH3
LGH3_ΔPEST3
g
LGH3
LGH3_ΔPEST1

Figure 4

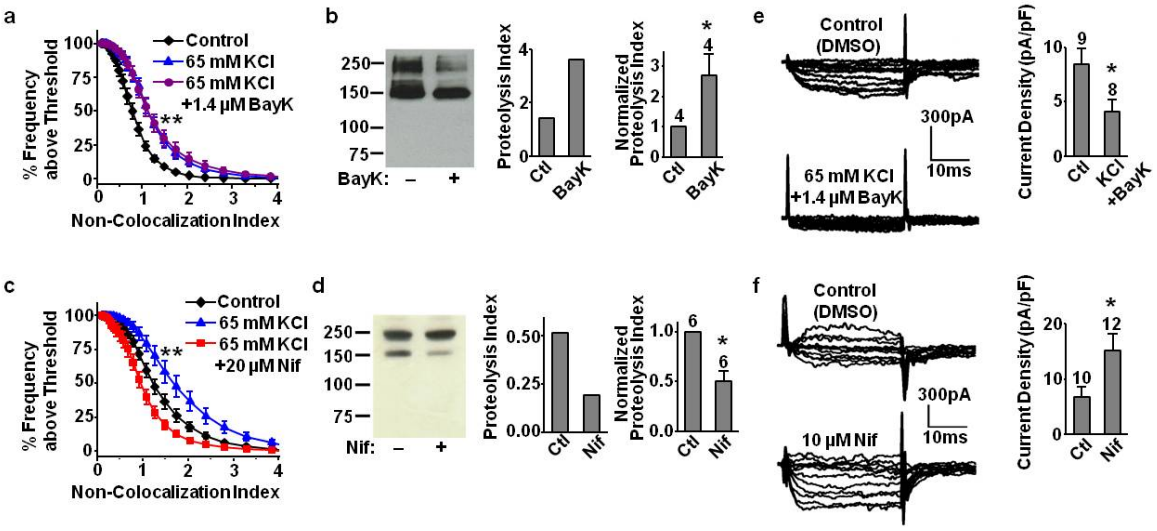

Figure 5

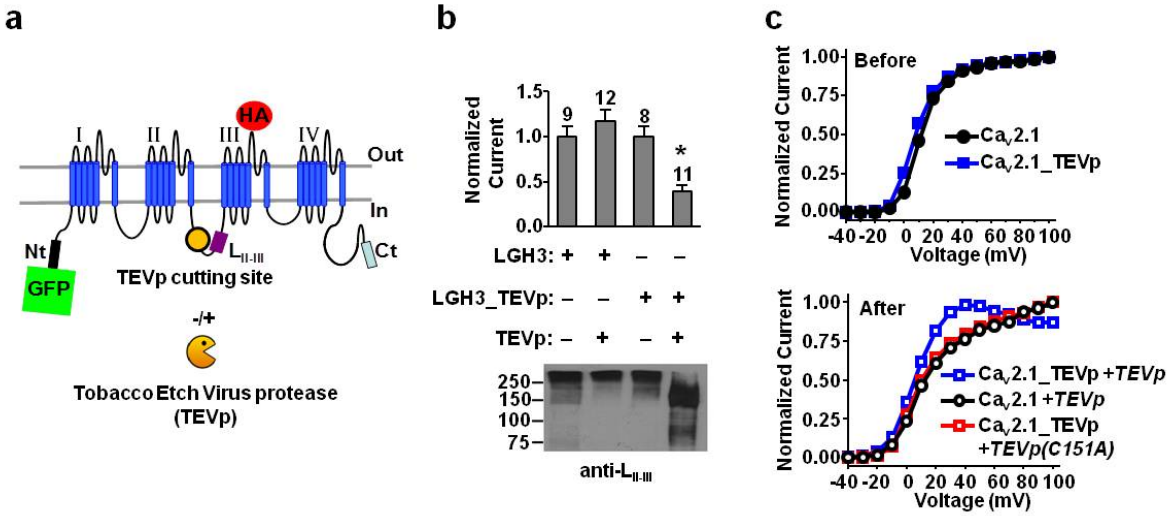

Figure 6

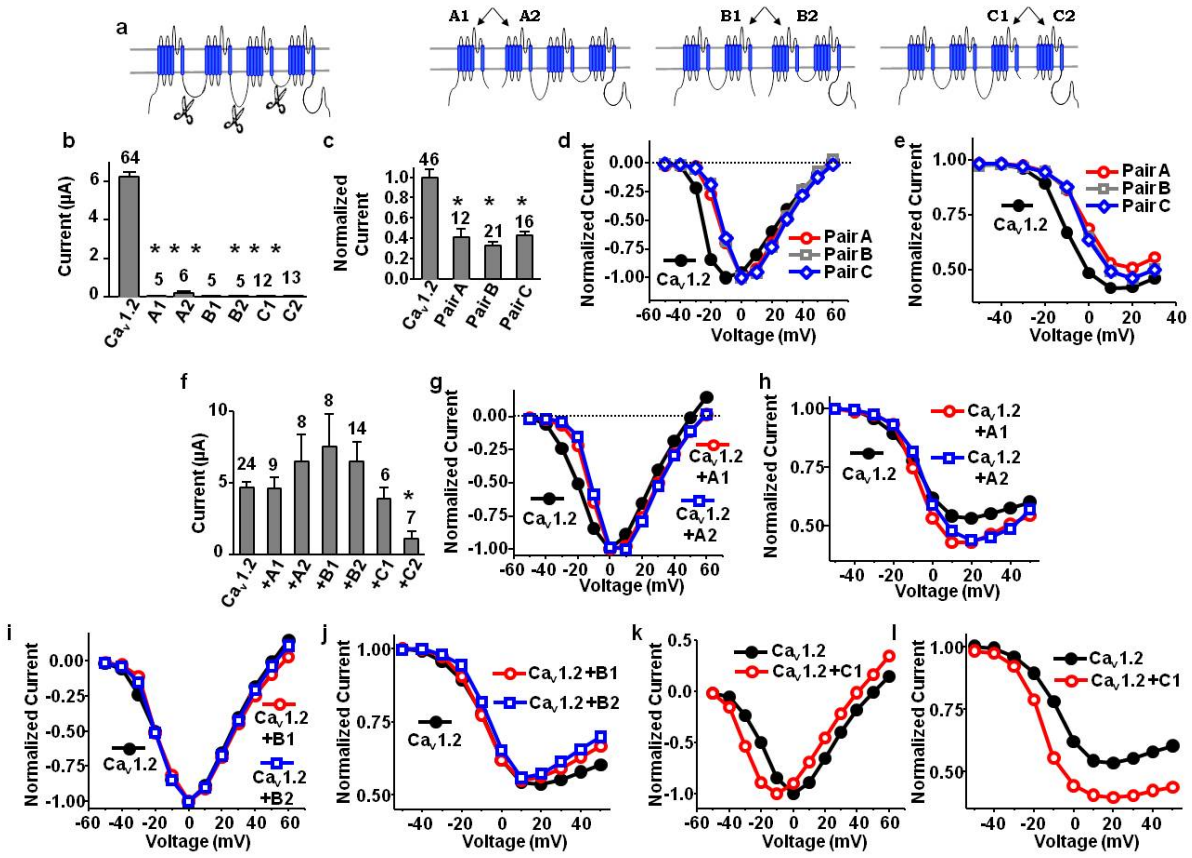
a
A1
A2
B1
B2
C1
C2
b
Current (μA)
64
5
6
5
5
12
13
Cav1.2
A1
A2
B1
B2
C1
C2
c
Normalized Current
46
12
21
16
Cav1.2
Pair A
Pair B
Pair C
d
Normalized Current
Cav1.2
Pair A
Pair B
Pair C
Voltage (mV)
e
Normalized Current
Cav1.2
Pair A
Pair B
Pair C
Voltage (mV)
f
Current (μA)
24
9
8
8
14
6
7
Cav1.2
+A1
+A2
+B1
+B2
+C1
+C2
g
Normalized Current
Cav1.2
Cav1.2 +A1
Cav1.2 +A2
Voltage (mV)
h
Normalized Current
Cav1.2
Cav1.2 +A1
Cav1.2 +A2
Voltage (mV)
i
Normalized Current
Cav1.2
Cav1.2 +B1
Cav1.2 +B2
Voltage (mV)
j
Normalized Current
Cav1.2
Cav1.2+B1
Cav1.2+B2
Voltage (mV)
k
Normalized Current
Cav1.2
Cav1.2+C1
Voltage (mV)
l
Normalized Current
Cav1.2
Cav1.2+C1
Voltage (mV)

Figure 7

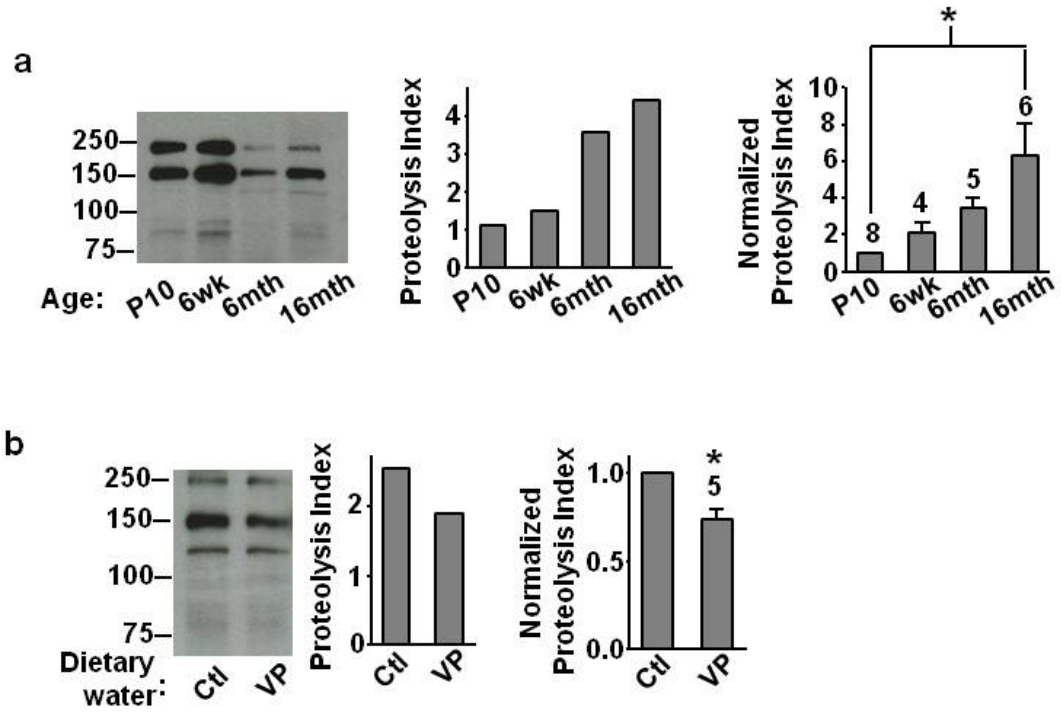
a
250–
150–
100–
75–
Age:
P10
6wk
6mth
16mth
Proteolysis Index
Normalized Proteolysis Index
*
8
4
5
6
b
Dietary water:
Ctl
VP
Proteolysis Index
Normalized Proteolysis Index
*
5